

Copyright

by

William Frederick Spotz

1995

**High-Order Compact Finite Difference Schemes
for Computational Mechanics**

by

William Frederick Spotz, B.S., M.S.

Dissertation

Presented to the Faculty of the Graduate School of

The University of Texas at Austin

in Partial Fulfillment

of the Requirements

for the Degree of

Doctor of Philosophy

The University of Texas at Austin

December 1995

High-Order Compact Finite Difference Schemes for Computational Mechanics

**Approved by
Dissertation Committee:**

To my wife Katherine Simons Spotz,
for her love, support and patience.

Acknowledgments

I would like to thank my advisor, Dr. Graham Carey, and my dissertation committee members, Dr. Robert MacKinnon of Ecodynamics Research Associates, Inc., Dr. David Dolling and Dr. John Kallinderis of the Aerospace Engineering Department, Dr. Chris Maziar of the Electrical Engineering Department, and Dr. Kamy Sepehrnoori of the Petroleum Engineering Department.

It is both common and expected to thank your thesis advisor for his or her support, guidance, and technical advice. For these things of Dr. Carey I am dutifully appreciative, but I am equally thankful for his offer to allow me to move from Austin to continue my research in Houston in the latter stages of my program. Both my wife and I are extremely grateful for his flexibility and generosity.

In the same vein, I would like to thank the Rice University Office of Networking Services, especially Richard Schafer and Cathy Foulston, for their policy of providing dial-in computer accounts to non-Rice students for educational purposes. This provided me with local access to the Internet, allowing me to work and research remotely. I would also like to thank Dr. Mary Wheeler and her assistant Daria Lawrence, for their help in obtaining the account.

This working arrangement also required frequent trips to Austin, and I would like to thank Brian Burgess and Shawn and Dylan Stricklin for their generosity in opening up their homes to me. I imposed on them frequently, often with little notice, and I will probably never be able to repay their hospitality.

I owe a huge debt of gratitude to all the experts in the Computational Fluid

Dynamics Laboratory, especially its administrator, Dr. Robert McLay, as well as my fellow consultants Dr. Steve Bova, Alfred Lorber, Dr. Anand Pardhanani, Spencer Swift, Dr. Scott Runnels, Dr. Harjit Kohli, Dr. Vijayan Sarathy, Andy Berner and Vincent Liu. Not only were they helpful with hardware and software advice, but also in theoretical discussions and some even for some much-needed socializing (made necessary by long days spent preparing for or taking qualifying exams, wrestling with the debugger, or convincing hardware to do what it was designed to do).

Other past and present members of the lab who made my life easier are Dr. Wayne Joubert, Dr. Yun Shen, Dr. Christophe Harle and especially my former roommate, Bruce Davis, whose parallel life has been both scary and reassuring.

The one member of the lab on whom everyone else depends is Pat Bozeman, Dr. Carey's administrative assistant. I am afraid that I leaned on her more than most, and she always cheerfully agreed to help me in any way that I needed. She deserves a special thank-you.

Finally, I would like to thank my wife, Katie Spatz, for her love, support, encouragement, and patience throughout the sometimes tedious process of producing a dissertation. She is both an outstanding engineer and writer, and I would like to thank her for her editorial contributions. I can't thank her enough.

This work has been supported by a grant from ARPA, the Texas Advanced Technology Program, the industrial associates of the U.T. Enhanced Oil and Gas Recovery Research Project, and the Semiconductor Research Corporation.

WILLIAM FREDERICK SPOTZ

The University of Texas at Austin

December 1995

High-Order Compact Finite Difference Schemes for Computational Mechanics

Publication No. _____

William Frederick Spatz, Ph.D.

The University of Texas at Austin, 1995

Supervisor: Graham F. Carey

A class of high-order compact (HOC) finite difference schemes is developed that exhibits higher-order accuracy at the grid points yet utilizes only a compact stencil. This is achieved by using the governing differential equation to approximate leading truncation error terms in the central difference scheme. The method is first developed for steady convection diffusion problems on uniform grids. The high-order accuracy of HOC schemes is demonstrated, as well as their tendency to suppress false oscillations. Second, this class of approximations is used to solve the stream-function vorticity form of the 2D, steady, incompressible Navier-Stokes equations. Numerical results for this application compare favorably with previously published results in the literature, despite use of coarser grids with the HOC scheme. Third, HOC iterative performance is analyzed, revealing that even though HOC condition numbers are higher than those of more standard schemes, certain gradient-type algorithms actually converge slightly faster for HOC formulations than for standard formulations on problems of equivalent size. HOC theory is then extended to nonuniform grids in 1D and 2D by mapping to a computational domain with a uniform

mesh. It is found that the derivatives of the mapping functions can degrade the overall accuracy of the HOC formulation if they are not approximated to sufficient order. A method is proposed for computing high-order compact grid metrics for the case where the grid is obtained by solving a differential equation, as happens with a Helmholtz grid generator. In the absence of such a differential equation, more standard non-compact differencing can be used to obtain high-order metrics. In 2D, the nonuniform grids must be orthogonal to maintain fourth-order accuracy. Finally, other restrictions to previous HOC schemes are removed by extending the theory to transient problems, nonlinear Poisson problems, and 3D linear Poisson problems. Transient HOC formulas are found to have slightly stricter stability requirements on the time step for forward Euler than for more standard schemes, although this is alleviated by the fact that coarser grids may be used. However, HOC forward Euler is an implicit formulation, making backward Euler and Crank-Nicolson more attractive because they are unconditionally stable.

Contents

Acknowledgments	v
Abstract	vii
List of Tables	xii
List of Figures	xiii
Chapter 1 Introduction	1
1.1 Background and Objectives	1
1.2 Contributions	4
Chapter 2 High-Order Compact Methodology	6
2.1 Introduction	6
2.2 Model Equation	8
2.3 1D Convection Diffusion	10
2.3.1 HOC Formulation	10
2.3.2 Oscillations	12
2.3.3 Numerical Studies	16
2.4 2D Convection Diffusion	17
2.4.1 HOC Formulation	17
2.4.2 Numerical Studies	22

2.5	2D Linear Poisson Equation	26
2.6	Summary	30
Chapter 3 Stream-Function Vorticity		31
3.1	Introduction	31
3.2	Governing Equations	31
3.3	HOC Formulation	33
3.3.1	Boundary Conditions	33
3.3.2	Coupled and Decoupled Forms	37
3.4	Numerical Results	39
3.4.1	Model Problem Results	39
3.4.2	Driven Cavity Results	41
3.4.3	Cascading Plates Results	47
3.4.4	Backward-Facing Step Results	58
3.5	Summary	59
Chapter 4 Performance Issues		61
4.1	Introduction	61
4.2	Condition Number Analysis	62
4.3	Numerical Studies	68
4.4	Parallel HOC	72
4.5	Summary	76
Chapter 5 HOC Schemes on Nonuniform Grids		79
5.1	Introduction	79
5.2	1D Convection Diffusion	79
5.2.1	HOC Formulation	80
5.2.2	Numerical Studies	81
5.2.3	HOC Metrics	85
5.3	2D Convection Diffusion	88

5.3.1	HOC Formulation	89
5.3.2	Numerical Studies	93
5.4	Summary	94
Chapter 6 Other Extensions to HOC Theory		95
6.1	Introduction	95
6.2	Transient 1D Convection Diffusion	95
6.2.1	Semi-Discrete HOC Formulation	96
6.2.2	Temporal Differencing	96
6.2.3	Stability Analysis	97
6.3	Transient 1D Diffusion	100
6.4	Transient 2D Diffusion	102
6.5	Nonlinear Poisson	103
6.6	3D Linear Poisson	106
6.6.1	HOC Formulation	106
6.6.2	Global Error Norm	109
6.6.3	Numerical Experiments	111
6.7	Summary	113
Chapter 7 Conclusions		115
Appendix A Truncation Errors for Compact Difference Operators		120
A.1	1D Difference Operators	120
A.2	2D Cross Derivative Operators	121
Appendix B General Stability for Compact Schemes		122
Bibliography		125
Vita		143

List of Tables

2.1	Definitions of 1D δ -Operators on a Uniform Mesh	11
2.2	Definitions of 2D Cross Derivative δ -Operators on a Uniform Mesh .	20
3.1	HOC Wall Boundary Conditions	36
3.2	HOC Corner Boundary Conditions	37
3.3	HOC Driven Cavity Results	45
4.1	Condition Numbers for 1D HOC Matrices	63
6.1	Definition of 3D Cross Derivative δ -Operator on a Uniform Mesh . .	109

List of Figures

2.1	Ratio of Adjacent Slopes for 1D CDS and HOC	14
2.2	Exact 1D Model Problem Solutions	15
2.3	Exact, HOC, and Oscillatory CDS 1D Solutions	16
2.4	1D Convection Diffusion Results	18
2.5	Solution to 2D Model Problem 1	23
2.6	HOC Oscillation Suppression for 2D Model Problem 1	24
2.7	Results for 2D Model Problem 1	25
2.8	Solution to 2D Model Problem 2	26
2.9	Results for 2D Model Problem 2	27
3.1	HOC Vorticity Convergence for Model Stokes Flow	40
3.2	HOC ψ Solution to Analytic Model Problem	42
3.3	HOC ζ Solution to Analytic Model Problem	42
3.4	Problem Description for the Lid-Driven Cavity	43
3.5	HOC Driven Cavity Contours for $Re = 0$	44
3.6	Driven Cavity Results for ζ , $Re = 100$	44
3.7	Driven Cavity Results for u , $Re = 100$	46
3.8	Driven Cavity Results for v , $Re = 100$	46
3.9	Driven Cavity Results for ζ , $Re = 400$	47
3.10	Driven Cavity Results for u , $Re = 400$	48
3.11	Driven Cavity Results for v , $Re = 400$	48

3.12 Oscillating HOC Boundary Conditions	49
3.13 Driven Cavity Results for ζ , $Re = 1000$	49
3.14 Driven Cavity Results for u , $Re = 1000$	50
3.15 Driven Cavity Results for v , $Re = 1000$	50
3.16 Problem Description for the Cascading Plates	51
3.17 Cascading Plates Grids	54
3.18 Cascading Plates Stream Function Contours	55
3.19 Cascading Plates Vorticity Contours	56
3.20 Cascading Plates Velocity	57
3.21 Cascading Plates Wall Vorticity	57
3.22 Problem Description for a Backward-Facing Step.	58
3.23 HOC Backward Facing Step Solutions	60
4.1 Condition Number Limit for HOC, CDS and UDS	64
4.2 Tensor Product $\sigma(ch)\sigma(dh)$	67
4.3 Gershgorin Circles for 2D HOC Matrices	68
4.4 Eigenvalues for 2D HOC, $Re_h = 1$	69
4.5 Eigenvalues for 2D HOC, $Re_h = 2$	70
4.6 Eigenvalues for 2D HOC, $Re_h = 4$	70
4.7 Eigenvalues for 2D HOC, $Re_h = 8$	71
4.8 Eigenvalues for 2D HOC, $Re_h = 16$	71
4.9 Residuals for HOC and CDS, $Re = 0$	73
4.10 Residuals for HOC, CDS and UDS, $Re_h = 1$	73
4.11 Residuals for HOC, CDS and UDS, $Re_h = 2$	74
4.12 Residuals for HOC, CDS and UDS, $Re_h = 4$	74
4.13 Residuals for HOC, CDS and UDS, $Re_h = 8$	75
4.14 Matrix-Vector Product MFLOP rates	76
4.15 Parallel HOC Solution	77
4.16 Speedup Curve for HOC and CDS	77

5.1	Convergence on 1D Nonuniform Grids with Exact Metrics	82
5.2	Convergence on 1D Nonuniform Grids with Differenced Metrics . . .	83
5.3	Non-oscillating HOC Solution on Nonuniform Grid	84
5.4	Boundary Layer Results on Nonuniform Grids	86
5.5	Convergence on 1D Nonuniform Grid with Auxiliary Metrics	88
5.6	2D Test Problem for Nonuniform Grids	94
6.1	Compact, Time-Dependent, 1D Stencil	98
6.2	Stability Restrictions for HOC, CDS and UDS	100
6.3	7-Point $O(h^2)$ CDS Stencil in 3D	107
6.4	19-Point $O(h^4)$ HOC Stencil in 3D	108
6.5	27-Point $O(h^6)$ HOC Stencil in 3D	110
6.6	3D Convergence Rates for HOC and CDS	112
B.1	Compact, Time-Dependent, 1D Stencil	123

Chapter 1

Introduction

1.1 Background and Objectives

Finite difference methods have long been used to approximate the solution of ordinary or partial differential equations (PDEs). These methods involve discretizing the domain of interest into a structured mesh of grid points and approximating derivatives by difference quotients. At each grid point, the value of the desired function or functions are treated as unknowns, and the governing differential equation or equations are approximated by a sparse system of algebraic equations that can then be solved with an appropriate matrix solution algorithm. This approximation process and the resulting system characteristics are what distinguish one finite difference method from another.

Finite differencing is a relatively straightforward method of developing numerical approximations to boundary value problems. However, it does suffer the disadvantage of requiring a structured mesh¹. This is in contrast to finite element methods, which are designed to accommodate highly unstructured meshes, as well as irregular problem data and solutions by virtue of finding approximations to the

¹There is an exception to this. Tworzydło [139] proposed a finite difference method for arbitrary curvilinear coordinates which did not require a structured mesh. However, this was accomplished at the expense of a considerably more complicated formulation and is not utilized in this dissertation.

weak, or variational form of the problem. On the other hand, finite difference methods lend themselves quite easily to Taylor series analysis of truncation errors, and this property is exploited in the present work to develop rigorous high-order approximations.

The simplest (and most familiar) finite difference scheme for second order elliptic PDEs is the central difference scheme (CDS) on a uniform structured mesh. In this method, first and second partial derivatives at a grid point are represented by linear combinations of the three function values at, and directly adjacent to, the grid point in the corresponding coordinate directions. Higher derivatives require additional points. In general, derivatives of order p can be approximated in the CDS with $p+1$ symmetrically-located points if p is even. The coefficients for this case are also symmetric. For odd p , $p+2$ nodes are required, although the coefficients are anti-symmetric, meaning the center coefficient for odd derivatives is always zero. The CDS was named to reflect this symmetry in the stencils and coefficients. Taylor series analysis of the truncation errors for central difference approximations shows that the scheme asymptotically approaches the values of the approximated derivatives as $O(h^2)$ as the mesh size h approaches zero.

Methods with accuracy better than $O(h^2)$ are called higher-order methods. These methods are desirable because their greater accuracy allows coarser meshes to be used, thus lowering computational costs. The standard method for achieving higher-order accuracy is to include additional grid points into the approximations representing the derivatives. In general on a structured mesh, a derivative of order p may be approximated to order m with $p+m-1$ points if p is even. If p is odd, $p+m$ points are required. A general finite difference theory was developed by Patterson [110] for approximating first and second derivatives up to $O(h^{N-1})$ on a grid of N nodes.

High-order methods achieved in this manner always require non-compact stencils that utilize grid points located beyond those directly adjacent to the node

about which the differences are taken. This complicates formulations near boundaries, increases matrix bandwidth, and increases communication requirements for implementation on parallel computer architectures. Still, non-compact high-order schemes are a popular choice. See, for example, Leonard [81, 53] or Bradley [11], who use non-compact differencing for the first derivatives. A. Datta Gupta, *et al.* [29] also implement this strategy in the context of a total variation diminishing (TVD) flux limiting scheme implemented in `UTCMP` and `UTCHEM` [4]. Other examples include the essentially non-oscillatory (ENO) schemes of Harten [54, 55], the high-order schemes of Jain [64] and Lele [79]², or the mimetic and support-operator differencing of Castillo [19, 20].

In light of the problems caused by non-compact finite difference schemes, it is desirable to develop a class of schemes that are both high-order and compact. Hirsh [60] conducted numerical experiments with a class of high-order compact schemes in which the first and second derivatives are treated as unknowns resulting in a mixed method, unlike the schemes developed in the present work. Forester [39] proposed a high-order filter that allowed the underlying method to remain compact. Defect correction techniques [56] take advantage of certain aspects of multi-level schemes to obtain high-order accuracy compactly. Also of interest are the discrete weighted mean approximations of Gartland [41], Noye’s [100, 104] weighted modified equation method and the higher-order upwind difference scheme of Wilkes [148].

High-order compact (HOC) schemes of the type studied here increase the accuracy of the standard central difference approximation from $O(h^2)$ to $O(h^4)$ by including compact approximations to the leading truncation error terms. They are a spatial implementation of the temporal Lax-Wendroff [78] idea and were first proposed in the context of the present methodology by MacKinnon and Carey [86] for material discontinuities. MacKinnon, Carey, Johnson and Langerman followed with similar research (see [87, 88, 90, 91]) for convection diffusion problems. About

²Lele’s “compact” schemes are actually non-compact, although they are relatively compact compared to spectral methods; hence their name

the same time, Abarbanel and Kumar [1] independently developed an HOC scheme for the Euler equations. These schemes are similar to the methods proposed by Dukowicz [37], Wong [151], Dennis [34, 35] and M. M. Gupta [51, 52], although they are derived in a different manner. They also have the added advantage of suppressing or reducing numerical oscillations. For example, the HOC scheme presented in Section 2.3 has been proven to be non-oscillatory for steady and homogenous 1D convection diffusion with constant coefficients [90, 131].

The early study of HOC methods was restricted to a single, steady 1D or 2D equation on uniform meshes. Analysis of these methods was also limited to their accuracy and oscillation properties. In an effort to improve the practical applications of HOC methods, this dissertation addresses these limitations. An outline of the thesis is as follows: The main ideas of the HOC methodology are developed in Chapter 2, and then formulated for the set of stream-function vorticity equations for steady, 2D, incompressible flow in Chapter 3. Issues related to the performance of HOC schemes are then addressed in Chapter 4. Chapter 5 covers the extension of the HOC method to nonuniform grids in 1D and 2D, and finally, Chapter 6 extends the HOC methodology to a variety of problem types, including transient, nonlinear, and 3D applications.

1.2 Contributions

The following list is a description of the new and original work presented in this dissertation:³

Chapter 2 provides a systematic approach to HOC theory, and a new $O(h^6)$ formulation for the 2D Poisson equation for the special case where the fourth derivatives of the forcing function are known (for example, when the analytic form of the forcing function is known).

³Some aspects of these contributions have been accepted for publication [134, 133].

Chapter 3 develops new HOC stencils for the stream-function vorticity equations and wall boundary conditions, including applications to a number of model problems.

Chapter 4 is an original analysis of the eigenvalues, condition numbers, convergence properties and parallelizability of HOC schemes.

Chapter 5 covers the first extension of HOC methodology to nonuniform grids in 1D and 2D.

Chapter 6 provides several new HOC extensions, including formulations for transient convection diffusion in 1D, transient diffusion in 2D, nonlinear Poisson problems, and 3D linear Poisson problems.

Chapter 2

High-Order Compact Methodology

2.1 Introduction

This chapter provides a systematic treatment and overview of high-order compact theory [90, 131, 132] as applied to the steady convection diffusion equation. It covers 1D and 2D problems with variable convection coefficients solved on uniform grids.

To introduce the main ideas, consider a typical two-point boundary value problem (BVP)

$$-a \frac{d^2 \phi}{dx^2} + u \frac{d\phi}{dx} + \phi = S(x), \quad (2.1)$$

with constant coefficients a and u , source term S and Dirichlet boundary data $\phi(0) = \phi_0$ and $\phi(1) = \phi_1$. This model problem is representative of a class of transport problems and permits the main steps of the formulation to be clearly presented. Assume that the domain $[0, 1]$ is divided into evenly spaced cells of length h , and that ϕ_i refers to the approximation of $\phi(x_i)$, where x_i is the coordinate of a typical node. Taylor series expansions of ϕ_{i-1} and ϕ_{i+1} yield the standard central

difference model of (2.1) at grid point i :

$$-a \frac{\phi_{i-1} - 2\phi_i + \phi_{i+1}}{h^2} + u \frac{\phi_{i+1} - \phi_{i-1}}{2h} + \phi_i - \tau_i = S(x_i), \quad (2.2)$$

where τ_i is the truncation error at node i given by

$$\tau_i = \frac{h^2}{12} \left[2u \frac{d^3\phi}{dx^3} - a \frac{d^4\phi}{dx^4} \right]_i + O(h^4). \quad (2.3)$$

We obtain the $O(h^2)$ central difference scheme (CDS) when τ_i is dropped from the formulation in (2.2).

Clearly, if the leading term in (2.3) vanished the scheme would be at least $O(h^4)$. Alternatively, if the leading term in (2.3) is approximated to $O(h^4)$, and retained in (2.2) then we would have a modified scheme that is $O(h^4)$. To obtain a high-order compact (HOC) scheme, we approximate the derivatives on the right hand side of equation (2.3) and include them in the discrete equation. Relations for $\frac{d^3\phi}{dx^3}$ and $\frac{d^4\phi}{dx^4}$ can be constructed by differentiating (2.1) to get

$$\frac{d^3\phi}{dx^3} = \frac{u}{a} \frac{d^2\phi}{dx^2} + \frac{1}{a} \left(\frac{d\phi}{dx} - \frac{dS}{dx} \right), \quad (2.4)$$

$$\begin{aligned} \frac{d^4\phi}{dx^4} &= \frac{u}{a} \frac{d^3\phi}{dx^3} + \frac{1}{a} \left(\frac{d^2\phi}{dx^2} - \frac{d^2S}{dx^2} \right), \\ &= \left(\frac{u^2 + a}{a^2} \right) \frac{d^2\phi}{dx^2} + \frac{u}{a^2} \left(\frac{d\phi}{dx} - \frac{dS}{dx} \right) - \frac{1}{a} \frac{d^2S}{dx^2}. \end{aligned} \quad (2.5)$$

By including the $O(h^2)$ approximations to the derivatives on the right hand sides of (2.4) and (2.5) in our formulation, the rate of convergence is increased to $O(h^4)$, as desired, and the resulting scheme remains compact. The system is still tridiagonal. It will be shown later that this new formulation has other attractive properties.

The source term S plays an important role in approximating $\frac{d^3\phi}{dx^3}$ and $\frac{d^4\phi}{dx^4}$. If the derivatives of S are known analytically, this knowledge can be used in equations (2.4) and (2.5). However, if only a discrete approximation to S is available, $O(h^2)$ central differences can be used to approximate $\frac{dS}{dx}$ and $\frac{d^2S}{dx^2}$, which still results

in $O(h^4)$ convergence for the difference equation. Note that the use of (2.4) and (2.5) implies strong regularity assumptions on the solutions and data, and increases the mathematical complexity for deriving the discrete model. Successively higher-order compact schemes could be devised by repeating the above procedure to obtain a scheme that is of some arbitrary high-order.

2.2 Model Equation

Consider the steady convection diffusion equation in 1D,

$$-a \frac{d^2 \phi}{dx^2} + u \frac{d\phi}{dx} = S, \quad (2.6)$$

on some domain Ω where ϕ is the transport variable of interest, a is a positive diffusion constant (for example, viscosity in fluid mechanics or the permeability in a reservoir simulation), u is a variable convection velocity and S is a source term such as a body force. Equations in the form of (2.6) arise frequently in engineering fields such as fluid mechanics, heat transfer, oil and gas reservoir simulation, and semiconductor device modeling.

If we wish to model (2.6) numerically, we can simplify our task by non-dimensionalizing the problem. Choosing a characteristic length L , velocity U , and solution value ϕ^* (either from the boundary conditions or a combination of other characteristic values), and letting $\hat{\phi} = \frac{\phi}{\phi^*}$, $\hat{u} = \frac{u}{U}$, and $\hat{x} = \frac{x}{L}$, the non-dimensional convection diffusion equation is

$$-\frac{d^2 \hat{\phi}}{d\hat{x}^2} + \frac{UL}{a} \hat{u} \frac{d\hat{\phi}}{d\hat{x}} = \frac{L^2}{a\phi^*} S. \quad (2.7)$$

The quantity $\frac{UL}{a}$ that appears in (2.7) is extremely important in both the physics and numerics of the solution and is called the Reynolds number (Re) in fluid mechanics and the Peclet number (Pe) in the fields of reservoir simulation and heat transfer. In a general discussion of convection diffusion processes, the terms are essentially interchangeable. For analysis of numerical approximations to problems

with constant convection velocities, $u = U$, examination of a local Reynolds number, based on a characteristic length Δx (the size of the grid cells of the discretization) is appropriate. This leads to the definition of the cell Reynolds or cell Peclet numbers,

$$Re_h = Pe_h = \frac{u\Delta x}{a} = \frac{UL}{a}h = Re \cdot h,$$

where $h = \frac{\Delta x}{L}$ is the non-dimensional mesh size. This quantity is important in the study of spurious numerical oscillations, the stability of time-dependent problems, and the convergence properties of numerical approximations to (2.7).

To further ease the development of high-order compact approximations to the non-dimensional model equation (2.7) and comparisons to other more standard schemes, we define $c = Re \cdot \hat{u}$ and $f = \frac{L^2 S}{a\phi^*}$, and drop the hats from the governing equation, with the understanding that we are always discussing non-dimensional quantities. The model convection diffusion equation in 1D is therefore

$$-\frac{d^2\phi}{dx^2} + c\frac{d\phi}{dx} = f. \quad (2.8)$$

We remark that in general, c and f can each vary in space, and are assumed to be sufficiently smooth for the following formulations. Note also that the cell Reynolds number for the constant coefficient case is ch .

Balancing the numerical contributions of the central difference approximations to convection-dominated problems requires refining the grid to prohibitively small sizes. Grids that are too coarse (that is, that violate the cell-Peclet condition $ch < 2$ [6]) result in non-physical oscillations. Many approaches for resolving this problem have been proposed and implemented by researchers. The simplest is to use one-sided differencing on the convection term rather than central differencing. This is equivalent to the addition of an artificial (or numerical) diffusion term [122]. The side on which to apply the differencing is determined by the sign of the convection coefficient, so this technique is called upwinding, and the method is called the upwind difference scheme (UDS). This method has the advantage of being unconditionally non-oscillatory, but the accuracy is reduced to $O(h)$. It has been shown

that upwinding is numerically equivalent to adding artificial viscosity, so in effect, UDS models the wrong problem at coarser grids. This implies a need for finer and finer grids, which is also one of the problems with CDS. This motivates the construction of a method that has higher-order accuracy, yet suppresses or eliminates oscillations.

2.3 1D Convection Diffusion

We now discretize equation (2.8) using central differencing. We first consider differencing on a uniform grid, and will generalize the problem to nonuniform grids in a later chapter.

We define $\delta_x^n \phi_i$, for $n = 1, 2$ to be the standard central difference operator for the n -th derivative of ϕ at grid point i on a uniform grid of mesh size h (see Table 2.1 for a list of 1D central and one-sided difference operators). Central differencing (2.8) yields

$$-\delta_x^2 \phi_i + c_i \delta_x \phi - \tau_i = f_i, \quad (2.9)$$

where τ_i is the local truncation error at node i , derived from Taylor series analysis,

$$\tau_i = \frac{h^2}{12} \left[2c \frac{d^3 \phi}{dx^3} - \frac{d^4 \phi}{dx^4} \right]_i + O(h^4). \quad (2.10)$$

A compilation of the truncation errors of interest in this dissertation are provided in Appendix A.

2.3.1 HOC Formulation

The central difference scheme (CDS) for (2.8) is obtained by neglecting τ_i in (2.9). The truncation error at grid point i is $O(h^2)$, corresponding to the leading term in (2.10). The basic idea behind the HOC approach is to find compact approximations to the derivatives in (2.10) by differentiating the governing equation. This

Table 2.1: Definitions of 1D δ -Operators on a Uniform Mesh

Operator	Formula
$\delta_x \phi_i$	$\frac{\phi_{i+1} - \phi_{i-1}}{2h}$
$\delta_x^+ \phi_i$	$\frac{\phi_{i+1} - \phi_i}{h}$
$\delta_x^- \phi_i$	$\frac{\phi_i - \phi_{i-1}}{h}$
$\delta_x^2 \phi_i$	$\frac{\phi_{i+1} - 2\phi_i + \phi_{i-1}}{h^2}$

gives

$$\begin{aligned} \left. \frac{d^3 \phi}{dx^3} \right|_i &= \left[c \frac{d^2 \phi}{dx^2} + \frac{dc}{dx} \frac{d\phi}{dx} - \frac{df}{dx} \right]_i, \\ &= c_i \delta_x^2 \phi_i + \delta_x c_i \delta_x \phi_i - \delta_x f_i + O(h^2), \end{aligned} \quad (2.11)$$

and

$$\begin{aligned} \left. \frac{d^4 \phi}{dx^4} \right|_i &= \left[c \frac{d^3 \phi}{dx^3} + 2 \frac{dc}{dx} \frac{d^2 \phi}{dx^2} + \frac{d^2 c}{dx^2} \frac{d\phi}{dx} - \frac{d^2 f}{dx^2} \right]_i, \\ &= c_i \left. \frac{\partial^3 \phi}{\partial x^3} \right|_i + 2\delta_x c_i \delta_x^2 \phi_i + \delta_x^2 c_i \delta_x \phi_i - \delta_x^2 f_i + O(h^2). \end{aligned} \quad (2.12)$$

Relations (2.11) and (2.12) can be combined with (2.10) to yield the new truncation error expression,

$$\tau_i = \frac{h^2}{12} \left[(c_i^2 - 2\delta_x c_i) \delta_x^2 \phi_i + (c_i \delta_x c_i - \delta_x^2 c_i) \delta_x \phi_i - c_i \delta_x f_i + \delta_x^2 f_i \right] + O(h^4). \quad (2.13)$$

We can use (2.13) to increase the accuracy of our approximation in (2.9). The resulting high-order compact scheme is therefore

$$-A_i \delta_x^2 \phi_i + C_i \delta_x \phi_i = F_i + O(h^4), \quad (2.14)$$

where

$$A_i = 1 + \frac{h^2}{12} (c_i^2 - 2\delta_x c_i),$$

$$\begin{aligned} C_i &= c_i + \frac{h^2}{12} \left(\delta_x^2 c_i - c_i \delta_x c_i \right), \\ F_i &= f_i + \frac{h^2}{12} \left(\delta_x^2 f_i - c_i \delta_x f_i \right). \end{aligned}$$

For the constant coefficient case, this simplifies to

$$- \left(1 + \frac{c^2 h^2}{12} \right) \delta_x^2 \phi_i + c \delta_x \phi_i = F_i + O(h^4). \quad (2.15)$$

Equations (2.14) and (2.15) provide compact approximations to (2.8) with fourth-order asymptotic rates of convergence.

2.3.2 Oscillations

A serious problem associated with central difference (and other) approximations to the convection diffusion equation is that under certain conditions an oscillatory approximation is obtained even though the analytical solution is smooth and monotonic. An undesirable side effect of this phenomenon is that certain nodes can have negative solution values where positive values are the only physically possible ones; for example, concentrations in a species transport problem may oscillate with negative values and these can be coupled adversely to other solution field variables in biological production models [63] or chemical reactions [143]. In the standard central difference approximation to the one-dimensional, homogeneous problem with constant coefficients, the solution will be oscillatory if the so-called cell-Peclet condition [6],

$$|ch| \leq 2, \quad (2.16)$$

is violated.

The problem of false oscillations and what to do about them is a topic of spirited debate in the literature (see, for example, Gresho [47], Leonard [81], Mokhtari [97], Price [114] or Roache [122]). The simplest proposal is to decrease the mesh size such that relationship (2.16) holds, which can be costly in terms of

memory and computation time. A second solution is to change to some type of upwinding approach [120], which usually prevents oscillations at the cost of decreasing accuracy to $O(h)$. A common proposal is to use CDS when cell-Peclet holds and UDS when cell-Peclet is violated [53, 130], but this simply degenerates to UDS for strongly convective flows. Many researchers support using some type of guaranteed non-oscillatory scheme such as uniformly non-oscillatory (UNO), essentially non-oscillatory (ENO), and total variation diminishing (TVD). See Suresh and Huynh [137] for a description and comparison of these and other schemes.

The HOC approximation provides a more attractive alternative, because it is more accurate for coarser grids. Moreover, in 1D the steady homogeneous scheme is unconditionally non-oscillatory, as will now be shown.

We begin with the homogenous, constant-coefficient form of (2.8), where $c = \text{const}$ and $f = 0$, and we define the solution differences to either side of node i as

$$\begin{aligned}\Delta\phi_i^- &= \phi_i - \phi_{i-1}, \\ \Delta\phi_i^+ &= \phi_{i+1} - \phi_i.\end{aligned}$$

The central difference operators can be expressed as

$$\begin{aligned}\delta_x\phi_i &= \frac{1}{2h}(\Delta\phi_i^+ + \Delta\phi_i^-), \\ \delta_x^2\phi_i &= \frac{1}{h^2}(\Delta\phi_i^+ - \Delta\phi_i^-).\end{aligned}$$

Substituting these expressions into (2.15) yields

$$-\left(\frac{1}{h^2} + \frac{c^2}{12}\right)(\Delta\phi_i^+ - \Delta\phi_i^-) + \frac{c}{2h}(\Delta\phi_i^+ + \Delta\phi_i^-) = 0.$$

Rearranging to isolate $\Delta\phi_i^-$ and $\Delta\phi_i^+$ gives

$$\Delta\phi_i^- \left(\frac{c}{2h} + \frac{1}{h^2} + \frac{c^2}{12}\right) + \Delta\phi_i^+ \left(\frac{c}{2h} - \frac{1}{h^2} - \frac{c^2}{12}\right) = 0,$$

and the ratio of adjacent slopes for the HOC scheme is

$$\frac{\Delta\phi_i^+/h}{\Delta\phi_i^-/h} = \frac{c^2h^2 + 6ch + 12}{c^2h^2 - 6ch + 12}. \quad (2.17)$$

The corresponding ratio for the standard central difference scheme is

$$\frac{\Delta\phi_i^+/h}{\Delta\phi_i^-/h} = \frac{2+ch}{2-ch}, \quad (2.18)$$

and for the upwind difference scheme,

$$\frac{\Delta\phi_i^+/h}{\Delta\phi_i^-/h} = \begin{cases} 1+ch, & c > 0, \\ \frac{1}{1-ch}, & c < 0. \end{cases} \quad (2.19)$$

A negative ratio of adjoining slopes corresponds to oscillations in the solution. Clearly this is the case in (2.18) when the cell-Peclet condition (2.16) is violated. The ratio of adjacent slopes for the HOC scheme in (2.17), however, is *always* positive, with a minimum of $\frac{2-\sqrt{3}}{2+\sqrt{3}}$ at $ch = -2\sqrt{3}$ and a maximum of $\frac{2+\sqrt{3}}{2-\sqrt{3}}$ at $ch = 2\sqrt{3}$. Both ratio curves are graphed in Figure 2.1. The limits at $\pm\infty$ are +1 for the HOC scheme and -1 for the CDS.

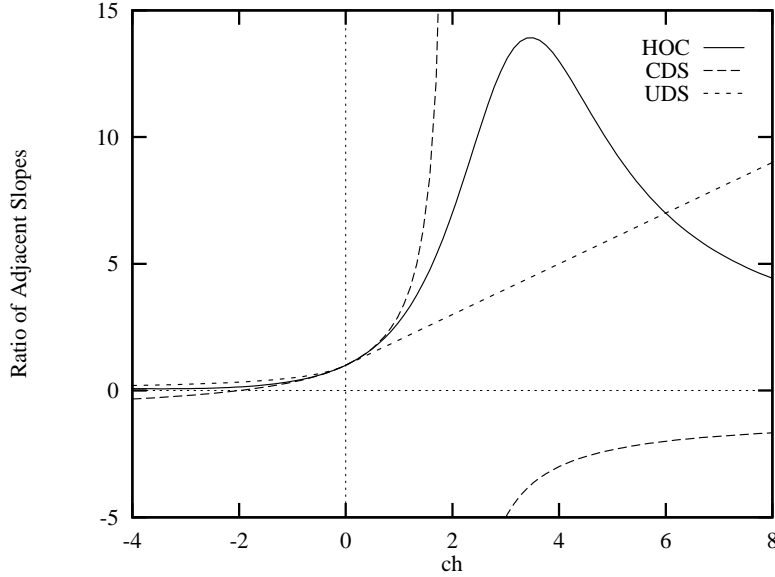


Figure 2.1: Ratio of adjacent slopes for the 1D CDS and HOC methods. A method is oscillatory anywhere its ratio is negative.

To illustrate these results, consider the 1D convection diffusion model problem with the following problem data: $c = Re$ and $f = 0$ for $0 \leq x \leq 1$ and boundary

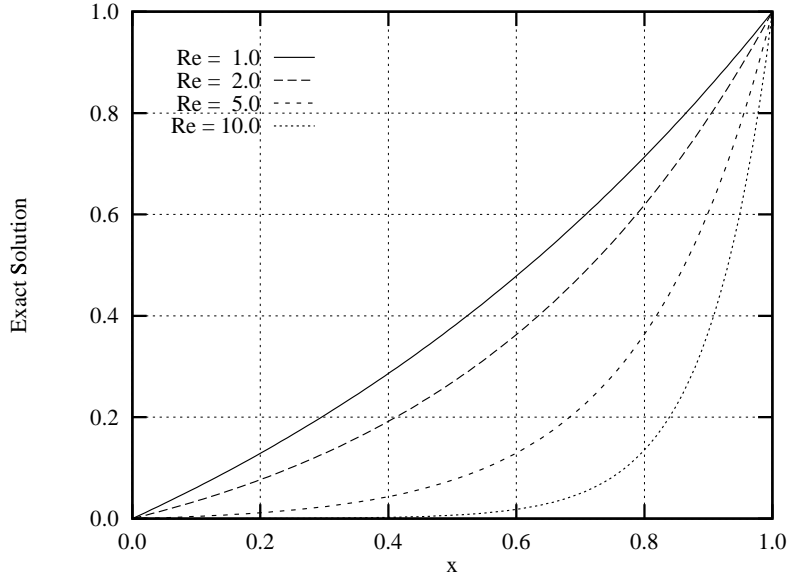


Figure 2.2: Exact 1D model problem solutions for $Re = 1, 2, 5$, and 10 .

conditions $\phi(0) = 0, \phi(1) = 1$, where the Reynolds number, Re , is a constant introduced as a measure of convection relative to diffusion. The resulting exact solution is

$$\phi(x) = \frac{e^{Re \cdot x} - 1}{e^{Re} - 1}, \quad (2.20)$$

that exhibits a layer at $x = 1$ for $Re \gg 1$. The exact solution is shown in Figure 2.2 for $Re = 1, 2, 5$, and 10 . Figure 2.3 shows the exact solution for $Re = 50$ along with the CDS and HOC approximations to the solution for $h = \frac{1}{8}$, which clearly violates the cell-Peclet condition. The oscillations in the CDS solution are obvious. As predicted, the HOC solution does not oscillate (although at this coarse grid level, the errors in the layer are evident). Since both formulas involve three-point schemes (but with different weights), the computational complexity of the solution methods are identical but the new formula offers increased accuracy and oscillatory stability.

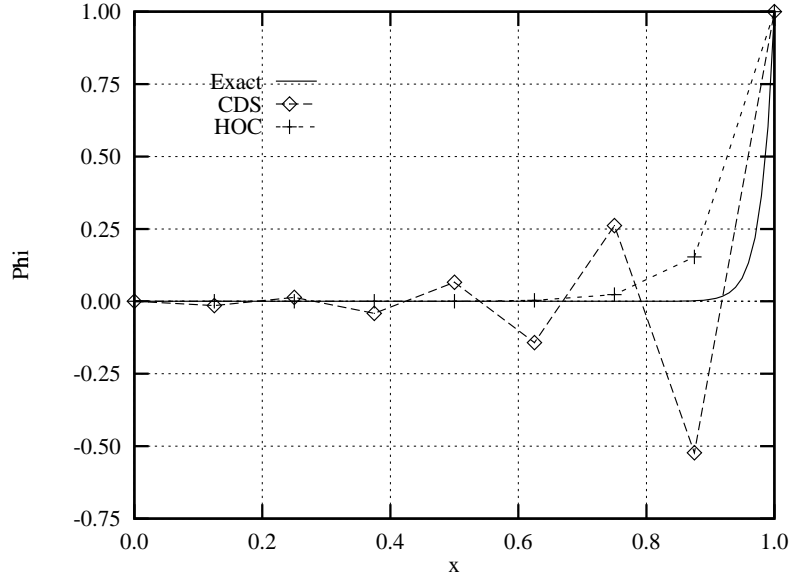


Figure 2.3: Exact, CDS, and HOC solutions to the 1D convection diffusion model problem for $c = 50$, $h = \frac{1}{8}$.

2.3.3 Numerical Studies

The truncation errors given by expressions (2.9), (2.14) and (2.15) represent the pointwise error in approximating the differential equation (but not necessarily the solution). Let the error at any grid point i be defined by

$$E = |\phi(x_i) - \phi_i|.$$

Moreover, let i be a grid point common to a set of uniformly refined grids. Then, asymptotically, we expect the pointwise error to converge as

$$E = Ch^m,$$

for some m . This implies

$$\log E = \log C + m \log h.$$

Hence, the data $\log E$ vs. $\log h$ should be asymptotic to a straight line with slope m , which provides us with a method for experimentally determining the order of accuracy of a given method.

For each of the following model problems, the cases $h = \frac{1}{4}, \frac{1}{8}, \frac{1}{16}, \frac{1}{32}$ and $\frac{1}{64}$ are solved and the error reported is the absolute solution error at the right-most interior grid point on the coarsest grid, where the error tends to be large. The convergence rate m is calculated from the formula

$$\frac{E(h = \frac{1}{32})}{E(h = \frac{1}{64})} = 2^m.$$

The 1D model problem was run for values of $Re = 1, 2, 5$, and 10 , and the solution error was measured at $x = 0.75$. The results are shown in Figure 2.4. The expected convergence rates were recovered; $m \simeq 1$ for UDS, $m = 2$ for CDS, and $m = 4$ for HOC. Note that in some cases, the errors for large h do not lie on the asymptotic line. This simply indicates that h is large enough for higher-order truncation terms to become significant and affect the error. Verification for the variable-coefficient case will be presented in Section 5.2.2.

2.4 2D Convection Diffusion

We turn our attention now to the 2D form of (2.8),

$$-\left(\frac{\partial^2 \phi}{\partial x^2} + \frac{\partial^2 \phi}{\partial y^2}\right) + c \frac{\partial \phi}{\partial x} + d \frac{\partial \phi}{\partial y} = f, \quad (2.21)$$

where the problem data c , d and f are sufficiently smooth to construct the following formulations.

2.4.1 HOC Formulation

For convenience in applying the HOC method to solve equation (2.21), we first consider the case where c and d are constants, and restrict the domain Ω to a union of rectangular shapes. Divide this domain into a uniform mesh of square cells, where each vertex serves as a node and the vertical and horizontal distance between two adjacent nodes is h , a constant.

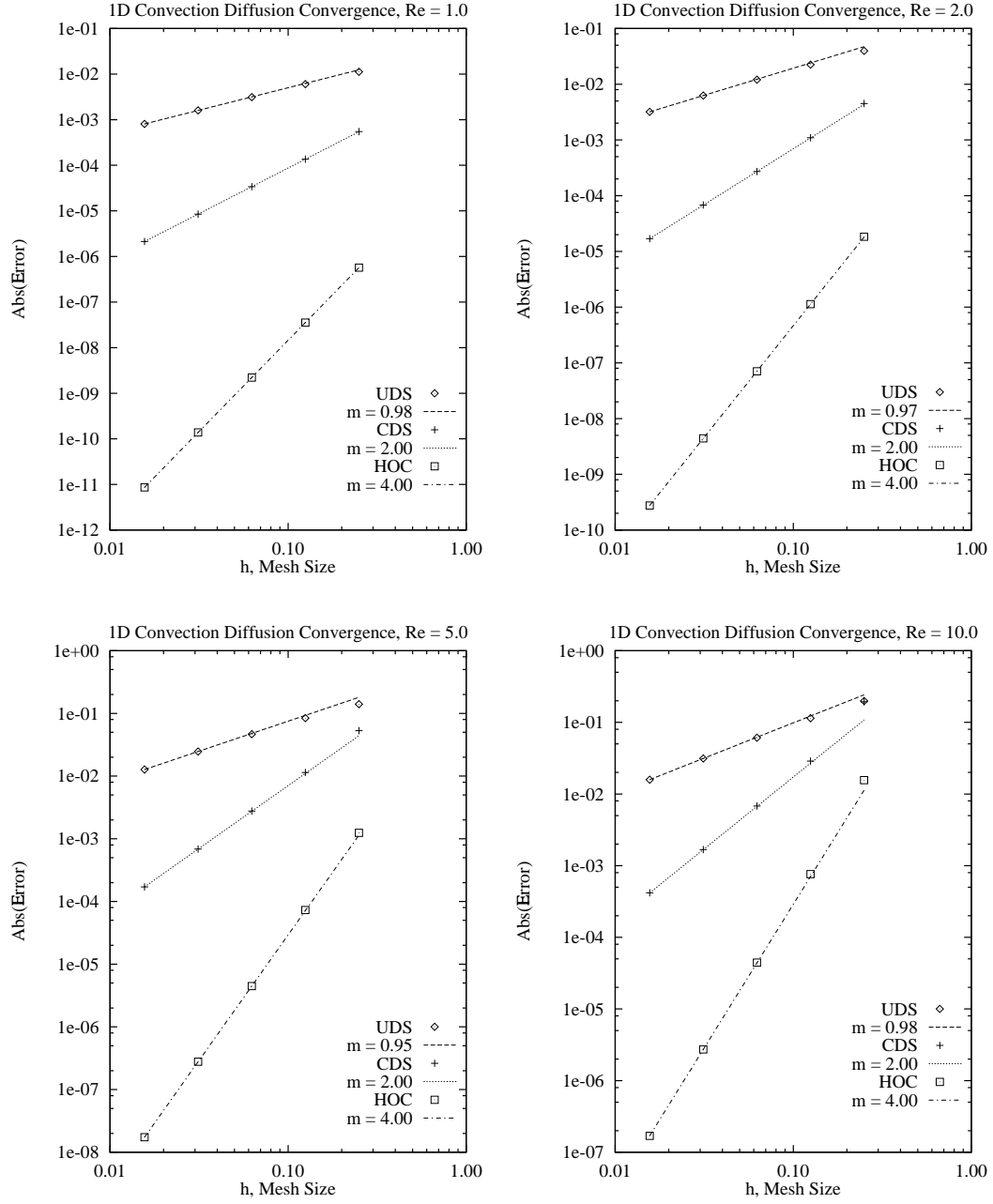


Figure 2.4: Convergence results for 1D convection diffusion, for $Re = 1, 2, 5$ and 10 , solved by CDS, UDS, and HOC scheme.

We let ϕ_{ij} denote $\phi(x_i, y_j)$, etc., and again substituting the standard central difference operators into equation (2.21) to yield

$$-\delta_x^2 \phi_{ij} - \delta_y^2 \phi_{ij} + c\delta_x \phi_{ij} + d\delta_y \phi_{ij} - \tau_{ij} = f_{ij}, \quad (2.22)$$

where the truncation error is

$$\tau_{ij} = \frac{h^2}{12} \left[2 \left(c \frac{\partial^3 \phi}{\partial x^3} + d \frac{\partial^3 \phi}{\partial y^3} \right) - \left(\frac{\partial^4 \phi}{\partial x^4} + \frac{\partial^4 \phi}{\partial y^4} \right) \right]_{ij} + O(h^4). \quad (2.23)$$

As before, we now seek approximations to the derivatives in (2.23) and include them in the finite difference formulation (2.22). Differentiating equation (2.21) yields

$$\frac{\partial^3 \phi}{\partial x^3} = -\frac{\partial^3 \phi}{\partial x \partial y^2} + c \frac{\partial^2 \phi}{\partial x^2} + d \frac{\partial^2 \phi}{\partial x \partial y} - \frac{\partial f}{\partial x}, \quad (2.24)$$

$$\frac{\partial^4 \phi}{\partial x^4} = -\frac{\partial^4 \phi}{\partial x^2 \partial y^2} + c \frac{\partial^3 \phi}{\partial x^3} + d \frac{\partial^3 \phi}{\partial x^2 \partial y} - \frac{\partial^2 f}{\partial x^2}, \quad (2.25)$$

$$\frac{\partial^3 \phi}{\partial y^3} = -\frac{\partial^3 \phi}{\partial x^2 \partial y} + c \frac{\partial^2 \phi}{\partial x \partial y} + d \frac{\partial^2 \phi}{\partial y^2} - \frac{\partial f}{\partial y}, \quad (2.26)$$

$$\frac{\partial^4 \phi}{\partial y^4} = -\frac{\partial^4 \phi}{\partial x^2 \partial y^2} + c \frac{\partial^3 \phi}{\partial x \partial y^2} + d \frac{\partial^3 \phi}{\partial y^3} - \frac{\partial^2 f}{\partial y^2}. \quad (2.27)$$

Note that all the terms on the right hand side of equation (2.24) have compact $O(h^2)$ approximations at node ij (see Table 2.2 for a complete list of 2D cross-derivative operators). For example,

$$\left. \frac{\partial^3 \phi}{\partial x \partial y^2} \right|_{ij} = \delta_x \delta_y^2 \phi_{ij} - \frac{h^2}{12} \left[2 \frac{\partial^5 \phi}{\partial x^3 \partial y^2} + \frac{\partial^5 \phi}{\partial x \partial y^4} \right]_{ij} + O(h^4),$$

etc. Therefore, $\frac{\partial^3 \phi}{\partial x^3}$ can be approximated to $O(h^2)$. Now all the terms on the right hand side of equation (2.25) have $O(h^2)$ approximations, so $\frac{\partial^4 \phi}{\partial x^4}$ can be approximated to $O(h^2)$. The same is true for $\frac{\partial^3 \phi}{\partial y^3}$ and $\frac{\partial^4 \phi}{\partial y^4}$. The result is that all the left hand side terms of equations (2.24)–(2.27) have $O(h^2)$ approximations.

Substituting equations (2.24)–(2.27) into equation (2.23) and simplifying

Table 2.2: Definitions of 2D Cross Derivative δ -Operators on a Uniform Mesh

Operator	Formula
$\delta_x \delta_y \phi_{ij}$	$\frac{\phi_{i+1,j+1} - \phi_{i-1,j+1} - \phi_{i+1,j-1} + \phi_{i-1,j-1}}{4h^2}$
$\delta_x^+ \delta_y^+ \phi_{ij}$	$\frac{\phi_{i+1,j+1} - \phi_{i,j+1} - \phi_{i+1,j} + \phi_{ij}}{h^2}$
$\delta_x^+ \delta_y^- \phi_{ij}$	$\frac{\phi_{i+1,j} - \phi_{ij} - \phi_{i+1,j-1} + \phi_{i,j-1}}{h^2}$
$\delta_x^- \delta_y^+ \phi_{ij}$	$\frac{\phi_{i,j+1} - \phi_{i-1,j+1} - \phi_{ij} + \phi_{i-1,j}}{h^2}$
$\delta_x^- \delta_y^- \phi_{ij}$	$\frac{\phi_{ij} - \phi_{i-1,j} - \phi_{i,j-1} + \phi_{i-1,j-1}}{h^2}$
$\delta_x^2 \delta_y \phi_{ij}$	$\frac{2(\phi_{i,j-1} - \phi_{i,j+1}) + \phi_{i+1,j+1} - \phi_{i+1,j-1} + \phi_{i-1,j+1} - \phi_{i-1,j-1}}{2h^3}$
$\delta_x^2 \delta_y^+ \phi_{ij}$	$\frac{2(\phi_{i,j} - \phi_{i,j+1}) + \phi_{i+1,j+1} - \phi_{i+1,j} + \phi_{i-1,j+1} - \phi_{i-1,j}}{h^3}$
$\delta_x^2 \delta_y^- \phi_{ij}$	$\frac{2(\phi_{i,j-1} - \phi_{i,j}) + \phi_{i+1,j} - \phi_{i+1,j-1} + \phi_{i-1,j} - \phi_{i-1,j-1}}{h^3}$
$\delta_x \delta_y^2 \phi_{ij}$	$\frac{2(\phi_{i-1,j} - \phi_{i+1,j}) + \phi_{i+1,j+1} - \phi_{i-1,j+1} + \phi_{i+1,j-1} - \phi_{i-1,j-1}}{2h^3}$
$\delta_x^+ \delta_y^2 \phi_{ij}$	$\frac{2(\phi_{i,j} - \phi_{i+1,j}) + \phi_{i+1,j+1} - \phi_{i,j+1} + \phi_{i+1,j-1} - \phi_{i,j-1}}{h^3}$
$\delta_x^- \delta_y^2 \phi_{ij}$	$\frac{2(\phi_{i-1,j} - \phi_{ij}) + \phi_{i,j+1} - \phi_{i-1,j+1} + \phi_{i,j-1} - \phi_{i-1,j-1}}{h^3}$
$\delta_x^2 \delta_y^2 \phi_{ij}$	$\frac{4\phi_{ij} - 2(\phi_{i+1,j} + \phi_{i-1,j} + \phi_{i,j+1} + \phi_{i,j-1})}{h^4} +$ $\frac{\phi_{i+1,j+1} + \phi_{i+1,j-1} + \phi_{i-1,j+1} + \phi_{i-1,j-1}}{h^4}$

yields an error term of the form

$$\begin{aligned}
\tau_{ij} = & \frac{h^2}{12} \left[c^2 \frac{\partial^2 \phi}{\partial x^2} + 2cd \frac{\partial^2 \phi}{\partial x \partial y} + d^2 \frac{\partial^2 \phi}{\partial y^2} + 2 \frac{\partial^4 \phi}{\partial x^2 \partial y^2} - 2c \frac{\partial^3 \phi}{\partial x \partial y^2} - 2d \frac{\partial^3 \phi}{\partial x^2 \partial y} \right]_{ij} + \\
& \frac{h^2}{12} \left[\frac{\partial^2 f}{\partial x^2} + \frac{\partial^2 f}{\partial y^2} - c \frac{\partial f}{\partial x} - d \frac{\partial f}{\partial y} \right]_{ij} + O(h^4). \tag{2.28}
\end{aligned}$$

Now, substituting the $O(h^2)$ approximations to the derivatives in (2.28) and insert-

ing in (2.22),

$$\begin{aligned}
& - \left(1 + \frac{c^2 h^2}{12}\right) \delta_x^2 \phi_{ij} - \left(1 + \frac{d^2 h^2}{12}\right) \delta_y^2 \phi_{ij} + c \delta_x \phi_{ij} + d \delta_y \phi_{ij} - \\
& \frac{h^2}{6} \left[\delta_x^2 \delta_y^2 \phi_{ij} - c \delta_x \delta_y^2 \phi_{ij} - d \delta_x^2 \delta_y \phi_{ij} + cd \delta_x \delta_y \phi_{ij} \right] = \\
& f_{ij} + \frac{h^2}{12} \left[\frac{\partial^2 f}{\partial x^2} + \frac{\partial^2 f}{\partial y^2} - c \frac{\partial f}{\partial x} - d \frac{\partial f}{\partial y} \right]_{ij} + O(h^4). \tag{2.29}
\end{aligned}$$

If the convection coefficients c and d are allowed to vary over the domain, this increases the algebraic manipulation required to derive the HOC formula. Using the same procedure as for constant coefficients, the HOC formula for variable coefficients is

$$\begin{aligned}
& -A_{ij} \delta_x^2 \phi_{ij} - B_{ij} \delta_y^2 \phi_{ij} + C_{ij} \delta_x \phi_{ij} + D_{ij} \delta_y \phi_{ij} - \\
& \frac{h^2}{6} \left[\delta_x^2 \delta_y^2 \phi_{ij} - c_{ij} \delta_x \delta_y^2 \phi_{ij} - d_{ij} \delta_x^2 \delta_y \phi_{ij} - G_{ij} \delta_x \delta_y \phi_{ij} \right] = \tag{2.30} \\
& F_{ij} + O(h^4),
\end{aligned}$$

where the coefficients A_{ij} , B_{ij} , C_{ij} , D_{ij} , F_{ij} and G_{ij} are given by

$$\begin{aligned}
A_{ij} &= 1 + \frac{h^2}{12} (c_{ij}^2 - 2\delta_x c_{ij}), \\
B_{ij} &= 1 + \frac{h^2}{12} (d_{ij}^2 - 2\delta_y d_{ij}), \\
C_{ij} &= c_{ij} + \frac{h^2}{12} (\delta_x^2 c_{ij} + \delta_y^2 c_{ij} - c_{ij} \delta_x c_{ij} - d_{ij} \delta_y c_{ij}), \\
D_{ij} &= d_{ij} + \frac{h^2}{12} (\delta_x^2 d_{ij} + \delta_y^2 d_{ij} - c_{ij} \delta_x d_{ij} - d_{ij} \delta_y d_{ij}), \\
F_{ij} &= f_{ij} + \frac{h^2}{12} (\delta_x^2 f_{ij} + \delta_y^2 f_{ij} - c_{ij} \delta_x f_{ij} - d_{ij} \delta_y f_{ij}), \\
G_{ij} &= \delta_y c_{ij} + \delta_x d_{ij} - c_{ij} d_{ij}.
\end{aligned}$$

Note that in 2D both HOC stencils involve all nine points due to the introduction of cross derivatives of ϕ into the formulation, as compared to the standard five-point CDS stencil. Due to the compact nature of the stencil, there is only a minor increase in matrix bandwidth. For example, for a square domain of N total grid points, the half-bandwidth w for CDS is given by $w = \sqrt{N} + 1$ while the HOC half-bandwidth

is $w = \sqrt{N} + 2$. Since the operation count for the elimination procedure of a band solver is approximately $w^2 N$ [135] for large N , the HOC scheme results in an increase in elimination operations of $O(N^{3/2})$. This is negligible at large N compared to the total elimination operations, which is $O(N^2)$. The back-substitution stage requires $O(N^{3/2})$ operations for both schemes, which is also negligible compared to the elimination stage. (Note that iterative performance will be studied in Chapter 4.)

The more complicated matrix coefficients and right-hand side vector for the HOC scheme compared to CDS also incur additional operations. The number of multiplications and divides required to compute the HOC system for variable convection coefficients is approximately $56N$, compared to approximately $6N$ for the CDS. While this is a greater than nine-fold increase in operations, it is also negligible compared to the elimination stage.

A comparison of operations between CDS and HOC should not neglect the savings obtained by the increased HOC accuracy, which allows for coarser grids. If we roughly equate the errors on a CDS mesh of size h_{CDS} and an HOC mesh of size h_{HOC} , then

$$h_{CDS}^2 \approx h_{HOC}^4, \quad (2.31)$$

and use the fact that $h = N^{-1/2}$ for a 2D problem, we can estimate that the number of grid points required to solve a HOC system is $N_{HOC} \approx \sqrt{N_{CDS}}$. The ratio of required operations is therefore

$$\frac{CDS}{HOC} \approx \frac{N_{CDS}^2}{N_{HOC}^2} = N_{CDS},$$

hence the computation is approximately a factor of N_{CDS} faster.

2.4.2 Numerical Studies

We now consider two 2D model problems to test the HOC formulation for convection diffusion with constant coefficients and variable coefficients, respectively.

Problem 1. Gartland [41] proposed the following model problem,

$$\begin{aligned} c &= Re, d = 0, & f &= 0, & 0 \leq x, y \leq 1, \\ \phi(x, 0) &= 0, & \phi(x, 1) &= 0, & 0 \leq x \leq 1, \\ \phi(0, y) &= \sin \pi y, & \phi(1, y) &= 2 \sin \pi y, & 0 \leq y \leq 1, \end{aligned}$$

with exact solution

$$\begin{aligned} \phi(x, y) &= e^{Re \cdot x/2} \sin \pi y \frac{2e^{-Re/2} \sinh \sigma x + \sinh \sigma(1-x)}{\sinh \sigma}, \\ \sigma &= \sqrt{\pi^2 + Re^2/4}. \end{aligned}$$

(See Figure 2.5 for a surface and contour plot of the exact solution.) This model problem produces a layer along the line $x = 1$, but convection is limited to the x direction only. It also provides a good example of how the HOC scheme suppresses oscillations for 2D problems. Figure 2.6 shows contour and surface plots for the CDS and HOC solutions to model problem 1 with $Re = 100$ and $h = \frac{1}{16}$, which violates the cell-Peclet condition for CDS but results in a smooth HOC solution.

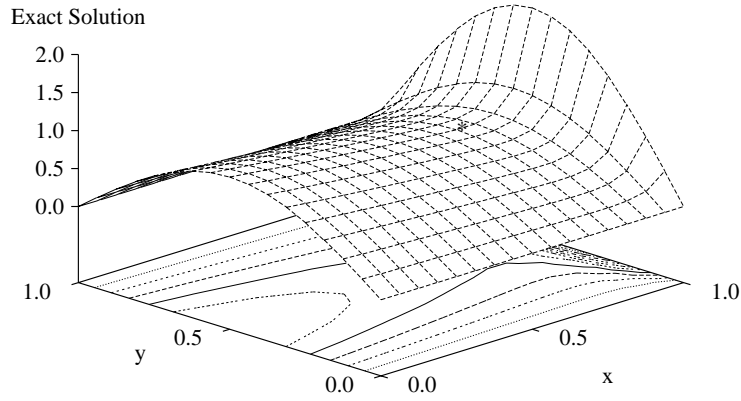


Figure 2.5: Surface and contour plot of the exact solution to the 2D model problem 1, for $Re = 20$. The asterisk (*) denotes where the error is measured.

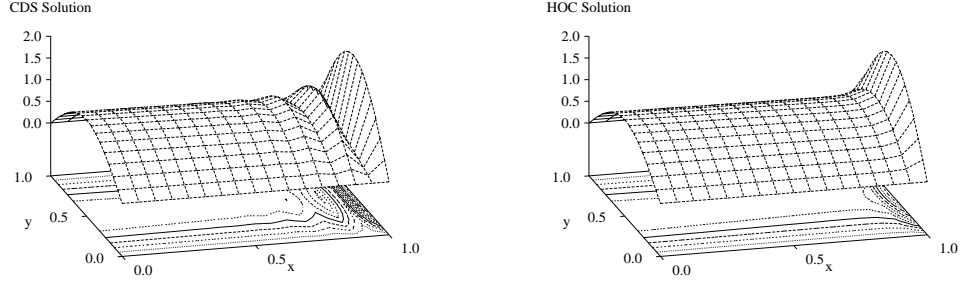


Figure 2.6: Surface and contour plots of the oscillating CDS and non-oscillating HOC solution to the 2D model problem 1 with $Re = 100$, $h = \frac{1}{16}$.

This model problem was tested for $Re = 2, 5, 10$ and 20 . The error was measured at a grid point located at $x = 0.75$, $y = 0.5$. The convergence rates, shown in Figure 2.7 are again $O(h^4)$ as predicted.

Problem 2. The previous model problem had constant convection coefficients. Gupta [52] proposed the following 2D model problem with variable convection coefficients:

$$\begin{aligned} c &= -Re \cdot x, d = Re \cdot y, \quad 0 \leq x, y \leq 1, \\ \phi(x, 0) &= \phi(x, 1) = 0, \quad 0 \leq x \leq 1, \\ \phi(0, y) &= \phi(1, y) = 0, \quad 0 \leq y \leq 1, \end{aligned}$$

combined with the following forcing function,

$$f = e^{x+y} \left[xy(6 - 2x - 2xy - 2y) + Re \cdot xy(x^2 - y^2) \right].$$

The resulting exact solution is

$$\phi(x, y) = xy(1 - x)(1 - y)e^{x+y}.$$

Clearly, this exact solution is independent of the Reynolds number, even though Re appears in the convection coefficients. Surface and contour plots of the exact solution are shown in Figure 2.8.

This model problem allowed HOC formulations for both constant coefficients, equation (2.29) labeled “HOC-C,” and variable coefficients, equation (2.30) labeled

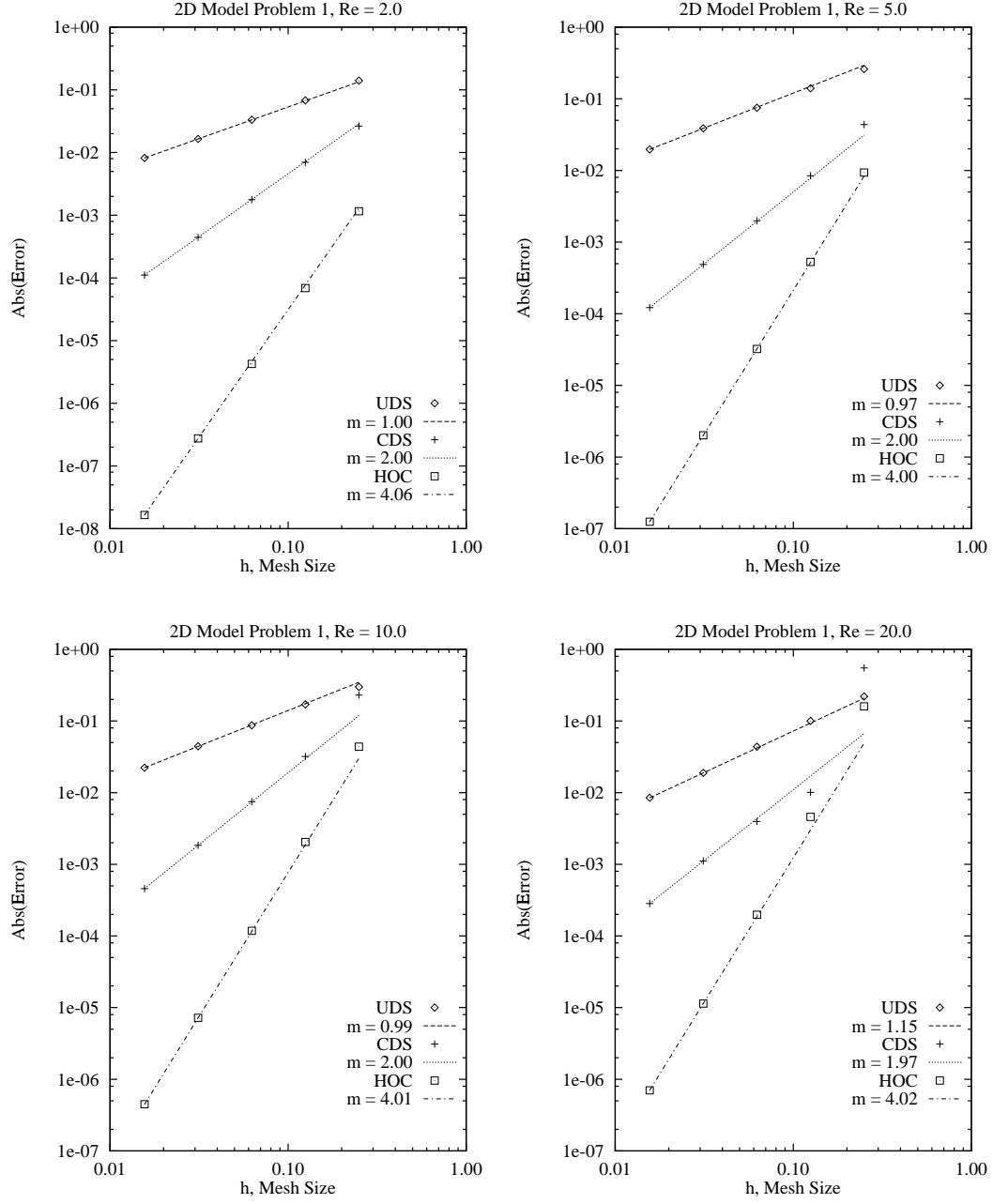


Figure 2.7: Convergence results for the 2D model problem 1, for $Re = 2, 5, 10$ and 20.

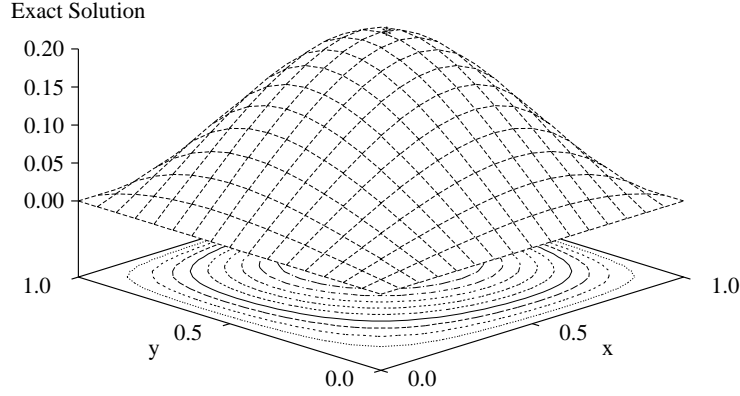


Figure 2.8: Surface and contour plot of the exact solution to the 2D model problem 2. The asterisk (*) denotes where the error is measured. Note that the solution is independent of Re .

“HOC-V,” to be tested. The error was measured at the grid point $x = y = 0.75$. Reynolds numbers of $Re = 0, 1, 10$, and 100 were run, with the results presented in Figure 2.9. Note that for $Re = 0$, no convection is present and therefore UDS is equivalent to CDS, and HOC-C is equivalent to HOC-V. For this case, convergence rates of 2 and 4 respectively, are obtained. For the other cases, with non-zero convection, $m = 1$ for UDS, $m = 2$ for CDS and HOC-C, and $m = 4$ for HOC-V, all as predicted, with the exception of unexpected poor performance of UDS at $Re = 100$.

Further verification of the HOC schemes for the convection diffusion equation via additional model problems can be found in [90] and [132].

2.5 2D Linear Poisson Equation

The stationary diffusion equation can be treated here as a special case of the convection diffusion equation (2.21), with zero convection coefficients $c = d = 0$, and

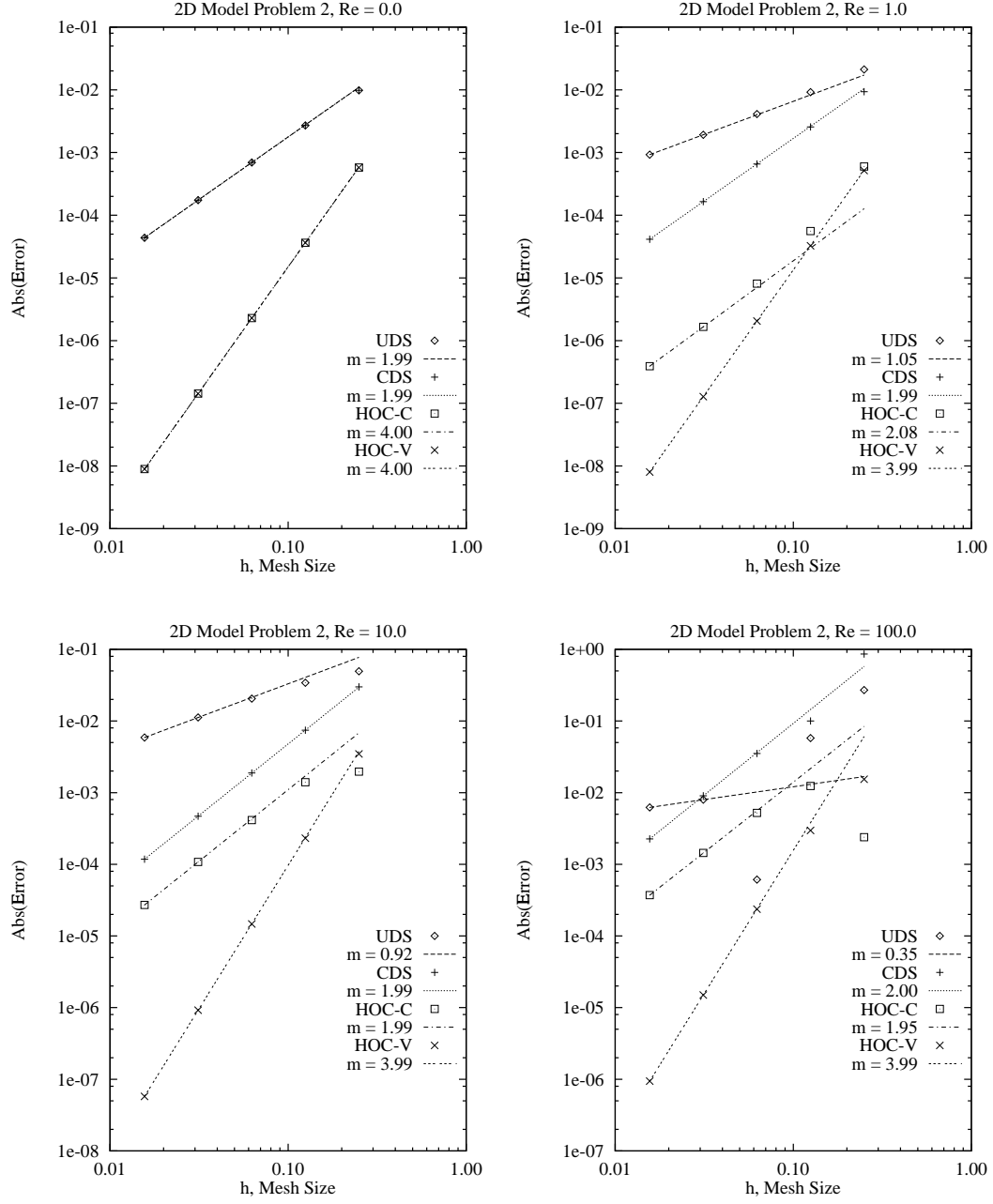


Figure 2.9: Convergence results for the 2D model problem 2, for $Re = 0, 1, 10$, and 100 .

we immediately obtain an $O(h^4)$ compact formula. However, this simplification allows (under certain conditions) even higher-order accuracy than we have previously obtained. In fact, an $O(h^6)$ finite-difference stencil was reported as early as 1967 by van de Vooren [140] for the 2D Laplace equation. In the present section we extend this result to include non-zero forcing functions. The simplification of ignoring convection will also provide a simple starting place for the study of the HOC scheme applied to 3D and nonlinear problems such as those encountered in reaction-diffusion applications. These are addressed in Sections 6.5 and 6.6.

Consider the Poisson equation,

$$-\nabla^2 \phi = f, \quad (2.32)$$

on some domain Ω with appropriate boundary conditions on $\partial\Omega$. The central difference scheme for (2.32) in 2D follows from (2.22) by setting convection coefficients $c = d = 0$ to obtain

$$-\delta_x^2 \phi_{ij} - \delta_y^2 \phi_{ij} - \tau_{ij} = f_{ij}, \quad (2.33)$$

where

$$\tau_{ij} = -\frac{h^2}{12} \left[\frac{\partial^4 \phi}{\partial x^4} + \frac{\partial^4 \phi}{\partial y^4} \right]_{ij} - \frac{h^4}{360} \left[\frac{\partial^6 \phi}{\partial x^6} + \frac{\partial^6 \phi}{\partial y^6} \right]_{ij} + O(h^6). \quad (2.34)$$

We have included both $O(h^2)$ and $O(h^4)$ terms in (2.34) because we wish to approximate all of them in order to construct an $O(h^6)$ scheme.

To obtain compact approximations to the $O(h^2)$ terms in (2.34), we simply take the appropriate derivatives of (2.32),

$$\frac{\partial^4 \phi}{\partial x^4} = -\frac{\partial^2 f}{\partial x^2} - \frac{\partial^4 \phi}{\partial x^2 \partial y^2}, \quad (2.35)$$

$$\frac{\partial^4 \phi}{\partial y^4} = -\frac{\partial^2 f}{\partial y^2} - \frac{\partial^4 \phi}{\partial x^2 \partial y^2}, \quad (2.36)$$

Substituting (2.35) and (2.36) into (2.34) yields

$$\tau_{ij} = \frac{h^2}{12} \left[\nabla^2 f_{ij} + 2 \frac{\partial^4 \phi}{\partial x^2 \partial y^2} \right]_{ij} - \frac{h^4}{360} \left[\frac{\partial^6 \phi}{\partial x^6} + \frac{\partial^6 \phi}{\partial y^6} \right]_{ij} + O(h^6). \quad (2.37)$$

We can easily get an $O(h^4)$ method in the same way as before by substituting difference expressions for the $O(h^2)$ terms in (2.37) and including these in the finite difference approximation (2.33). The resulting higher-order scheme follows from

$$-\delta_x^2 \phi_{ij} - \delta_y^2 \phi_{ij} - \frac{h^2}{6} \delta_x^2 \delta_y^2 \phi_{ij} + O(h^4) = f_{ij} + \frac{h^2}{12} [\delta_x^2 f_{ij} + \delta_y^2 f_{ij}]. \quad (2.38)$$

We can, however, obtain an $O(h^6)$ scheme for this governing equation. Note that the approximation to the cross derivative of ϕ in (2.37) introduces additional $O(h^4)$ terms that we must be careful to include in our derivation of an $O(h^6)$ scheme. More specifically, substituting the finite difference expressions for the cross derivative of ϕ and its truncation error terms into (2.37) gives us

$$\begin{aligned} \tau_{ij} = & \frac{h^2}{12} [\nabla^2 f_{ij} + 2\delta_x^2 \delta_y^2 \phi_{ij}] - \\ & \frac{h^4}{360} \left[\frac{\partial^6 \phi}{\partial x^6} + 5 \frac{\partial^6 \phi}{\partial x^4 \partial y^2} + 5 \frac{\partial^6 \phi}{\partial x^2 \partial y^4} + \frac{\partial^6 \phi}{\partial y^6} \right]_{ij} + O(h^6), \end{aligned} \quad (2.39)$$

Clearly, to get a *compact* $O(h^6)$ approximation, we require compact expressions for the four derivatives of order 6 in (2.39). This can actually be done by further differentiating (2.32). The required expressions are

$$\frac{\partial^6 \phi}{\partial x^6} = -\frac{\partial^4 f}{\partial x^4} - \frac{\partial^6 \phi}{\partial x^4 \partial y^2}, \quad (2.40)$$

$$\frac{\partial^6 \phi}{\partial y^6} = -\frac{\partial^4 f}{\partial y^4} - \frac{\partial^6 \phi}{\partial x^2 \partial y^4}, \quad (2.41)$$

and

$$\frac{\partial^6 \phi}{\partial x^4 \partial y^2} + \frac{\partial^6 \phi}{\partial x^2 \partial y^4} = -\frac{\partial^4 f}{\partial x^2 \partial y^2}, \quad (2.42)$$

The key here is that we can use (2.40)–(2.42) to algebraically eliminate all the

derivatives of ϕ . The 2D, $O(h^6)$ compact approximation¹ to (2.32) is therefore

$$-\delta_x^2 \phi_{ij} - \delta_y^2 \phi_{ij} - \frac{h^2}{6} \delta_x^2 \delta_y^2 \phi_{ij} + O(h^6) = f_{ij} + \frac{h^2}{12} \nabla^2 f_{ij} + \frac{h^4}{360} \left[\nabla^4 f + 2 \frac{\partial^4 f}{\partial x^2 \partial y^2} \right]_{ij}, \quad (2.43)$$

where ∇^4 is the biharmonic operator.

We have previously verified the $O(h^4)$ theory for diffusion *and* convection, including one case where $Re = 0$, so numerical studies of that formulation would be redundant. The $O(h^6)$ results have been verified in the literature [140] for $f = 0$, leaving only the $O(h^6)$ theory for $f \neq 0$ unverified. However, in Section 6.6 we extend the treatment to 3D and provide supporting numerical experiments, and the 3D theory contains the 2D theory as a special case.

2.6 Summary

In this chapter, we have provided a framework for HOC theory for 1D and 2D convection diffusion with variable convection coefficients on uniform grids. The 1D, homogeneous, constant coefficient case was demonstrated to be non-oscillatory for all cell-Peclet numbers. The predicted $O(h^4)$ convergence rates were verified for 1D and 2D cases, including the variable coefficient case in 2D. Also, a new $O(h^6)$ HOC formula for the Poisson equation was developed for the case when the fourth derivatives of the source term are known or can be approximated to sufficient accuracy.

¹If we compute the matrix coefficients from the left-hand side of (2.43) or (2.38), we see that they are the same as the coefficients published by van de Vooren [140] for the $O(h^6)$ approximation to the Laplacian. Indeed, we see that (2.38) and (2.43) are the $O(h^6)$ approximation to the Laplacian, if we merely substitute $f = 0$. But we now have a sixth-order approximation for the Poisson equation as well, provided the indicated derivatives of f are known analytically or can be approximated to sufficient accuracy.

Chapter 3

Stream-Function Vorticity

3.1 Introduction

We now develop the HOC scheme for the stream-function vorticity form of the steady, incompressible, 2D Navier-Stokes equations. This form is desirable for a number of reasons. The three governing equations (continuity and vector momentum) in three unknowns (pressure and two velocity components) are reduced to two equations in two unknowns (stream function, ψ , and vorticity, ζ), with the pressure dropping out of the formulation. More importantly, the governing equations are composed of a coupled pair of transport equations to which our theory can be directly extended. There are also two auxiliary equations relating the velocities to the stream function that will have to be considered, as well as the boundary conditions, which are always a concern with the (ψ, ζ) formulation.

3.2 Governing Equations

For a non-dimensionalized velocity field $\mathbf{V} = u\hat{\mathbf{i}} + v\hat{\mathbf{j}}$, where $\hat{\mathbf{i}}$ and $\hat{\mathbf{j}}$ are unit vectors in the x and y directions, respectively, the stream function ψ may be defined to

within an arbitrary constant by

$$u = \frac{\partial \psi}{\partial y}, \quad (3.1)$$

$$v = -\frac{\partial \psi}{\partial x}. \quad (3.2)$$

The definition of ψ implies that the incompressible continuity condition is satisfied. The 2D scalar vorticity is defined as the signed magnitude of the curl of the velocity, $\zeta = \frac{\partial v}{\partial x} - \frac{\partial u}{\partial y}$, and implies from (3.1) and (3.2) that

$$-\nabla^2 \psi = \zeta. \quad (3.3)$$

Taking the curl of the 2D vector momentum equation, we obtain the scalar vorticity transport equation

$$-\nabla^2 \zeta + Re \mathbf{V} \cdot \nabla \zeta = f, \quad (3.4)$$

where f is a non-dimensional forcing function, and $Re = \frac{UL}{\nu}$ is the Reynolds number, with U a characteristic velocity, L a characteristic length scale, and ν the kinematic viscosity of the fluid.

For the purposes of this study, we will consider wall boundary conditions, as these present some difficulty in maintaining high-order accuracy. The definition of the stream function, (3.1) and (3.2), can be used to relate any velocity boundary conditions to the stream function. For a wall boundary moving tangentially to its surface with a constant velocity V_w , the no-slip, no-penetration condition becomes

$$\frac{\partial \psi}{\partial n} = \pm V_w, \quad (3.5)$$

$$\frac{\partial \psi}{\partial s} = 0, \quad (3.6)$$

where n is the direction normal to the wall, and s is tangent to the wall. The latter equation implies ψ is constant on the boundary. Transport equations (3.3) and (3.4), together with velocity relations (3.1) and (3.2), plus boundary conditions (3.5) and (3.6) complete the mathematical description of the fully coupled stream-function vorticity problem.

3.3 HOC Formulation

The HOC formulation for the stream-function equation (3.3) follows by substituting ψ for ϕ , and ζ for f in equation (2.38) to obtain

$$-\delta_x^2 \psi_{ij} - \delta_y^2 \psi_{ij} - \frac{h^2}{6} \delta_x^2 \delta_y^2 \psi_{ij} = \zeta_{ij} + \frac{h^2}{12} [\delta_x^2 \zeta_{ij} + \delta_y^2 \zeta_{ij}]. \quad (3.7)$$

Note that we do not know the fourth derivatives of ζ , so we cannot use the $O(h^6)$ expression (2.43).

The HOC approximation to the vorticity equation (3.4) is obtained by substituting ζ for ϕ , and setting $c = Re \cdot u$ and $d = Re \cdot v$ in equation (2.30). However, u and v are derived from ψ by (3.1) and (3.2) and therefore these equations should also be represented to sufficient order. For example,

$$\begin{aligned} u_{ij} &= \left. \frac{\partial \psi}{\partial y} \right|_{ij}, \\ &= \delta_y \psi_{ij} - \frac{h^2}{6} \left. \frac{\partial^3 \psi}{\partial y^3} \right|_{ij} + O(h^4), \end{aligned}$$

and using (3.3),

$$\begin{aligned} u_{ij} &= \delta_y \psi_{ij} - \frac{h^2}{6} \left[-\frac{\partial \zeta}{\partial y} - \frac{\partial^3 \psi}{\partial x^2 \partial y} \right]_{ij} + O(h^4), \\ &= \delta_y \psi_{ij} + \frac{h^2}{6} (\delta_y \zeta_{ij} + \delta_x^2 \delta_y \psi_{ij}) + O(h^4). \end{aligned} \quad (3.8)$$

Likewise, for the y component of the velocity (3.2),

$$v_{ij} = -\delta_x \psi_{ij} - \frac{h^2}{6} (\delta_x \zeta_{ij} + \delta_x \delta_y^2 \psi_{ij}) + O(h^4). \quad (3.9)$$

Neglecting the $O(h^4)$ terms in equations (3.8) and (3.9), we obtain the high-order compact approximations for the velocity components, u_{ij} and v_{ij} , to be used in the vorticity transport equation.

3.3.1 Boundary Conditions

We seek now to construct compact high-order formulas for wall boundary conditions. Let us first consider boundary condition (3.5), applied for convenience at a vertical

wall $x = 0$, so that the normal direction is simply the x -direction. For an arbitrary node (x_1, y_j) along this boundary, the given velocity is

$$\begin{aligned} v_{1j} &= -\left.\frac{\partial\psi}{\partial x}\right|_{1j}, \\ &= -\delta_x^+ \psi_{1j} + \frac{h}{2} \left.\frac{\partial^2\psi}{\partial x^2}\right|_{1j} + \frac{h^2}{6} \left.\frac{\partial^3\psi}{\partial x^3}\right|_{1j} + \frac{h^3}{24} \left.\frac{\partial^4\psi}{\partial x^4}\right|_{1j} + O(h^4), \end{aligned} \quad (3.10)$$

where δ_x^+ represents the forward difference operator in the x direction. Using (3.3), $\frac{\partial^2\psi}{\partial x^2}$ in (3.10) can be written as

$$\begin{aligned} \left.\frac{\partial^2\psi}{\partial x^2}\right|_{1j} &= -\zeta_{1j} - \left.\frac{\partial^2\psi}{\partial y^2}\right|_{1j}, \\ &= -\zeta_{1j}, \end{aligned}$$

where we have used the fact that $\frac{\partial^2\psi}{\partial y^2} = 0$ on a vertical wall. Furthermore,

$$\begin{aligned} \left.\frac{\partial^3\psi}{\partial x^3}\right|_{1j} &= -\left.\frac{\partial\zeta}{\partial x}\right|_{1j} - \left.\frac{\partial^3\psi}{\partial x\partial y^2}\right|_{1j}, \\ &= -\left.\frac{\partial\zeta}{\partial x}\right|_{1j} + \left.\frac{\partial^2v}{\partial y^2}\right|_{1j}, \\ &= -\left.\frac{\partial\zeta}{\partial x}\right|_{1j}, \end{aligned}$$

where we have used (3.2) to relate ψ and v and the fact that $\frac{\partial^2v}{\partial y^2}$ is also zero on a vertical wall. Finally,

$$\left.\frac{\partial^4\psi}{\partial x^4}\right|_{1j} = -\left.\frac{\partial^2\zeta}{\partial x^2}\right|_{1j} + \left.\frac{\partial^3v}{\partial x\partial y^2}\right|_{1j}.$$

Substituting these expressions into (3.10) yields

$$v_{1j} = -\delta_x^+ \psi_{1j} - \frac{h}{2} \zeta_{1j} - \frac{h^2}{6} \left.\frac{\partial\zeta}{\partial x}\right|_{1j} - \frac{h^3}{24} \left.\frac{\partial^2\zeta}{\partial x^2}\right|_{1j} + \frac{h^3}{24} \left.\frac{\partial^3v}{\partial x\partial y^2}\right|_{1j} + O(h^4). \quad (3.11)$$

A second-order compact approximation can be easily obtained by simply neglecting the third, fourth, and fifth terms on the right of (3.11). That is,

$$v_{1j} = -\delta_x^+ \psi_{1j} - \frac{h}{2} \zeta_{1j} + O(h^2), \quad (3.12)$$

and setting $v_{1j} = V_w$. However, this scheme will locally pollute the accuracy of the HOC solution near the boundary.

A third-order compact approximation can be obtained by utilizing a one-sided difference approximation for $\frac{\partial \zeta}{\partial x}$ in (3.11) so that

$$v_{1j} = -\delta_x^+ \psi_{1j} - \frac{h}{2} \zeta_{1j} - \frac{h^2}{6} \delta_x^+ \zeta_{1j} + O(h^3). \quad (3.13)$$

To obtain fourth-order accuracy in (3.11), we need three approximations at the wall: (1) an $O(h^2)$ approximation to $\frac{d\zeta}{dx}$; (2) an $O(h)$ approximation to $\frac{d^2\zeta}{dx^2}$; and (3) an $O(h)$ approximation to $\frac{\partial^3 v}{\partial x \partial y^2}$. The third requirement is the easiest, simply

$$\left. \frac{\partial^3 v}{\partial x \partial y^2} \right|_{1j} = \delta_x^+ \delta_y^2 v_{1j} + O(h). \quad (3.14)$$

Examining the terms involving $\frac{\partial \zeta}{\partial x}$ and $\frac{\partial^2 \zeta}{\partial x^2}$,

$$\begin{aligned} \frac{h^2}{6} \left. \frac{\partial \zeta}{\partial x} \right|_{1j} + \frac{h^3}{24} \left. \frac{\partial^2 \zeta}{\partial x^2} \right|_{1j} &= \frac{h^2}{6} \left[\delta_x^+ \zeta_{1j} - \frac{h}{2} \left. \frac{\partial^2 \zeta}{\partial x^2} \right|_{1j} + O(h^2) \right] + \frac{h^3}{24} \left. \frac{\partial^2 \zeta}{\partial x^2} \right|_{1j}, \\ &= \frac{h^2}{6} \delta_x^+ \zeta_{1j} - \frac{h^3}{24} \left. \frac{\partial^2 \zeta}{\partial x^2} \right|_{1j} + O(h^4), \end{aligned} \quad (3.15)$$

and using (3.4) we can write

$$\begin{aligned} \left. \frac{\partial^2 \zeta}{\partial x^2} \right|_{1j} &= Re \cdot u_{1j} \left. \frac{\partial \zeta}{\partial x} \right|_{1j} + Re \cdot v_{1j} \left. \frac{\partial \zeta}{\partial y} \right|_{1j} - \left. \frac{\partial^2 \zeta}{\partial y^2} \right|_{1j} - f_{1j}, \\ &= \left[Re \cdot v_{1j} \delta_y \zeta_{1j} - \delta_y^2 \zeta_{1j} \right] - f_{1j} + O(h^2), \end{aligned} \quad (3.16)$$

where we have used the fact that $u_{1j} = 0$. Applying (3.14)–(3.16) in (3.11), the complete, fourth-order, compact approximation to the boundary condition is therefore

$$\begin{aligned} -\delta_x^+ \psi_{1j} - \frac{h}{2} \zeta_{1j} - \frac{h^2}{6} \delta_x^+ \zeta_{1j} + \frac{h^3}{24} \left(Re \cdot v_{1j} \delta_y \zeta_{1j} - \delta_y^2 \zeta_{1j} \right) &= \\ v_{1j} - \frac{h^3}{24} \left(\delta_x^+ \delta_y^2 v_{1j} - f_{1j} \right) + O(h^4) \end{aligned} \quad (3.17)$$

Similar formulations can easily be derived for the remaining three walls of a rectangular cavity and are provided in Table 3.1.

Table 3.1: HOC $O(h^4)$ wall boundary conditions for a rectangular cavity with an $M \times N$ mesh in stream-function vorticity form.

Wall	Formula
Left	$-\delta_x^+ \psi_{1j} - \left[\frac{h}{2} + \frac{h^2}{6} \delta_x^+ - \frac{h^3}{24} (Re \cdot v_{1j} \delta_y - \delta_y^2) \right] \zeta_{1j} =$ $v_{1j} - \frac{h^3}{24} (\delta_x^+ \delta_y^2 v_{1j} - f_{1j})$
Right	$-\delta_x^- \psi_{Mj} + \left[\frac{h}{2} - \frac{h^2}{6} \delta_x^- - \frac{h^3}{24} (Re \cdot v_{Mj} \delta_y - \delta_y^2) \right] \zeta_{Mj} =$ $v_{Mj} + \frac{h^3}{24} (\delta_x^- \delta_y^2 v_{Mj} - f_{Mj})$
Top	$\delta_y^- \psi_{iN} - \left[\frac{h}{2} - \frac{h^2}{6} \delta_y^- - \frac{h^3}{24} (Re \cdot u_{iN} \delta_x - \delta_x^2) \right] \zeta_{iN} =$ $u_{iN} + \frac{h^3}{24} (\delta_x^2 \delta_y^- u_{iN} + f_{iN})$
Bottom	$\delta_y^+ \psi_{i1} + \left[\frac{h}{2} + \frac{h^2}{6} \delta_y^+ - \frac{h^3}{24} (Re \cdot u_{i1} \delta_x - \delta_x^2) \right] \zeta_{i1} =$ $u_{i1} - \frac{h^3}{24} (\delta_x^2 \delta_y^+ u_{i1} + f_{i1})$

Boundary conditions at the corners are handled in a similar manner. The restricted geometry at the corners prevents the derivation of a fourth-order compact formula, but a third-order approximation is possible. For example, at the upper left corner (x_1, y_M) , we can approximate (3.5) in both the horizontal and vertical directions. Summing these results and replacing high-order terms with appropriate difference expressions, we obtain

$$\begin{aligned} \frac{h}{2} \zeta_{1N} + \frac{h^2}{6} [\delta_x^+ \zeta_{1N} - \delta_y^- \zeta_{1N}] &= - [\delta_x^+ \psi_{1N} + \delta_y^- \psi_{1N}] - \\ &u_{1N} - v_{1N} - \frac{h^2}{6} [\delta_x^+ \delta_y^- u_{1N} + \delta_x^+ \delta_y^- v_{1N}] + O(h^3), \end{aligned} \quad (3.18)$$

where N is the index of nodes along $y = 1$. A complete list of all $O(h^3)$ corner boundary conditions is given in Table 3.2.

A second-order corner formula, the lowest-order approximation of (3.5) that still involves the vorticity, can be obtained by dropping the $O(h^2)$ terms from (3.18):

$$\frac{h}{2} \zeta_{1N} = - [\delta_x^+ \psi_{1N} + \delta_y^+ \psi_{1N}] - u_{1N} - v_{1N} + O(h^2).$$

Note that when $\psi = 0$ on the boundary, this reduces to

$$\frac{h}{2} \zeta_{1N} = -u_{1N} - v_{1N} + O(h^2),$$

Table 3.2: HOC $O(h^3)$ corner boundary conditions for a rectangular $M \times N$ cavity in stream-function vorticity form.

Corner	Formula
Lower left	$\left[\delta_x^+ + \delta_y^+ \right] \psi_{11} + \frac{h}{2} \zeta_{11} + \frac{h^2}{6} \left[\delta_x^+ + \delta_y^+ \right] \zeta_{11} =$ $u_{11} - v_{11} - \frac{h^2}{6} \left[\delta_x^+ \delta_y^+ u_{11} - \delta_x^+ \delta_y^+ v_{11} \right]$
Lower right	$- \left[\delta_x^- - \delta_y^+ \right] \psi_{M1} + \frac{h}{2} \zeta_{M1} - \frac{h^2}{6} \left[\delta_x^- - \delta_y^+ \right] \zeta_{M1} =$ $u_{M1} + v_{M1} + \frac{h^2}{6} \left[\delta_x^- \delta_y^+ u_{M1} + \delta_x^- \delta_y^+ v_{M1} \right]$
Upper left	$\left[\delta_x^+ - \delta_y^- \right] \psi_{1N} + \frac{h}{2} \zeta_{1N} + \frac{h^2}{6} \left[\delta_x^+ - \delta_y^- \right] \zeta_{1N} =$ $-u_{1N} - v_{1N} - \frac{h^2}{6} \left[\delta_x^+ \delta_y^- u_{1N} - \delta_x^+ \delta_y^- v_{1N} \right]$
Upper right	$- \left[\delta_x^- + \delta_y^- \right] \psi_{MN} + \frac{h}{2} \zeta_{MN} - \frac{h^2}{6} \left[\delta_x^- + \delta_y^- \right] \zeta_{MN} =$ $-u_{MN} + v_{MN} + \frac{h^2}{6} \left[\delta_x^- \delta_y^- u_{MN} - \delta_x^- \delta_y^- v_{MN} \right]$

which reduces even further to $\zeta_{1N} = 0$ when the wall velocities are zero.

3.3.2 Coupled and Decoupled Forms

Solution to the nonlinear problem proceeds by iteration. Let us consider a typical iterative step. The current iterates are given by the solution at the previous step. Using these current iterates in a successive approximation scheme, we can compute higher-order compact approximations to the velocities from (3.8) and (3.9). Using this result in (2.30) with $c = Re \cdot u$, $d = Re \cdot v$ to approximate the vorticity transport equation (3.4), we obtain the HOC approximation at the interior nodes:

$$\tilde{\mathbf{C}}^{(n)} \boldsymbol{\zeta} = \tilde{\mathbf{F}}^{(n)}, \quad (3.19)$$

where $\tilde{\mathbf{C}}^{(n)}$ represents the HOC matrix for (3.4) and $\tilde{\mathbf{F}}^{(n)}$ is the current HOC forcing vector. Note that $\tilde{\mathbf{C}}^{(n)}$ is not a square matrix; it has only as many rows as there are interior grid points. The remaining HOC equations at the boundary nodes follow from our choice of (3.12), (3.13), or (3.17). Similarly, let \mathbf{L} and $\tilde{\mathbf{L}}$ be the non-square CDS and HOC matrices for the Laplacian that correspond to the interior nodes.

The HOC matrix representation of (3.7) at the interior nodes is therefore

$$\tilde{\mathbf{L}}\boldsymbol{\psi} + \left[\mathbf{I} + \frac{h^2}{12}\mathbf{L} \right] \boldsymbol{\zeta} = \mathbf{0}. \quad (3.20)$$

Finally, the boundary conditions (3.5) and (3.6) may be expressed

$$\mathbf{N}\boldsymbol{\psi} + \mathbf{B}\boldsymbol{\zeta} = \tilde{\mathbf{U}}^{(n)}, \quad (3.21)$$

and

$$\boldsymbol{\psi}_B = \mathbf{0}, \quad (3.22)$$

where \mathbf{N} is the “normal derivative” matrix, \mathbf{B} is the vorticity boundary matrix, $\tilde{\mathbf{U}}^{(n)}$ is the current HOC velocity term, and the subscript B refers to boundary points only. (Similarly, the subscript I will refer to interior points in the block matrix notation.)

In the coupled algorithm, the current values of $\boldsymbol{\psi}$ and $\boldsymbol{\zeta}$ are computed simultaneously. For conceptual clarity, let us split $\boldsymbol{\psi}$ and $\boldsymbol{\zeta}$ into two parts, one containing only interior data, one containing only boundary data. The values at a successive approximate iterate $(n+1)$ are thus computed by solving (3.19)–(3.22) concurrently,

$$\begin{bmatrix} \tilde{\mathbf{L}}_{II} & \tilde{\mathbf{L}}_{IB} & \mathbf{I} + \frac{h^2}{12}\mathbf{L}_{II} & \frac{h^2}{12}\mathbf{L}_{IB} \\ \mathbf{O} & \mathbf{I} & \mathbf{O} & \mathbf{O} \\ \mathbf{O} & \mathbf{O} & \tilde{\mathbf{C}}_{II}^{(n)} & \tilde{\mathbf{C}}_{IB}^{(n)} \\ \mathbf{N}_{II} & \mathbf{N}_{IB} & \mathbf{B}_{IB} & \mathbf{B}_{BB} \end{bmatrix} \begin{bmatrix} \boldsymbol{\psi}_I \\ \boldsymbol{\psi}_B \\ \boldsymbol{\zeta}_I \\ \boldsymbol{\zeta}_B \end{bmatrix}^{(n+1)} = \begin{bmatrix} \mathbf{0} \\ \mathbf{0} \\ \tilde{\mathbf{F}} \\ \tilde{\mathbf{U}} \end{bmatrix}^{(n)}, \quad (3.23)$$

where $\tilde{\mathbf{L}}$, \mathbf{L} , $\tilde{\mathbf{C}}$, \mathbf{N} , and \mathbf{B} have been partitioned into sub-matrices corresponding to interior and boundary components. We emphasize that the last row represents (3.5), the normal derivative boundary condition on ψ . For the case $Re = 0$ (Stokes flow), the matrix $\tilde{\mathbf{C}}^{(n)}$ is constant and for $O(h^2)$ or $O(h^3)$ wall BCs the vector $\tilde{\mathbf{U}}^{(n)}$ is constant so these problem are linear and the system (3.23) is solved only once.

The decoupled algorithm is simply a block iterative form of the coupled algorithm. We solve for the stream function and vorticity separately by lagging the

appropriate terms:

$$\begin{aligned} \begin{bmatrix} \tilde{\mathbf{L}}_{II} & \tilde{\mathbf{L}}_{IB} \\ \mathbf{O} & \mathbf{I} \end{bmatrix} \begin{bmatrix} \psi_I \\ \psi_B \end{bmatrix}^{(n+1)} &= - \begin{bmatrix} \mathbf{I} + \frac{h^2}{12} \mathbf{L}_{II} & \frac{h^2}{12} \mathbf{L}_{IB} \\ \mathbf{O} & \mathbf{O} \end{bmatrix} \begin{bmatrix} \zeta_I \\ \zeta_B \end{bmatrix}^{(n)}, \\ \begin{bmatrix} \tilde{\mathbf{C}}_{II}^{(n)} & \tilde{\mathbf{C}}_{IB}^{(n)} \\ \mathbf{B}_{IB} & \mathbf{B}_{BB} \end{bmatrix} \begin{bmatrix} \zeta_I \\ \zeta_B \end{bmatrix}^{(n+1)} &= - \begin{bmatrix} \mathbf{O} & \mathbf{O} \\ \mathbf{N}_{II} & \mathbf{N}_{IB} \end{bmatrix} \begin{bmatrix} \psi_I \\ \psi_B \end{bmatrix}^{(n+1)} + \begin{bmatrix} \tilde{\mathbf{F}} \\ \tilde{\mathbf{U}} \end{bmatrix}^{(n)}. \end{aligned}$$

Note that we have not changed the equations that model the system, but only the procedure by which the successive approximations are defined. The bottom row in the second matrix problem *looks* like a vorticity boundary condition, but in reality it is not. It is a *stream function* boundary condition, in which the vorticity only serves to model higher-order terms.

All of the numerical experiments in the section that follows are computed using the decoupled algorithm, with the added provision that successive iterates may be under-relaxed to prevent divergence. That is to say, if ψ' is the stream function computed from the first half of the decoupled algorithm, then ψ^{n+1} is given by

$$\psi^{n+1} = \omega \psi' + (1 - \omega) \psi^n,$$

where $0 \leq \omega \leq 1$ is the relaxation factor.

3.4 Numerical Results

We now verify the HOC formulation of the (ψ, ζ) equations with a model problem with known analytic solution, as well as the lid-driven cavity problem, entrance flow into a cascade of thin plates, and the backward-facing step problem.

3.4.1 Model Problem Results

To construct a test problem with known solution we specify the stream-function

$$\psi = -8(x - x^2)^2(y - y^2)^2,$$

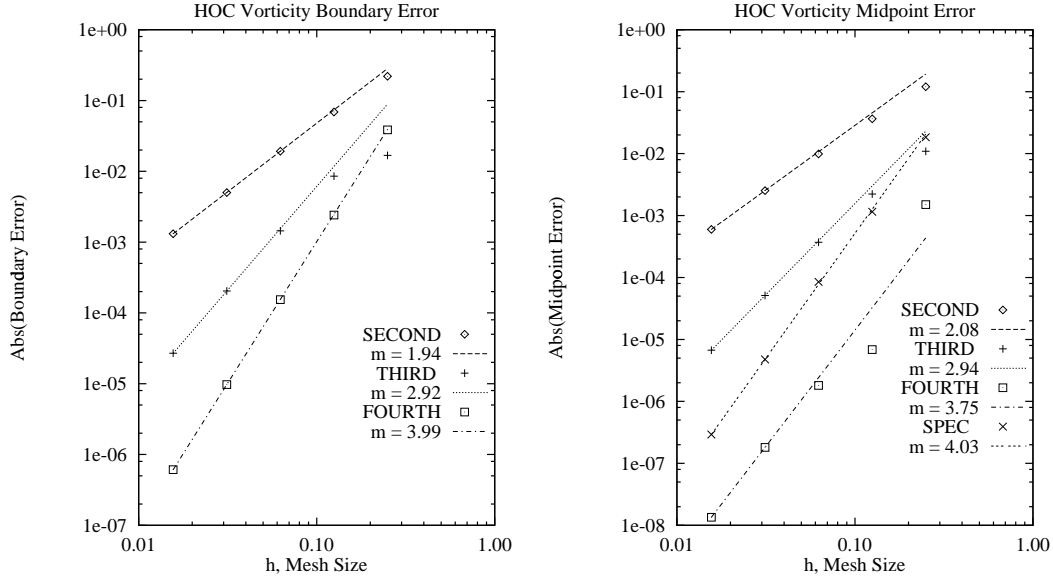


Figure 3.1: HOC vorticity error convergence plots on the boundary and at the midpoint for the model problem with $Re = 0$.

on the unit square. The corresponding vorticity solution, derived from equation (3.3), is

$$\zeta = 16[(6x^2 - 6x + 1)(y - y^2)^2 + (x - x^2)^2(6y^2 - 6y + 1)],$$

and the velocities, derived from (3.1) and (3.2), are

$$\begin{aligned} u &= -16(x - x^2)^2(y - y^2)(1 - 2y), \\ v &= 16(x - x^2)(1 - 2x)(y - y^2)^2. \end{aligned}$$

This problem was designed such that the no-slip, no-penetration condition holds for the velocities u and v on the boundary. The problem is driven by the forcing function f , which is constructed by substituting the above functions ζ , u and v in (3.4). In the following numerical test we solve the linear Stokes flow problem, $Re = 0$, to better isolate the effect of the choice of boundary conditions. The fourth-order scheme is applied in the interior and each of the boundary treatments is compared. In Figure 3.1 the vorticity error at a representative boundary point ($x = 0.5$, $y = 0$),

and at the midpoint ($x = y = 0.5$) are graphed for a succession of meshes and for each of the implementations of the boundary conditions discussed: $O(h^2)$ boundary conditions are labeled “SECOND” in the plots, $O(h^3)$ boundary conditions are labeled “THIRD,” and $O(h^4)$ boundary conditions are labeled “FOURTH.” Results for the case where we use our knowledge of ζ to provide specified boundary conditions (labeled “SPEC”) are also included for the vorticity error at the midpoint. The experimental asymptotic convergence rate m of the error E at the stated points is computed by using the results for the meshes $h = \frac{1}{32}$, $h = \frac{1}{64}$, and is included in the plot.

Figures 3.2 and 3.3 are surface and contour plots of the HOC stream function and vorticity on a 17×17 grid. They are visually indistinguishable from the exact surface and contour plots.

The boundary error plot indicates that the rates of convergence are as predicted by the boundary condition formulas. This verifies our interpretation of the boundary condition we use as that of the *stream function*. These rates of convergence are maintained on the interior. It is interesting to note that the $O(h^4)$ boundary conditions result in smaller errors at the midpoint than do specified exact boundary conditions using the known vorticity function.

3.4.2 Driven Cavity Results

The lid-driven cavity flow (described in Figure 3.4) is a standard test case for Navier-Stokes computations, and there are numerous published results that can be used for comparison purposes. However, this problem is complicated by the presence of two corner singularities [49]. We consider the unit cavity $\Omega = [0, 1] \times [0, 1]$ with horizontal lid velocity $u = 1, v = 0$. On the remaining sides $u = v = 0$.

Table 3.3 is a short description of the results for HOC driven cavity runs for selected combinations of Re , grid size, side boundary condition accuracy, and corner boundary condition accuracy. For Stokes flow ($Re = 0$), the most accu-

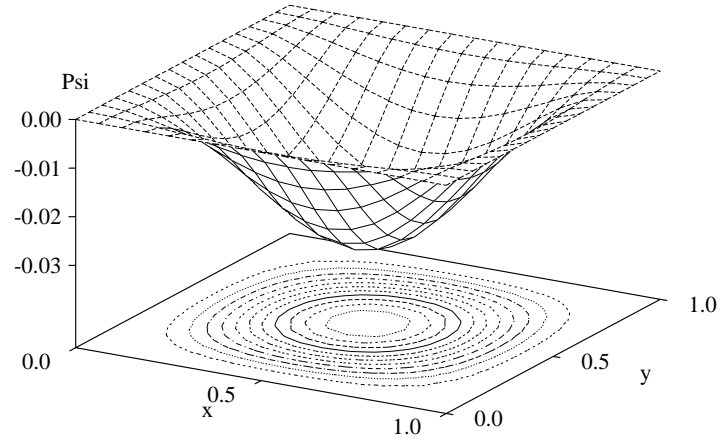


Figure 3.2: Surface and contour plot of the HOC stream function solution for the analytic model problem.

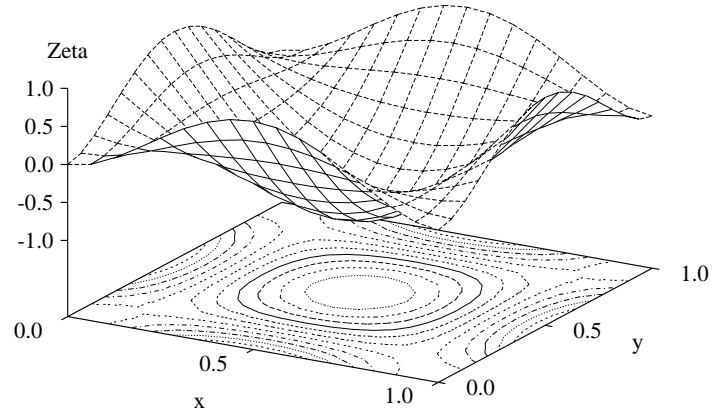


Figure 3.3: Surface and contour plot of the HOC vorticity solution for the analytic model problem.

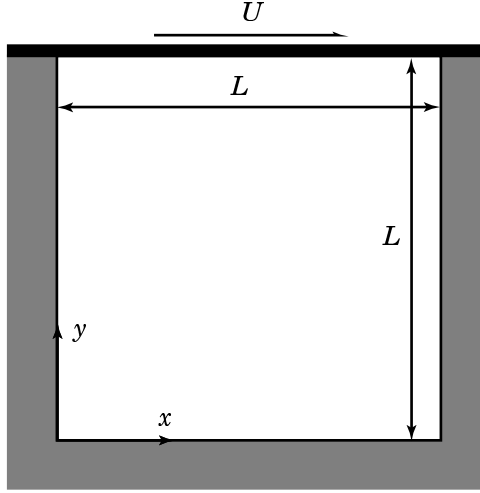


Figure 3.4: Problem description for the lid-driven cavity.

rate combination of boundary conditions produces good results at a grid as coarse as 11×11 .

However, for convection-dominated cases, we see that this combination of boundary conditions results in oscillations on coarse grids. When the corner boundary condition accuracy is reduced from $O(h^3)$ to $O(h^2)$, the magnitude of oscillations drops, indicating that the singularities are better represented by low-order approximations. Nevertheless, oscillations persist for this combination of boundary conditions, probably due to the convective component of the fourth-order side boundary condition. When we reduce the accuracy of the side boundary conditions from $O(h^4)$ to $O(h^3)$, these oscillations disappear, even on coarse grids. However, this pollutes the accuracy of the solution on the interior slightly.

Returning to Stokes flow, contours for ψ and ζ obtained from the HOC solution on a uniform 31×31 grid are shown in Figure 3.5. Next in Figures 3.6–3.8, for $Re = 100$ the vorticity along the moving wall, the horizontal velocity u along the vertical centerline and the vertical velocity v along the horizontal centerline are compared with the fine grid results of Ghia, *et al.* [43]. These HOC results are for a 21×21 grid and are comparable to the results from a 129×129 fine grid in [43].

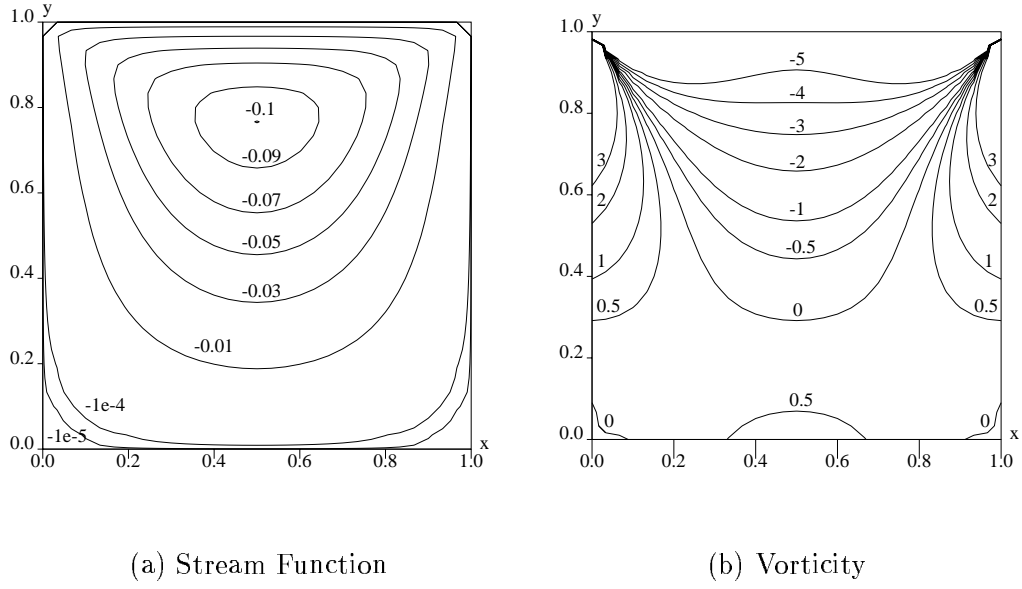


Figure 3.5: HOC driven cavity contours of the stream function and vorticity for $Re = 0$ on a 31×31 grid.

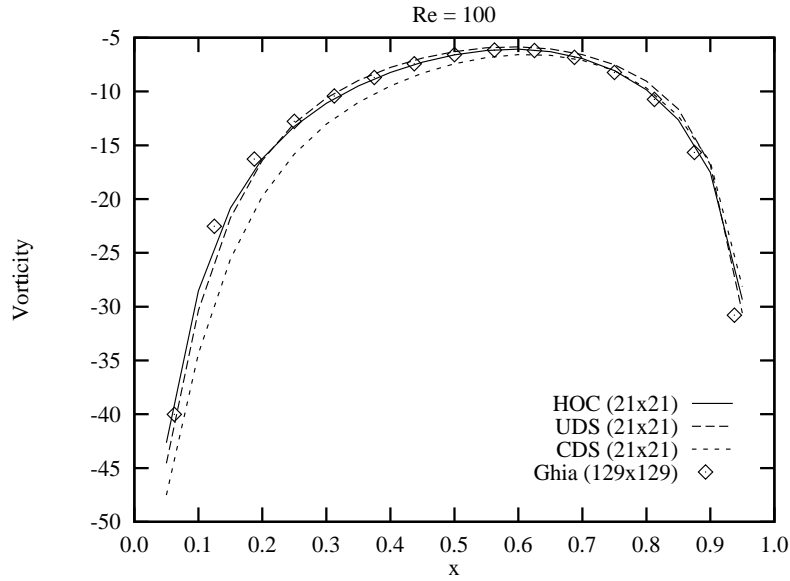


Figure 3.6: Driven cavity results for the vorticity along the moving wall, $Re = 100$. Note: results utilize $O(h^3)$ wall boundary conditions and $O(h^2)$ corner boundary conditions.

Table 3.3: Qualitative HOC driven cavity results for selected Re , grid size, and boundary conditions.

Re	Grid	Side BCs	Corner BCs	Comments
0	6×6	$O(h^4)$	$O(h^3)$	Very coarse, but no oscillations
0	11×11	$O(h^4)$	$O(h^3)$	Better resolution of flow features
100	11×11	$O(h^4)$	$O(h^3)$	Large oscillations in ζ on moving wall
100	11×11	$O(h^4)$	$O(h^2)$	Smaller oscillations in ζ on moving wall
100	11×11	$O(h^3)$	$O(h^2)$	No oscillations, but corner separation bubble is not resolved
100	21×21	$O(h^3)$	$O(h^2)$	No oscillations, accurate solutions, corner bubble appears
400	31×31	$O(h^4)$	$O(h^3)$	Large oscillations in ζ on moving wall
400	31×31	$O(h^4)$	$O(h^2)$	Very slight oscillations in ζ on moving wall
400	31×31	$O(h^3)$	$O(h^2)$	No oscillations, both corner separation bubbles resolved
400	41×41	$O(h^4)$	$O(h^2)$	Slight oscillations in ζ on moving wall (more than 31×31)
1000	31×31	$O(h^4)$	$O(h^3)$	Iterations stagnate
1000	41×41	$O(h^4)$	$O(h^3)$	Iterations stagnate
1000	41×41	$O(h^4)$	$O(h^2)$	Oscillations in ζ on moving wall
1000	41×41	$O(h^3)$	$O(h^2)$	No oscillations, good accuracy

Figures 3.9–3.11 are the same type of plots for the case $Re = 400$ on a 31×31 grid. Our results for this case also agree closely with the HOC primitive variable results in MacKinnon and Johnson [90] at this Reynolds number and grid size.

Figure 3.12 shows the HOC vorticity along the four borders of the cavity at $Re = 1000$, 41×41 grid, $O(h^4)$ side boundary conditions and $O(h^2)$ corner boundary conditions. Note that the vorticity oscillates along the moving wall, but not along the stationary walls, indicating that the oscillations are probably due to convection terms in the fourth-order boundary condition. Interestingly, these oscillations do not propagate into the interior.

We see from Figure 3.13 that decreasing the side boundary condition accu-

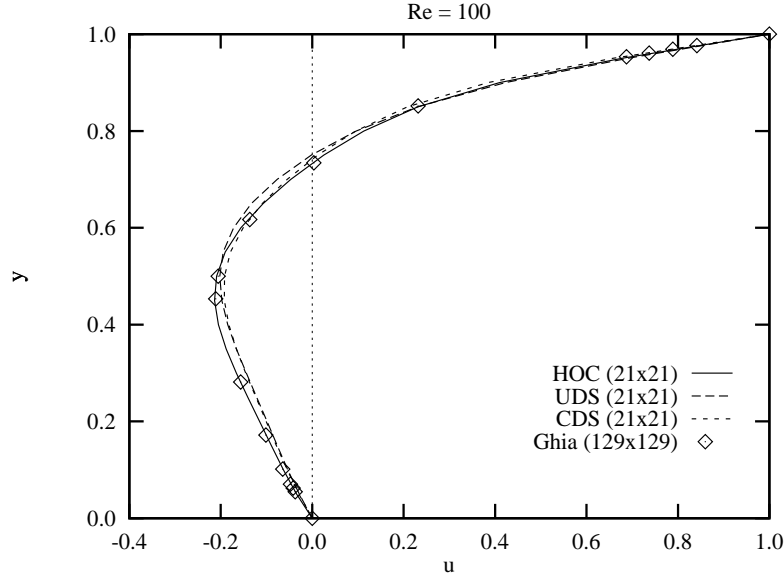


Figure 3.7: Driven cavity results for the horizontal velocity component along the vertical centerline, $Re = 100$. Note: results utilize $O(h^3)$ wall boundary conditions and $O(h^2)$ corner boundary conditions.

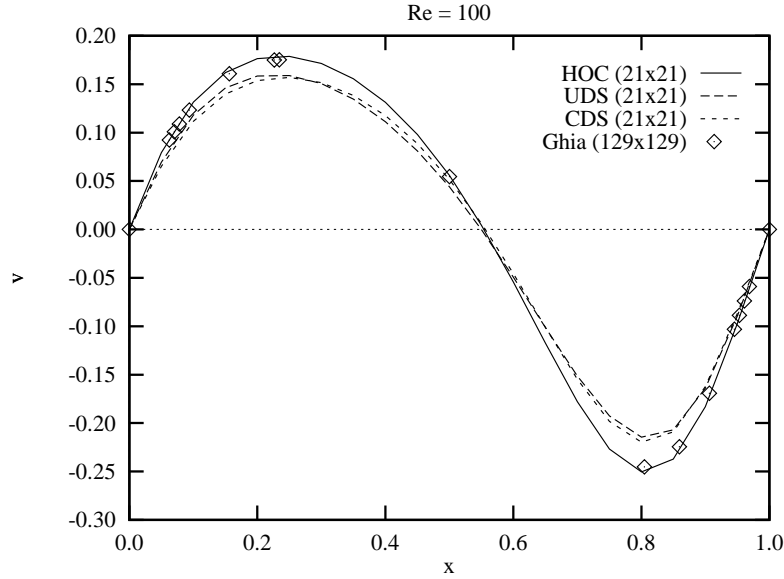


Figure 3.8: Driven cavity results for the vertical velocity component along the horizontal centerline, $Re = 100$. Note: results utilize $O(h^3)$ wall boundary conditions and $O(h^2)$ corner boundary conditions.

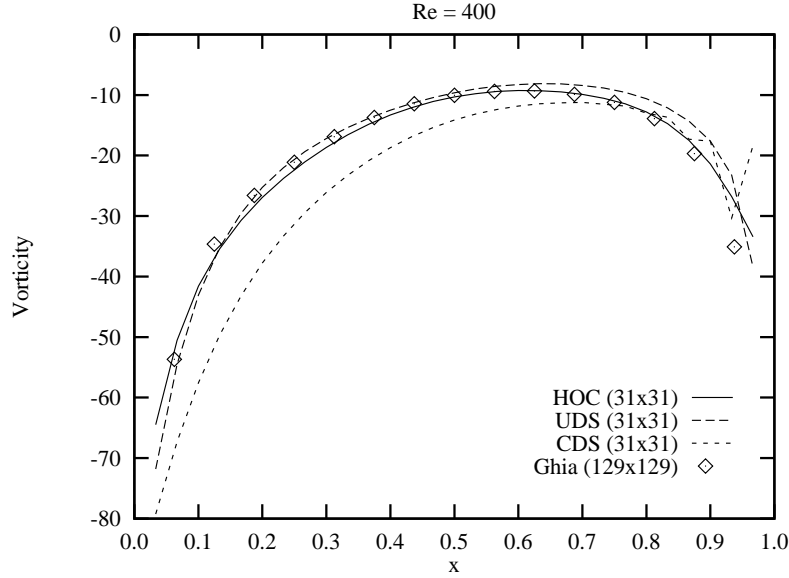


Figure 3.9: Driven cavity results for the vorticity along the moving wall, $Re = 400$. Note: results utilize $O(h^3)$ wall boundary conditions and $O(h^2)$ corner boundary conditions.

racy from $O(h^4)$ to $O(h^3)$ eliminates the oscillations and still results in a reasonably accurate approximation. The comparison to UDS is even more striking for the velocity components along the cavity centerlines, shown in Figures 3.14 and 3.15. The CDS solutions for this case suffer large-amplitude oscillations and are not included in the plots.

3.4.3 Cascading Plates Results

Another standard test problem for Navier-Stokes flows is the cascading plates model problem, considered first by Wang and Longwell [145] in 1964 and later by Panton [109]. Consider a cascade of semi-infinite thin plates in a fluid with kinematic viscosity ν separated by a distance $2L$ as depicted in Figure 3.16. A coordinate system is placed along the centerline of one channel with the origin aligned with the leading edge of the plates. Far upstream, the flow is uniform with velocity U . We assume that the flow pattern has the same symmetry as the problem geometry and

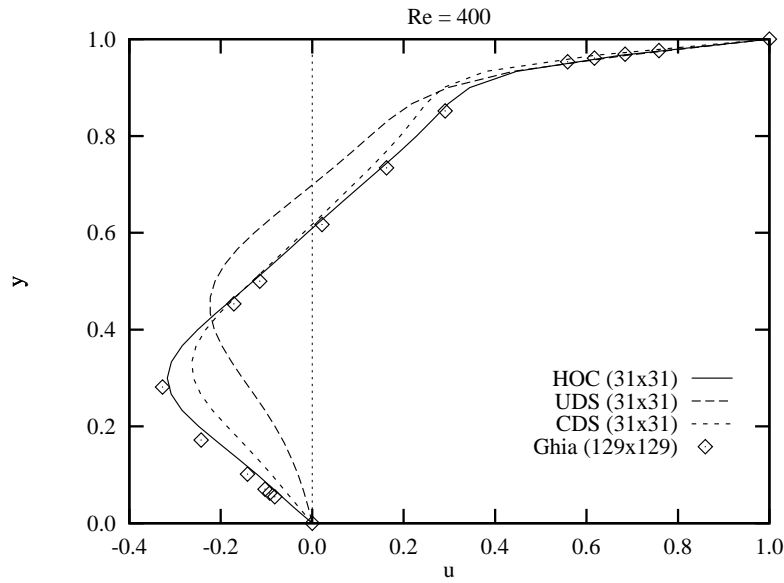


Figure 3.10: Driven cavity results for the horizontal velocity component along the vertical centerline, $Re = 400$. Note: results utilize $O(h^3)$ wall boundary conditions and $O(h^2)$ corner boundary conditions.

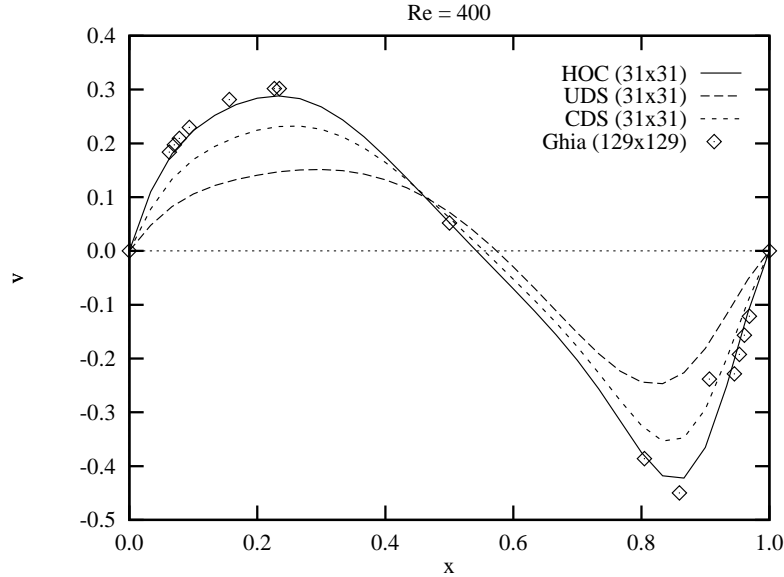


Figure 3.11: Driven cavity results for the vertical velocity component along the horizontal centerline, $Re = 400$. Note: results utilize $O(h^3)$ wall boundary conditions and $O(h^2)$ corner boundary conditions.

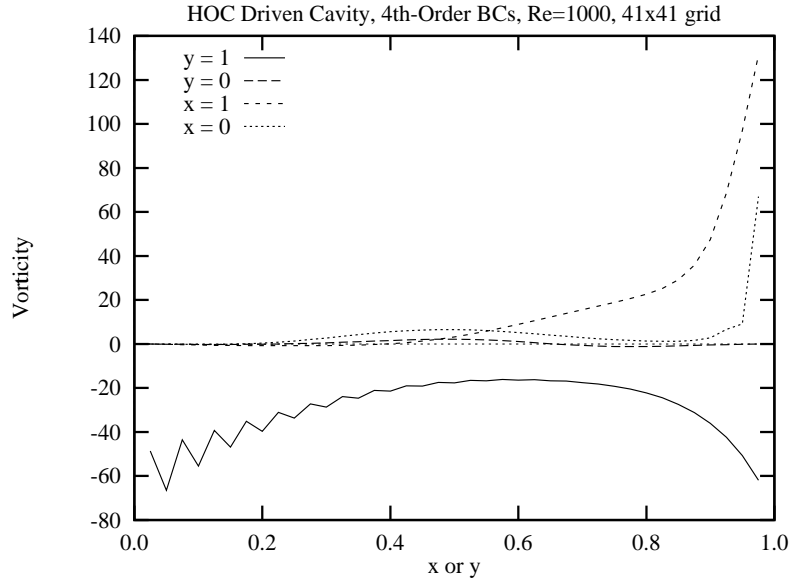


Figure 3.12: Vorticity on the four boundaries of the driven cavity problem for $Re = 1000$ and $O(h^4)$ boundary conditions.

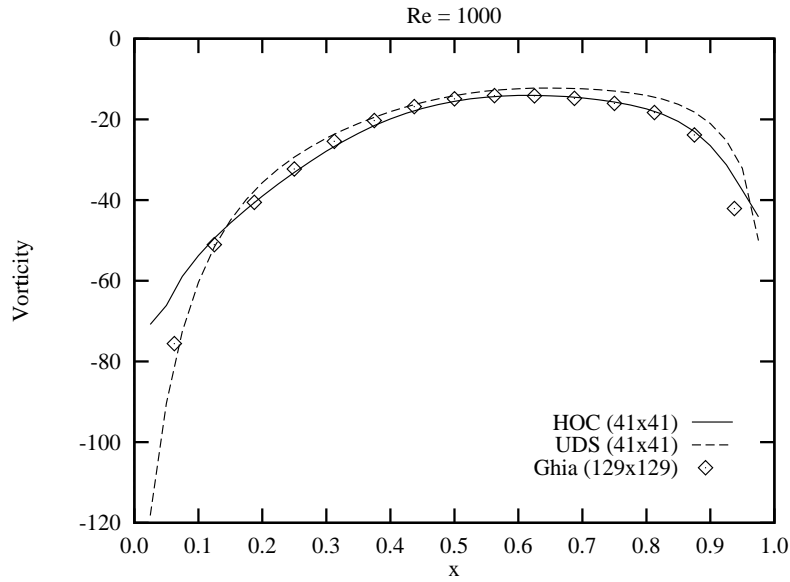


Figure 3.13: Driven cavity results for the vorticity along the moving wall, $Re = 1000$. Note: results utilize $O(h^3)$ wall boundary conditions and $O(h^2)$ corner boundary conditions.

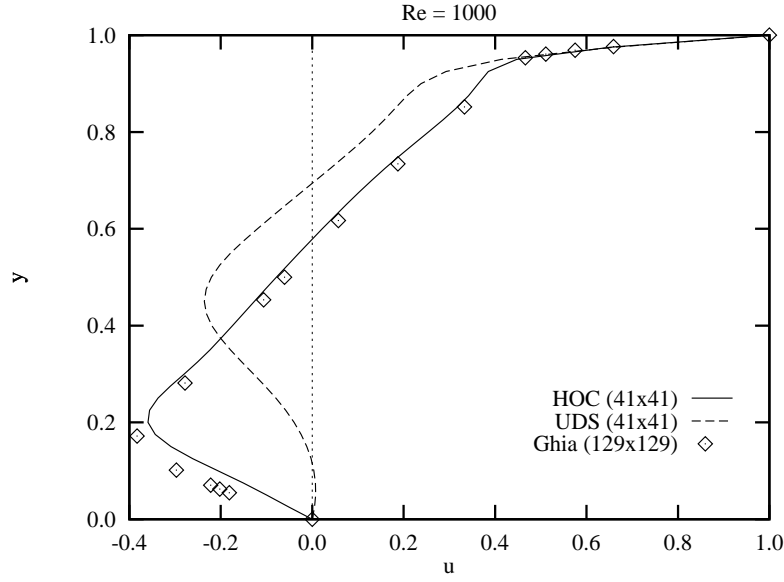


Figure 3.14: Driven cavity results for the horizontal velocity component along the vertical centerline, $Re = 1000$. Note: results utilize $O(h^3)$ wall boundary conditions and $O(h^2)$ corner boundary conditions.

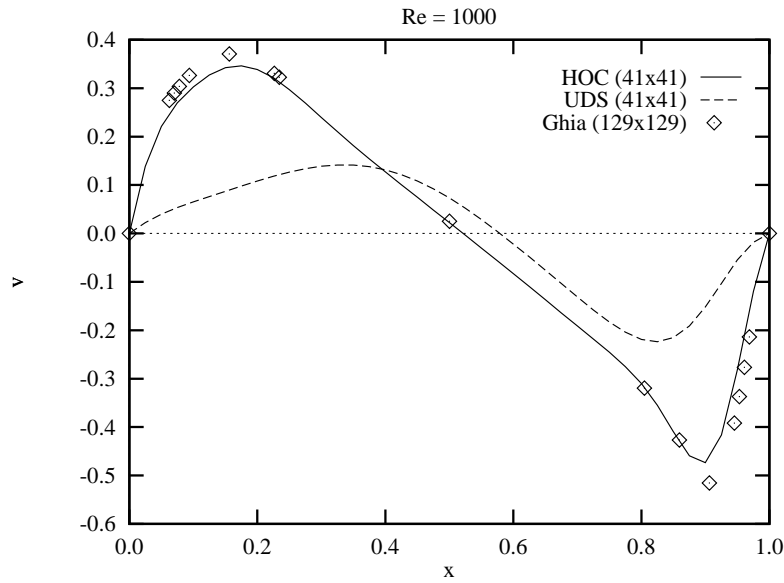


Figure 3.15: Driven cavity results for the vertical velocity component along the horizontal centerline, $Re = 1000$. Note: results utilize $O(h^3)$ wall boundary conditions and $O(h^2)$ corner boundary conditions.

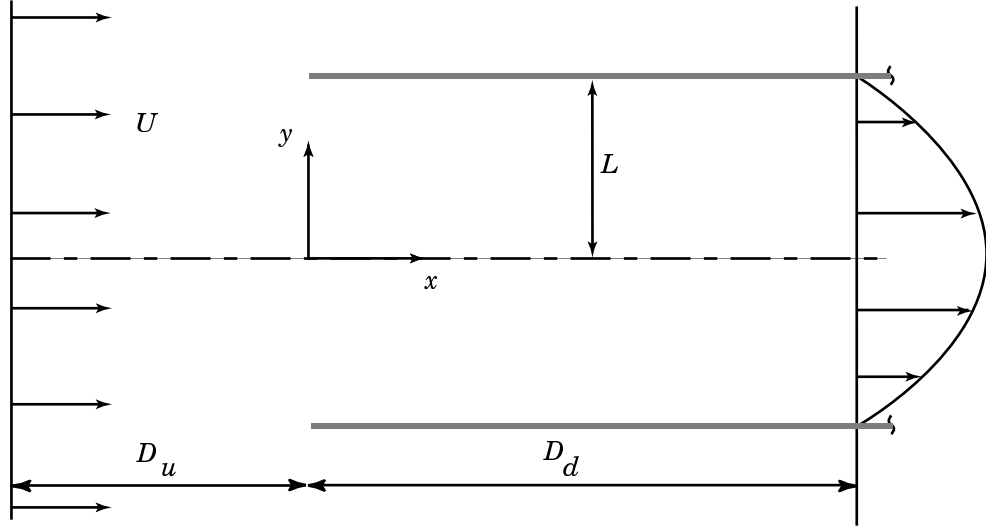


Figure 3.16: Problem description for an infinite cascade of thin plates.

select one half of one channel as the solution region.

To apply a finite difference method, we must truncate the domain a distance D_u upstream and a distance D_d downstream of the origin. In order to get an accurate solution, we must choose D_u and D_d large enough that they have an insignificant effect. Experience has shown that for highly diffusive flows, $Re = \frac{UL}{\nu} \rightarrow 0$, the effects of the plate can be felt reasonably forward of the leading edge, requiring at a minimum that $D_u = 2L$. The distance downstream required to develop the final flow profile grows in direct proportion to Re for large Reynolds numbers [109].

At the upstream boundary, the velocity boundary conditions are $u = 1$, $v = 0$. This results in a stream function at this boundary of the form $\psi = y + F(x)$. We choose $F(x) = 0$ so that $\psi = 0$ at the centerline and $\psi = 1$ at the top boundary. The uniform upstream flow is irrotational, so $\zeta = 0$ there.

At the outlet, the flow is fully developed and therefore u has a parabolic profile. The exact form of u can be found by matching the flow rate at the outlet with the flow rate at the inlet. This results in velocity outlet boundary conditions

$$u = \frac{3}{2} (1 - y^2), \quad v = 0.$$

The corresponding outlet stream function and vorticity are

$$\psi = \frac{3}{2}y - \frac{1}{2}y^3, \quad \zeta = 3y.$$

Along the plate, $y = 1$, $x > 0$, we use the compact wall boundary conditions of Section 3.3.1. Since it is a stationary wall ($u = 0$), we should not expect oscillations and can use the $O(h^4)$ formulation. The remainder of the top boundary, $y = 1$, $x < 0$, is a stagnation (and symmetry) streamline with $\psi = 1$. (The stream function is also unity along the wall.) The lower boundary along the channel centerline is also a symmetry streamline with $\psi = 0$. Along the symmetry streamlines, we have $\frac{\partial u}{\partial y} = 0$ and $v = 0$, which result in the vorticity boundary condition $\zeta = 0$. At the leading edge of the plate, there is a singularity in the vorticity. This is “handled” by orienting the grid such that plate tip is in the middle of a cell and not at a node.

Along the two streamline boundaries, we do not know u and must calculate it from the other problem data. However, we cannot use the HOC approximation to u at a boundary since it utilizes central difference operators. If we use one-sided differencing instead, this raises an issue about the accuracy of u on the boundary. However, we now show from symmetry arguments that one-sided differencing is sufficient to maintain $O(h^4)$ accuracy.

We know that the velocity u is symmetric about $y = 0$ (for all x) and $y = 1$ (when $x < 0$) because of the symmetry of the geometry. Equivalently, $\frac{\partial \psi}{\partial y}$ is symmetric about these lines, so if we temporarily consider the finite difference mesh extending above and below our solution domain, we can say that

$$\delta_y^+ \psi_{i1} = \delta_y^- \psi_{i1}, \quad (3.24)$$

for all x and

$$\delta_y^+ \psi_{iN} = \delta_y^- \psi_{iN}, \quad (3.25)$$

for $x < 0$ where N is the index such that $y_N = 1$. If we recall the identity

$$\delta_y \psi_{ij} = \frac{1}{2} \left(\delta_y^+ \psi_{ij} + \delta_y^- \psi_{ij} \right), \quad (3.26)$$

then it is clear from equations (3.24)–(3.26) that

$$\begin{aligned}\delta_y^+ \psi_{i1} &= \delta_y \psi_{i1}, \\ \delta_y^- \psi_{iN} &= \delta_y \psi_{iN}.\end{aligned}$$

In other words, one-sided differencing of ψ in the y -direction along symmetry streamlines has the same truncation error as central differencing. A similar argument can be made for the vorticity (both ζ and ψ will be odd functions—or anti-symmetric—with respect to symmetry streamlines, while u is an even function). The HOC velocity boundary conditions along these streamlines are therefore obtained from

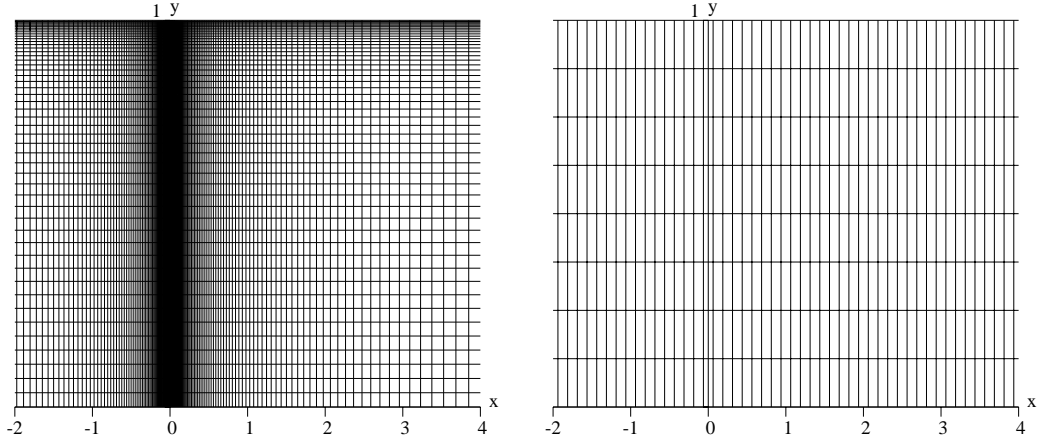
$$\begin{aligned}u_{i1} &= \delta_y^+ \psi_{i1} + \frac{h^2}{6} \left(\delta_y^+ \zeta_{i1} + \delta_x^2 \delta_y^+ \psi_{i1} \right) + O(h^4), \\ u_{iN} &= \delta_y^- \psi_{iN} + \frac{h^2}{6} \left(\delta_y^- \zeta_{iN} + \delta_x^2 \delta_y^- \psi_{iN} \right) + O(h^4).\end{aligned}$$

Comparison data for the cascading plates problem was obtained from Lorber [85], who solved the problem using central differencing on a nonuniform grid. It should be noted that Lorber, as well as Panton before him, define the Reynolds number differently than in the present work, using $2L$ as the characteristic length and then solving

$$\frac{\partial \zeta}{\partial t} + \mathbf{V} \cdot \nabla \zeta = \frac{2}{Re} \nabla^2 \zeta.$$

The Reynolds numbers reported in these sources are therefore greater than the Reynolds numbers reported here by a factor of 2. Comparison data was obtained for the incompressible cases where $Re = 0.5$ and $Re = 50$ on the nonuniform 150×51 grid depicted in Figure 3.17(a). The HOC solutions were computed on a much coarser uniform grid with $h = \frac{1}{8}$, shown in Figure 3.17(b). For $Re = 0.5$, a downstream distance $D_d \approx 6$ was used, and for $Re = 50$, $D_d \approx 10$. We are therefore trying to solve the problem with 7.6% and 11.6% of the number of grid points, respectively.

The coarse-grid HOC results compare extremely well with the fine-grid comparison data. Figure 3.18 depicts the stream function contours for both methods



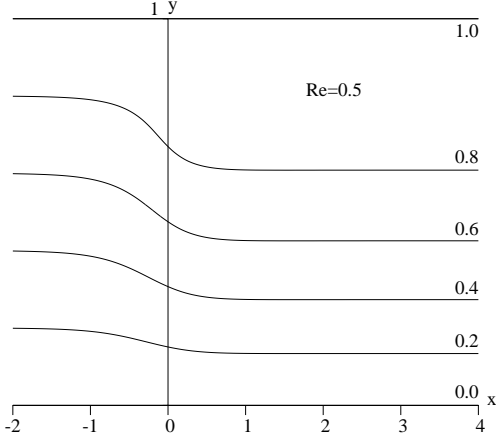
(a) Lorber, 150×51

(b) HOC, 65×9

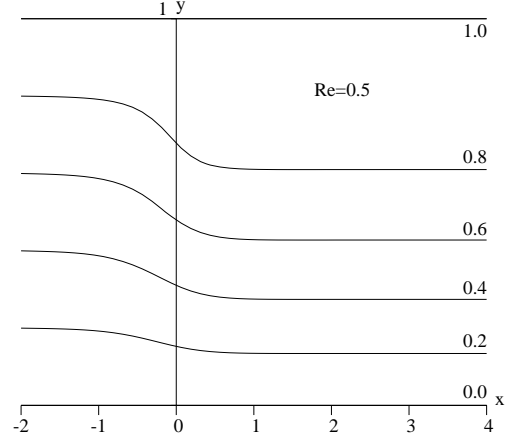
Figure 3.17: Detail of grids used to solve the cascading plates problem, (a) graded mesh by Lorber, 150×51 , used for comparison and (b) uniform HOC mesh, $h = \frac{1}{8}$ ($x = 0$ line is the y -axis, not a grid line). Note that $x : y = 1 : 5$.

at both Reynolds numbers studied. The results are visually indistinguishable. Figure 3.19 shows the vorticity contours for the same cases, and although the coarseness of the HOC grid is more apparent, the HOC results are still quite good.

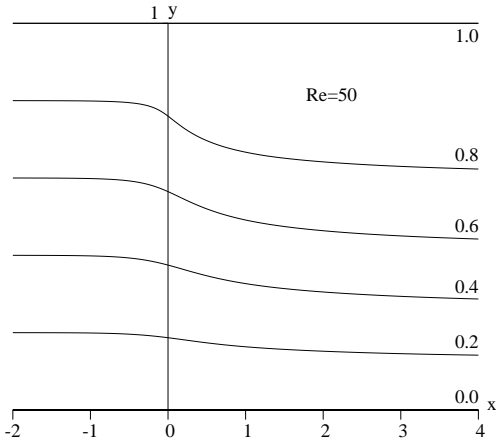
The x -component of the velocity along the channel center streamline and the stagnation streamline is plotted in Figure 3.20 for the HOC scheme and the comparison data at the two Reynolds numbers studied. Agreement is excellent. In fact, the most noticeable difference occurs where we should expect the grid coarseness to be most apparent, at the plate tip where there is a discontinuity in the velocity gradient but no grid point present. Figure 3.21 is a set of plots for the vorticity along the plate, and the agreement is again excellent, especially given the presence of a singularity at the tip. In fact, were the HOC data to be interpolated with a piecewise fourth-order polynomial rather than straight lines, the differences between the curves would be imperceptible.



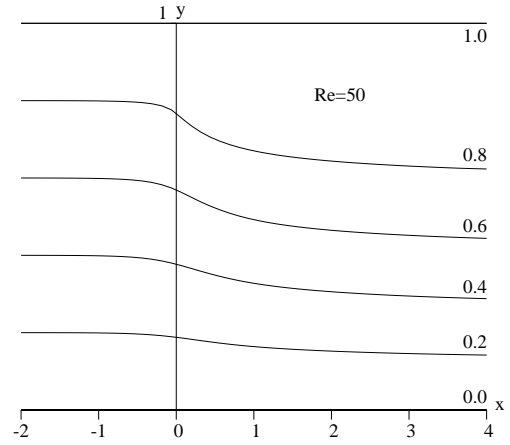
(a) $Re = 0.5$, Lorber, 150×51



(b) $Re = 0.5$, HOC, 65×9

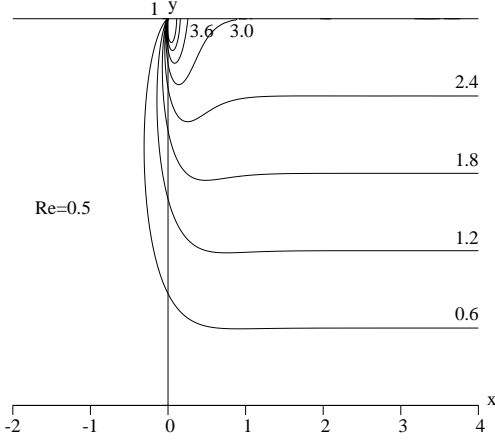


(c) $Re = 50$, Lorber, 150×51

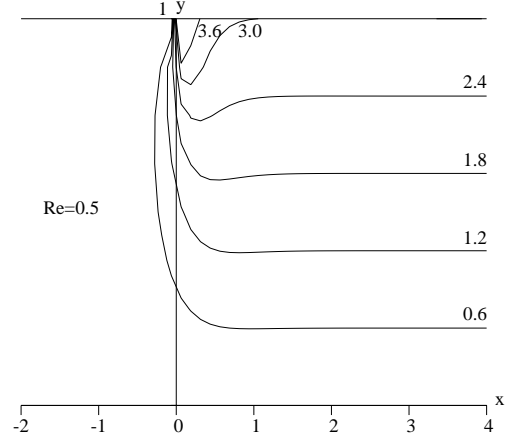


(d) $Re = 50$, HOC, 99×9

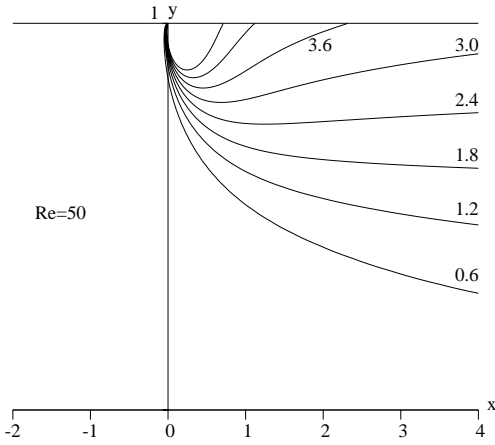
Figure 3.18: Stream function contours for the cascading plates problem for (a) $Re = 0.5$, Lorber, (b) $Re = 0.5$, HOC, (c) $Re = 50$, Lorber, and (d) $Re = 50$, HOC. Note that $x : y = 1 : 5$.



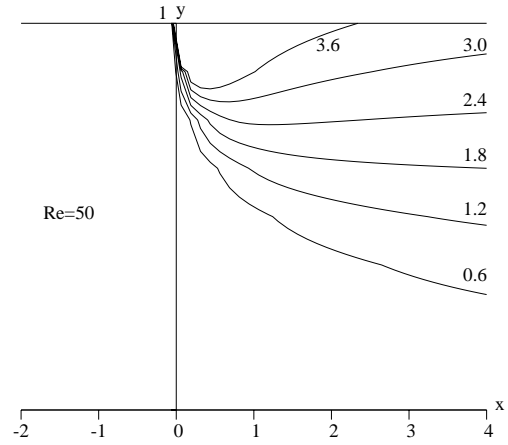
(a) $Re = 0.5$, Lorber, 150×51



(b) $Re = 0.5$, HOC, 65×9

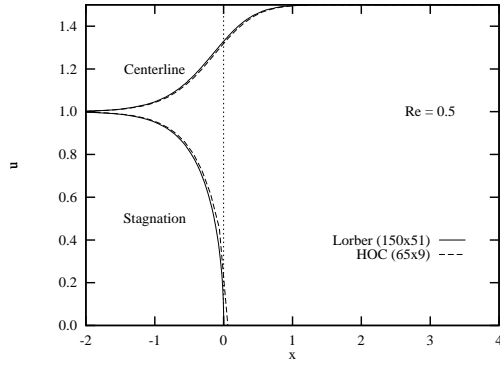


(c) $Re = 50$, Lorber, 150×51

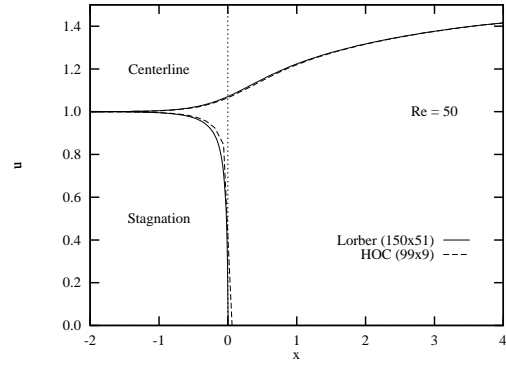


(d) $Re = 50$, HOC, 99×9

Figure 3.19: Vorticity contours for the cascading plates problem for (a) $Re = 0.5$, Lorber, (b) $Re = 0.5$, HOC, (c) $Re = 50$, Lorber, and (d) $Re = 50$, HOC. Note that $x : y = 1 : 5$.

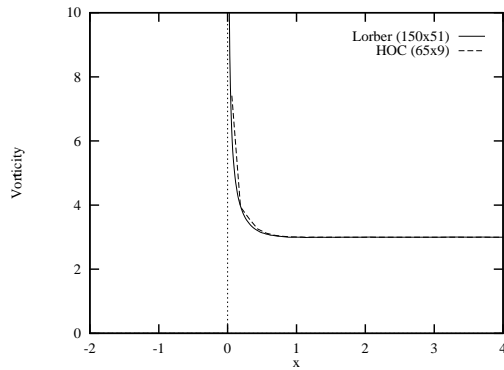


(a) $Re = 0.5$

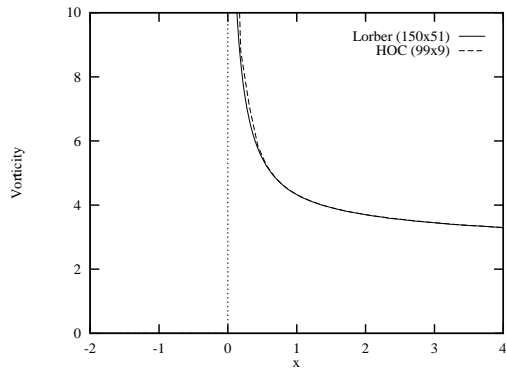


(b) $Re = 50$

Figure 3.20: Stagnation and Centerline velocity plots for the cascading plates model problem (a) $Re = 0.5$ and (b) $Re = 50$.



(a) $Re = 0.5$



(b) $Re = 50$

Figure 3.21: Wall vorticity plots for the cascading plates model problem for (a) $Re = 0.5$ and (b) $Re = 50$.

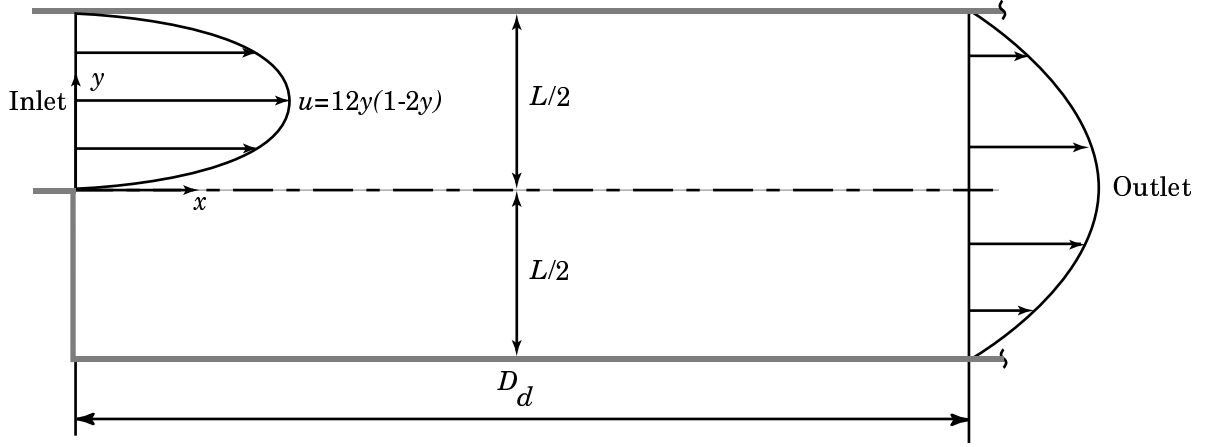


Figure 3.22: Problem description for a backward-facing step.

3.4.4 Backward-Facing Step Results

The final model problem for testing HOC modeling of steady incompressible flow is the backward-facing step problem. Many researchers have studied this problem, both experimentally [8] and numerically [9, 10, 42, 84], and we use Gartling's [42] problem definition. Consider a channel of width L downstream of the origin and width $\frac{L}{2}$ upstream of the origin, separated by a backward-facing step as depicted in Figure 3.22. Flow is assumed to be fully developed as it passes the inlet at $x = 0$ and has an average velocity U_{avg} . The problem domain is the channel starting at the inlet and extends downstream a distance D_d long enough for the flow to again become fully developed. The characteristic length is L , the characteristic velocity is U_{avg} , and thus the Reynolds number is $\frac{U_{avg}L}{\nu}$.

The top and bottom boundaries are stationary channel walls and thus we use the $O(h^4)$ compact wall boundary conditions with $u = v = 0$. The step face, located at $x = 0$, $-\frac{1}{2} \leq y < 0$, is also a stationary wall. At the inlet, the velocities are given by

$$u = 12y(1 - 2y), \quad v = 0,$$

and the corresponding stream function and vorticity are

$$\psi = 2y^2(3 - 4y), \quad \zeta = 12(4y - 1).$$

The stream function is chosen such that the stream function along the step face and bottom wall is 0 and the stream function value along the top wall is $\frac{1}{2}$.

The fully developed velocity profile at the outlet can be determined by equating the flow rates at the inlet and outlet. The outlet velocities are therefore

$$u = \frac{3}{4}(1 - 4y^2), \quad v = 0,$$

with corresponding stream function and vorticity

$$\psi = \frac{1}{4}(1 + 3y - 4y^3), \quad \zeta = 6y.$$

These boundary conditions, along with the suggested downstream distance $D_d \approx 30L$ [42], complete the specification of the backward-facing step model problem.

Figure 3.23 presents contour plots for the HOC stream function and vorticity solutions for Reynolds number $Re = 200$. A recirculation zone clearly forms behind the step. The length of the zone predicted by the HOC method is approximately 2.5, with $\psi_{min} = -0.0332$ at location $(0.8750, -0.1875)$. This is a slightly smaller recirculation zone than indicated by Barragy [9], who solved the coupled problem using high- p finite elements and predicted a recirculation length of 2.67 with $\psi_{min} = -0.0331$ at location $(1.0021, -0.2030)$.

3.5 Summary

Existing 2D HOC formulations for convection diffusion were used to model the (ψ, ζ) form of the steady, incompressible, Navier-Stokes equations. New HOC formulations for the velocity relationships were developed, as were HOC formulations for wall and corner boundary conditions. This system was determined to be $O(h^4)$ for a model problem with known analytic solution, and lower-order BCs were also shown to be

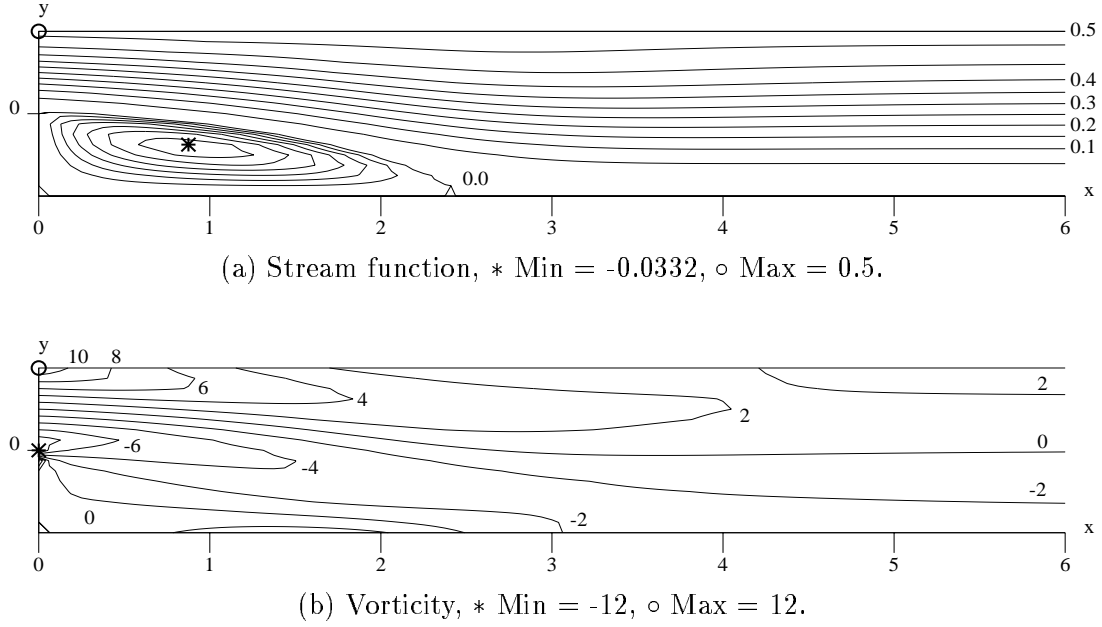


Figure 3.23: Contour plots for HOC solutions to the (a) stream function and (b) vorticity for the backward facing step problem, $Re = 200$.

the expected order of accuracy. Unfortunately, it was also discovered that the $O(h^4)$ BCs can lead to numerical oscillations in the vorticity on non-stationary walls. For this reason, $O(h^3)$ BCs were used to solve representative driven cavity problems. Results compared extremely favorably with fine-grid data published in the literature. The cascading plates problem was solved with $O(h^4)$ BCs since the plates are stationary, and results for this problem also compare well with lower-order results obtained on a fine, graded mesh. The backward-facing step problem proved difficult to solve using the HOC formulation at high Reynolds numbers, indicating that admitting more flexible grids might be useful and that an algorithm more sophisticated than successive approximations (such as Newton) should be implemented in order to converge to a solution.

Chapter 4

Performance Issues

4.1 Introduction

Heretofore in this dissertation, as well as in the literature involving this class of high-order compact schemes, evaluation of HOC formulations has been with respect to accuracy and other properties of the resulting approximate solution. In this chapter we seek to explore properties of HOC systems that are important to their application in practical situations. Specifically, we hope to determine how well HOC schemes can be expected to converge using typical iterative solvers and how well such schemes can be adapted to parallel computer architectures.

While some algorithms are more robust than others, most iterative matrix solvers can be expected to converge more quickly for matrices with a small condition number, κ , and more slowly or not at all for matrices with a large condition number. The condition number, in turn, is defined by

$$\kappa = \frac{\max |\lambda_k|}{\min |\lambda_k|}, \quad (4.1)$$

where $\{\lambda_k\}$ is the set of eigenvalues of the real matrix we wish to solve and can include complex conjugate pairs. Other factors also affect convergence of a given matrix. For instance, a matrix with tightly clustered eigenvalues will converge more quickly than a matrix with evenly distributed eigenvalues [44].

Most conjugate-gradient-type solvers require the matrix to be solved to be positive definite. This is equivalent to requiring $\Re(\lambda_k) > 0$, $k = 1 \dots N$, where \Re denotes the real component and N is the rank of the matrix. In Section 4.2, we seek to analyze HOC matrices to predict their condition numbers and check for positive-definiteness. Unfortunately, obtaining analytic estimates of the eigenvalues of an $N \times N$ matrix is equivalent to finding all the roots of an N -th degree polynomial, so we instead compute them explicitly for representative HOC systems in Section 4.3, as well as perform actual convergence tests to see how quickly HOC schemes converge compared to other schemes.

Finally, Section 4.4 is a case study of the parallelization of an HOC code to illustrate the issues that arise in porting an HOC code to a parallel architecture.

4.2 Condition Number Analysis

In seeking to determine the convergence properties of HOC schemes, our goal should be to analyze systems arising from 2D or 3D problems, since 1D problems are rarely large enough to require an iterative solver. Nevertheless, the tridiagonal matrices generated by compact 1D numerical schemes lend themselves to theoretical eigenvalue analysis, and our hope is that we can draw some conclusions from such analysis that might apply to higher dimensions.

Accordingly, we shall begin our analysis with 1D convection diffusion with constant coefficients on a uniform grid. The HOC scheme, given by (2.15) can be written in the form

$$-\left(\frac{1}{h^2} + \frac{c^2}{12} + \frac{c}{2h}\right)\phi_{i-1} + \left(\frac{2}{h^2} + \frac{c^2}{6}\right)\phi_i - \left(\frac{1}{h^2} + \frac{c^2}{12} - \frac{c}{2h}\right)\phi_{i+1} = F_i,$$

which illustrates the coefficients of the matrix that premultiplies the vector ϕ . The eigenvalues of such a tridiagonal matrix (see [17, p. 277]) are given by

$$\lambda_i = \frac{2}{h^2} + \frac{c^2}{6} - 2 \cos(i-1)\pi h \sqrt{\left(\frac{1}{h^2} + \frac{c^2}{12} + \frac{c}{2h}\right)\left(\frac{1}{h^2} + \frac{c^2}{12} - \frac{c}{2h}\right)}, \quad (4.2)$$

where $i = 2 \dots N - 1$. For the indices $i = 1$ or N , the matrix rows are determined by the boundary conditions and for Dirichlet data can easily be algebraically eliminated from the problem. It can be shown (as it was for the oscillation analysis of Section 2.3.2) that for any value of c and positive h , the two terms under the radical in (4.2) are both positive and thus the eigenvalues are guaranteed to be real and the coefficient matrix will be positive definite. The minimum eigenvalue occurs when $i = 2$ and the maximum eigenvalue occurs when $i = N - 1$. If we restrict our analysis to large N , then the factor $\cos(i - 1)\pi h$ is approximately ± 1 for these two extreme cases, and we can use (4.1) to derive an expression for the 1D HOC condition number limit,

$$\kappa_{HOC} = \frac{c^2 h^2 + 12 + \sqrt{(c^2 h^2 + 6ch + 12)(c^2 h^2 - 6ch + 12)}}{c^2 h^2 + 12 - \sqrt{(c^2 h^2 + 6ch + 12)(c^2 h^2 - 6ch + 12)}}. \quad (4.3)$$

We thus have an expression for the condition number limit as a function of ch , or the cell Reynolds (or Peclet) number. Unfortunately, as $ch \rightarrow 0$, the condition number behaves as $c^{-2}h^{-2}$ and for large ch , the condition number behaves as $c^2 h^2$. This means that for large N and $|ch|$ very large or very small, the condition number is extremely large and may pose some difficulty for an iterative solver.

Table 4.1: Condition Numbers for 1D HOC Matrices

	$ch = 2$		$ch = 5$		$ch = 10$		$ch = 20$	
h	c	κ	c	κ	c	κ	c	κ
1/8	16	4.1426	40	3.3550	80	8.096	160	16.215
1/16	32	4.6936	80	3.6955	160	10.640	320	31.395
1/32	64	4.8523	160	3.7898	320	11.526	640	40.699
Theory		4.9073		3.8229		11.853		45.129

As verification of (4.3), the eigenvalues for HOC matrices in 1D were computed by the linear algebra software package LAPACK [7]. Cases were run for different values of ch by varying c and h proportionately, and the results are shown in Table 4.1. Condition numbers on coarse meshes are lower than the theoretical limit and

approach the theory as the mesh is refined, so (4.3) provides a worst-case estimate of the condition number for a given cell Reynolds number.

For comparison purposes, the condition number limit for CDS is

$$\kappa_{CDS} = \begin{cases} \frac{2+\sqrt{4-c^2h^2}}{2-\sqrt{4-c^2h^2}}, & |ch| \leq 2, \\ \frac{|ch|}{2}, & |ch| > 2. \end{cases} \quad (4.4)$$

For UDS, the condition number limit is

$$\kappa_{UDS} = \frac{|ch| + 2 + 2\sqrt{|ch| + 1}}{|ch| + 2 - 2\sqrt{|ch| + 1}}. \quad (4.5)$$

Equations (4.3)–(4.5) are graphed in Figure 4.1. This is one instance where CDS and UDS appear to compare favorably with HOC, except of course for the fact that for $ch > 2$, CDS is oscillatory and for large ch , the UDS models an overly diffusive problem. Nevertheless, the HOC curve indicates that HOC schemes may require some form of preconditioning if a solution is to be obtained for large (or very small) values of ch .

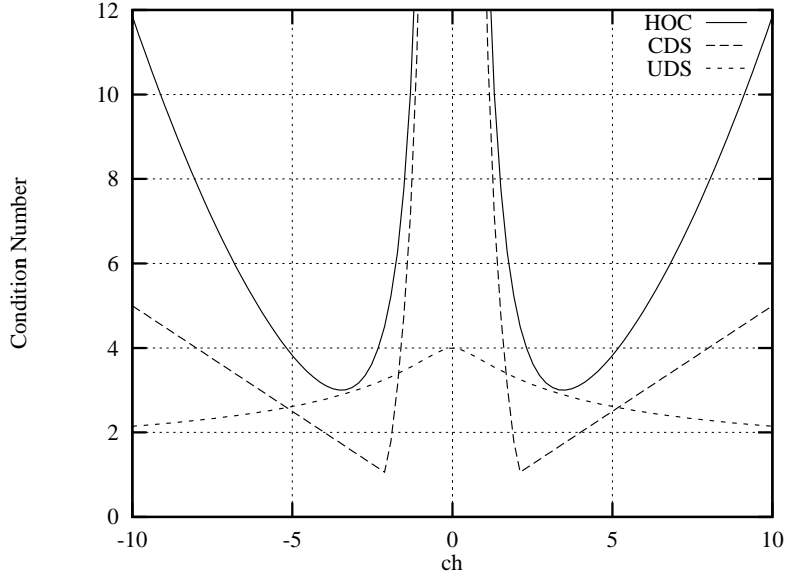


Figure 4.1: Condition number limit as a function of the cell Reynolds number for HOC, CDS and UDS

Theoretical estimates of eigenvalues (and thus the condition number) of systems resulting from 2D problems are more difficult because such systems lead to matrices that are not tridiagonal. Gershgorin [149] developed a theoretical bound on the eigenvalues of a matrix that affords a convenient geometric interpretation. The eigenvalues $\{\lambda_k\}$ of a matrix $\mathbf{M} = \{m_{ij}\}$ lie in the union of the Gershgorin circles in the complex plane defined by

$$|\lambda - m_{ii}| \leq \sum_{j \neq i} |m_{ij}|.$$

The circles in the complex λ -plane have centers located at points m_{ii} and radii of lengths equal to the sum of the magnitudes of the off-diagonal row entries. Thus we have a bound on all the eigenvalues of any matrix \mathbf{M} .

If we let M be the coefficient matrix generated by the HOC scheme on a uniform grid for the 2D convection diffusion equation with constant convection coefficients c and d , then the diagonal coefficient is given by

$$m_{ii} = \frac{1}{6h^2}(c^2h^2 + d^2h^2 + 20).$$

This term is always positive, so we know that the Gershgorin circle (all the circles collapse to a single disk when the convection and mesh size are constant) is centered in the right-half plane. To determine the Gershgorin radius, we need expressions for the off-diagonal matrix entries. The coefficients for the side nodes are given by

$$\begin{aligned} & -\frac{1}{12h^2}(c^2h^2 \pm 4ch + 8), \\ & -\frac{1}{12h^2}(d^2h^2 \pm 4dh + 8), \end{aligned}$$

in the x - and y -directions, respectively. The resulting expressions are everywhere negative for all values of ch and dh , so

$$\sum_{\text{sides}} |m_{ij}| = \frac{1}{6h^2}(c^2h^2 + d^2h^2 + 16).$$

The coefficients at the four corner nodes are given by the four permutations of

$$-\frac{1}{24h^2}(2 \pm ch)(2 \pm dh).$$

The resulting sum of coefficients at the corners is

$$\sum_{\text{corners}} |m_{ij}| = \frac{1}{6h^2} \sigma(ch) \sigma(dh),$$

where

$$\sigma(r) = \begin{cases} |r|, & |r| \geq 2, \\ 2, & |r| < 2. \end{cases}$$

This gives us the final result that

$$\sum_{j \neq i} |m_{ij}| = \frac{1}{6h^2} (c^2 h^2 + d^2 h^2 + \sigma(ch) \sigma(dh) + 16).$$

The radius of the Gershgorin circle is thus greater than the location of its center by the amount $\frac{\sigma(ch)\sigma(dh)-4}{6h^2}$, allowing for the possibility of negative eigenvalues if $|ch| > 2$ or $|dh| > 2$. The behavior of the tensor product $\sigma(ch)\sigma(dh)$ therefore becomes important in this analysis and is graphed in Figure 4.2.

By inspection we note that the resulting function is symmetric about the origin, so we can restrict our analysis to the quadrant $ch, dh > 0$ without loss of generality. Also, the direction of steepest ascent within this quadrant is along the ray $ch = dh > 2$. Accordingly, let us define

$$c = Re \cdot \cos \theta,$$

$$d = Re \cdot \sin \theta,$$

where Re is the Reynolds number for the problem. If we normalize the domain to unit scale, then $Re \cdot h = Re_h$, the cell Reynolds number. Further restricting the convection angle to $\frac{\pi}{4}$, we get

$$ch = dh = \frac{\sqrt{2}}{2} Re_h.$$

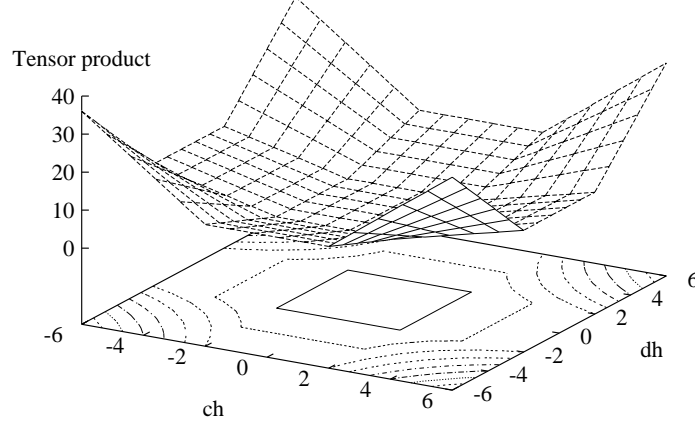


Figure 4.2: Surface and contour plot of the tensor product $\sigma(ch)\sigma(dh)$.

Under these assumptions, the Gershgorin eigenvalue bound becomes

$$\left| \lambda - \frac{1}{6h^2} (Re_h^2 + 20) \right| \leq \frac{1}{6h^2} \left(Re_h^2 + \sigma^2 \left(\frac{\sqrt{2}}{2} Re_h \right) + 16 \right). \quad (4.6)$$

If $\frac{\sqrt{2}}{2} Re_h < 2$ (that is, $Re_h < 2\sqrt{2}$), then we see that the Gershgorin circle center location equals the radius and thus we know that $\lambda \geq 0$ and that the matrix is guaranteed to be positive definite. However, if $Re_h > 2\sqrt{2}$, then $\sigma^2 \left(\frac{\sqrt{2}}{2} Re_h \right) = \frac{Re_h^2}{2}$, which gives

$$\left| \lambda - \frac{1}{6h^2} (Re_h^2 + 20) \right| \leq \frac{1}{6h^2} \left(\frac{3}{2} Re_h^2 + 16 \right).$$

The geometric interpretation of (4.6) is graphed in Figure 4.3, for $Re_h < 2\sqrt{2}$ (Case 1) and $Re_h > 2\sqrt{2}$ (Case 2). The circle for Case 1 is centered at $A = \frac{1}{6h^2}(Re_h^2 + 20)$ with equivalent radius, so that the imaginary axis is tangent to the circle. The circle for Case 2 is centered at B , which has the same expression as A , but for a larger Re_h . This circle extends a distance $C = -\frac{1}{6h^2} \left(\frac{1}{2} Re_h^2 - 4 \right)$ into the left-half plane.

While these results give us a good idea of the maximum possible eigenvalue magnitude, the theory allows $\min |\lambda_k|$ to be arbitrarily small. Therefore, no conclu-

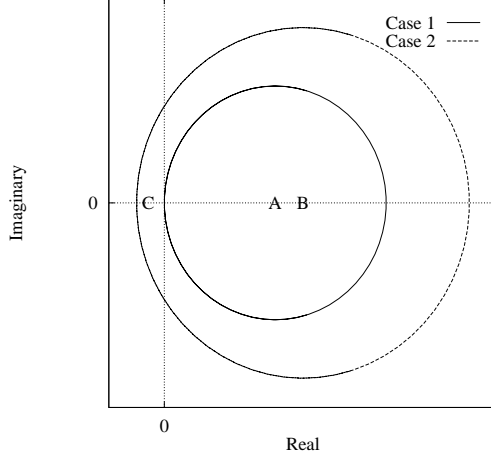


Figure 4.3: Gershgorin circles in the λ -plane for the 2D HOC scheme with constant and equal convection coefficients.

sions can be drawn regarding the condition number for the 2D case. In the following section, we will explicitly calculate the eigenvalues for representative 2D systems, compare the results to our Gershgorin theory, and compute the condition numbers for a variety of values of Re_h , as well as compare convergence of HOC systems to CDS and UDS.

4.3 Numerical Studies

The complex eigenvalues of selected HOC matrices were computed using the linear algebra library LAPACK in double precision on a Sun SparcStation. Five cell Reynolds numbers were examined, $Re_h = 1, 2, 4, 8$, and 16 . Each cell Reynolds number was examined for two mesh sizes, $h = \frac{1}{8}$ and $\frac{1}{16}$.

Figure 4.4 shows the eigenvalues for the case $Re_h = 1$. Since $Re_h < 2\sqrt{2}$, we predict that the real components of all the eigenvalues are positive, which is verified. We also note that the eigenvalues are all real, and that they all lie well within the Gershgorin limit. This is favorable, since it results in a lower condition number.

For $Re_h = 2$, which is still less than the critical cell Reynolds number in

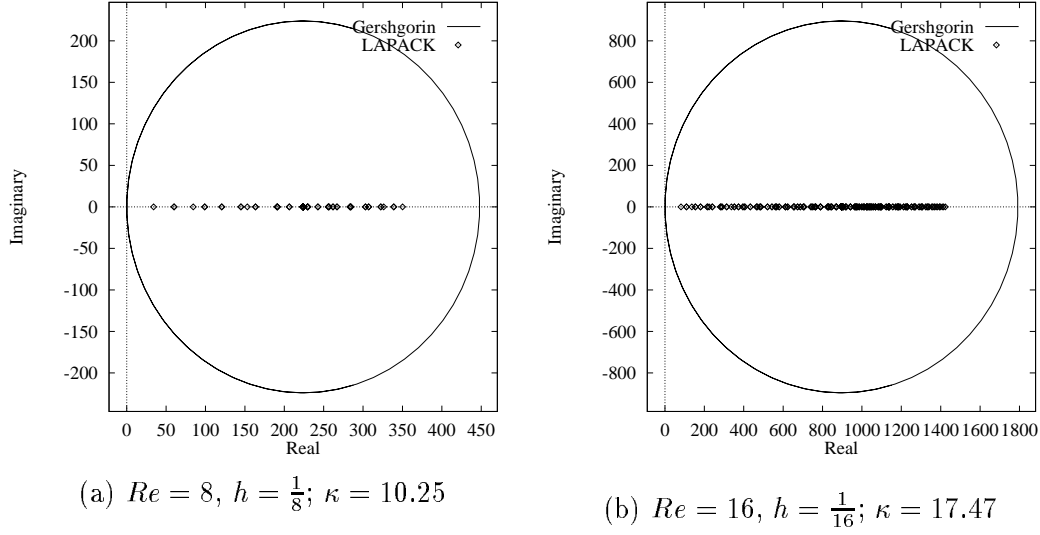


Figure 4.4: Eigenvalue plot for 2D HOC, $Re_h = 1$.

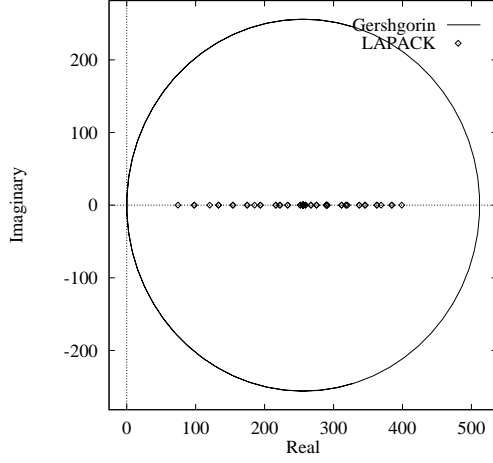
Gershgorin theory and depicted in Figure 4.5, we see the same trends as for $Re_h = 1$. Namely, that the eigenvalues are real and positive, and are well within the Gershgorin limit.

Figure 4.6 depicts the case $Re_h = 4$, and since $Re_h > 2\sqrt{2}$, is our first case that could theoretically allow for negative eigenvalues. However, it is apparent that this case does not have negative eigenvalues, as $\min |\lambda_k|$ is significantly greater than zero for both mesh sizes shown. Again, the eigenvalues are real and well within the Gershgorin limit.

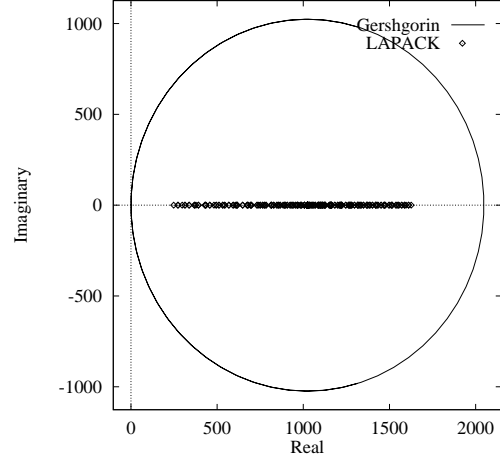
For the case $Re_h = 8$ in Figure 4.7 we see for the first time the appearance of complex conjugate eigenvalues. However, the imaginary parts are small compared to the real components of the eigenvalues. Furthermore, all the eigenvalues are located in the right-half plane.

Again in Figure 4.8, depicting eigenvalues for the case $Re_h = 16$, we see that the eigenvalues are all in the right-hand plane. Some of the eigenvalues are complex, but the imaginary components are still relatively small.

We have shown that the matrices for 2D HOC schemes are positive definite

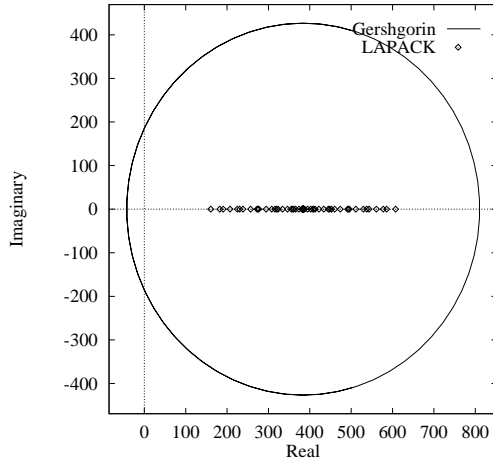


(a) $Re = 16, h = \frac{1}{8}; \kappa = 5.362$

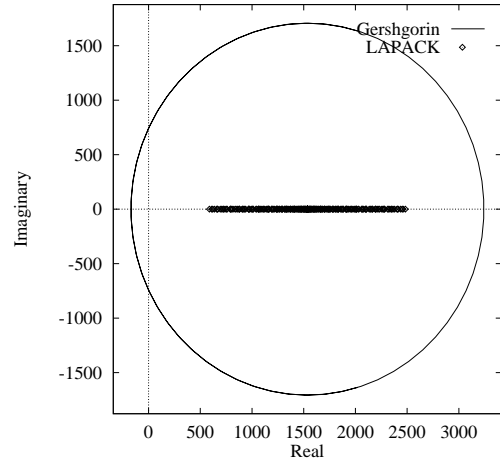


(b) $Re = 32, h = \frac{1}{16}; \kappa = 6.558$

Figure 4.5: Eigenvalue plot for 2D HOC, $Re_h = 2$.

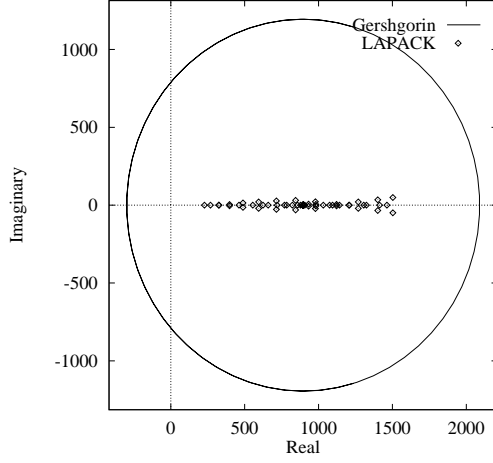


(a) $Re = 32, h = \frac{1}{8}; \kappa = 3.781$

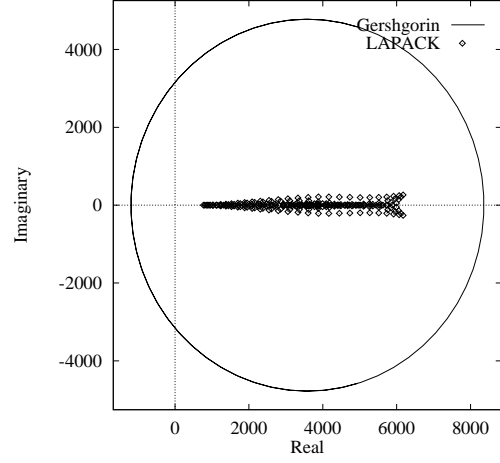


(b) $Re = 64, h = \frac{1}{16}; \kappa = 4.219$

Figure 4.6: Eigenvalue plot for 2D HOC, $Re_h = 4$.

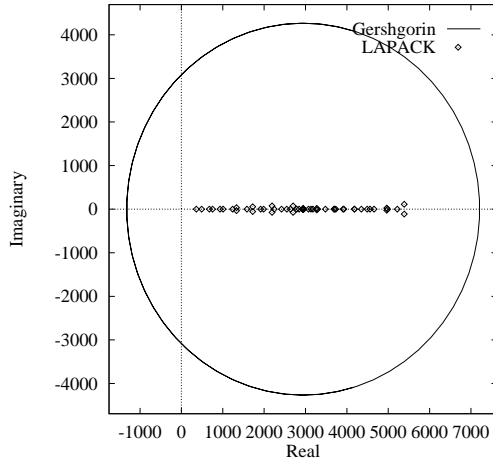


(a) $Re = 64, h = \frac{1}{8}; \kappa = 6.596$

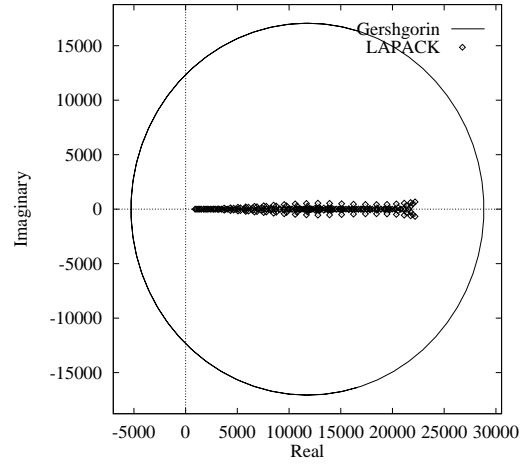


(b) $Re = 128, h = \frac{1}{16}; \kappa = 8.055$

Figure 4.7: Eigenvalue plot for 2D HOC, $Re_h = 8$.



(a) $Re = 128, h = \frac{1}{8}; \kappa = 14.94$



(b) $Re = 256, h = \frac{1}{16}; \kappa = 24.27$

Figure 4.8: Eigenvalue plot for 2D HOC, $Re_h = 16$.

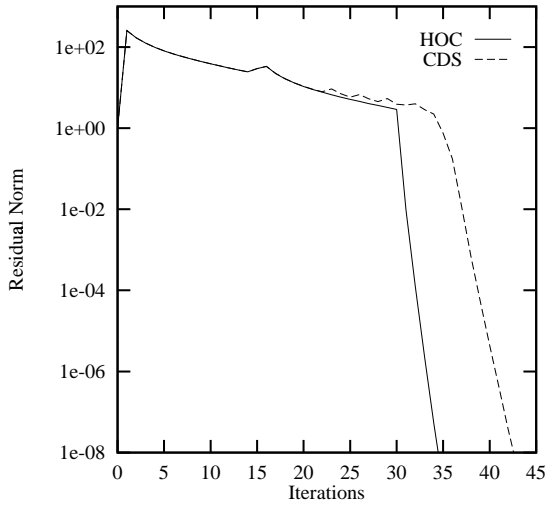
when $ch < 2$ and $dh < 2$. We have also determined experimentally that they seem to be positive definite even when these conditions are not met, and that the condition numbers remain moderate for reasonable cell Reynolds numbers. We now proceed to solve these systems iteratively to observe their iterative convergence behavior.

Accordingly, we solve systems for Stokes flow ($Re = 0$) and for four different cell Reynolds numbers, $Re_h = 1, 2, 4$ and 8 in Figures 4.9–4.13 respectively, where a norm of the residual is plotted at every iteration. We compare HOC, CDS and UDS on two finer grids, $h = \frac{1}{32}$ and $\frac{1}{64}$, than were considered for the eigenvalue studies. Since Stokes flow is symmetric, it is solved with conjugate gradient. The systems with $Re > 0$ are non-symmetric, and so we solve them by bi-conjugate gradient, and employ only a simple diagonal-scaling preconditioner. The results are somewhat surprising, given that the HOC condition number limit in 1D is always larger than the CDS and UDS condition number limits. In each example run, however, the HOC scheme converges slightly *more* quickly than the CDS and UDS counterparts. This may indicate that the HOC eigenvalues are somewhat clustered compared to CDS and UDS eigenvalues or that diagonal scaling is a more effective preconditioner for HOC systems than for CDS or UDS.

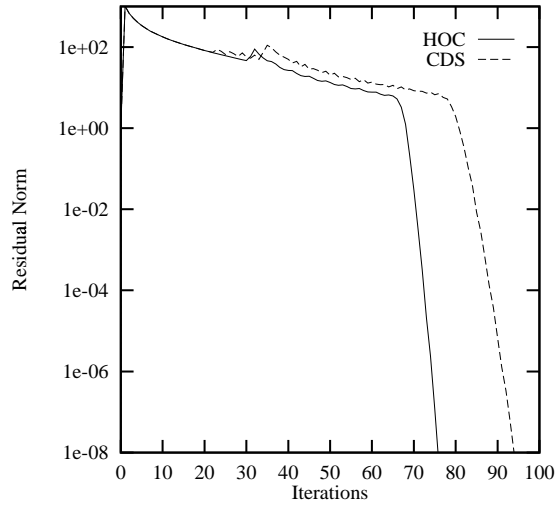
4.4 Parallel HOC

The code used to solve the HOC approximation to the 2D convection diffusion equation was parallelized by implementing the software library PCG (preconditioned conjugate gradient) [67], which is designed to iteratively solve systems arising from computational mechanics problems in parallel by domain decomposition. It supports a regular-grid storage format ideally suited to the problem being solved.

PCG computes the matrix-vector products of the gradient-type algorithms it supports by communicating the necessary problem data to neighboring processors. In the case of 9-point HOC stencils, this includes any corner data that might lie off-processor. For maximum efficiency, these data transfers are performed asyn-

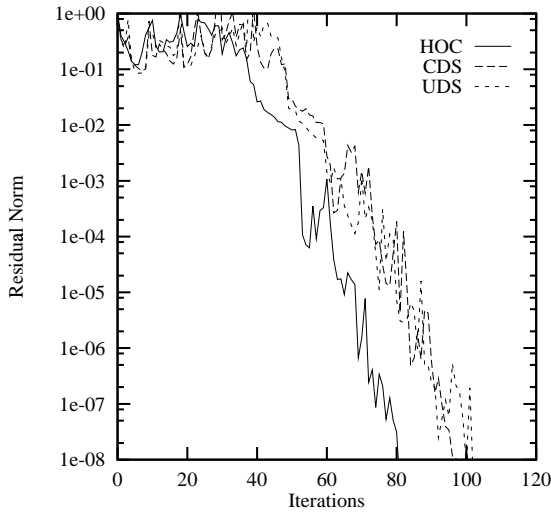


(a) $Re = 0, h = \frac{1}{32}$

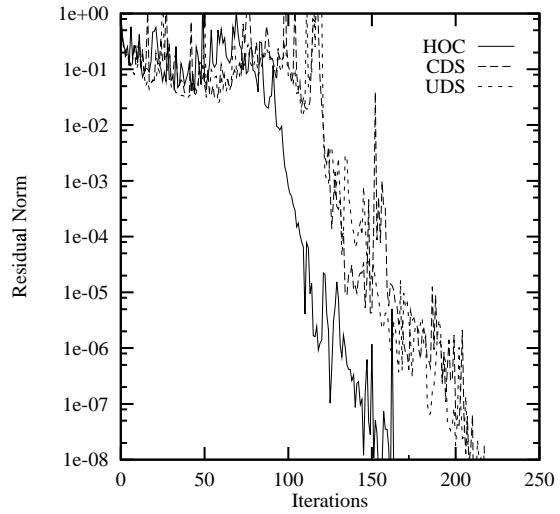


(b) $Re = 0, h = \frac{1}{64}$

Figure 4.9: Convergence plots for HOC and CDS using conjugate gradient with no diagonal scaling, $Re = 0$.

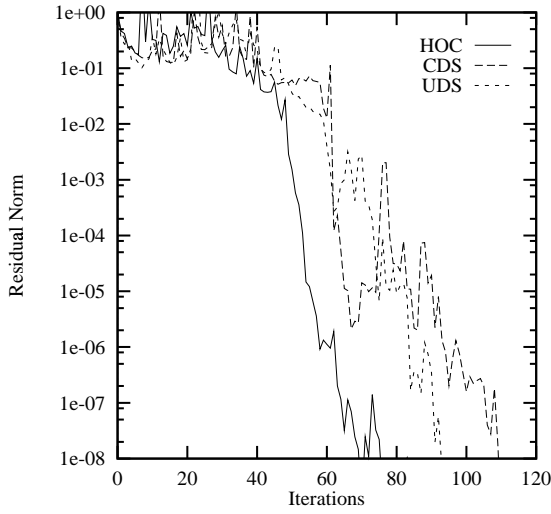


(a) $Re = 32, h = \frac{1}{32}$

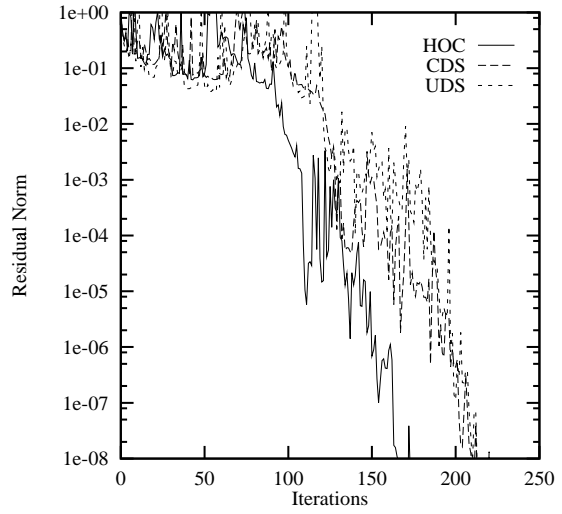


(b) $Re = 64, h = \frac{1}{64}$

Figure 4.10: Convergence plots for HOC, CDS and UDS using bi-conjugate gradient and diagonal scaling, $Re_h = 1$.

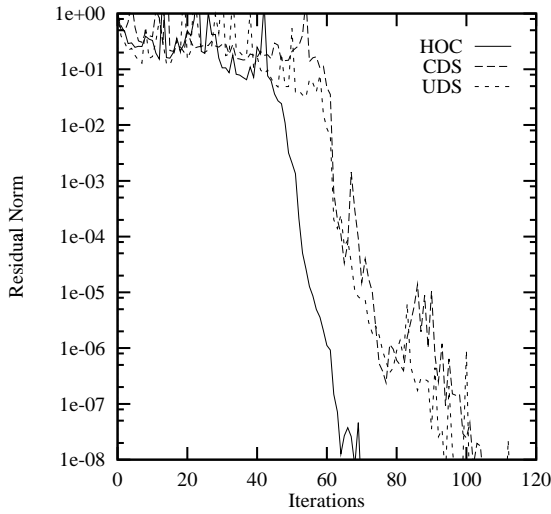


(a) $Re = 64, h = \frac{1}{32}$

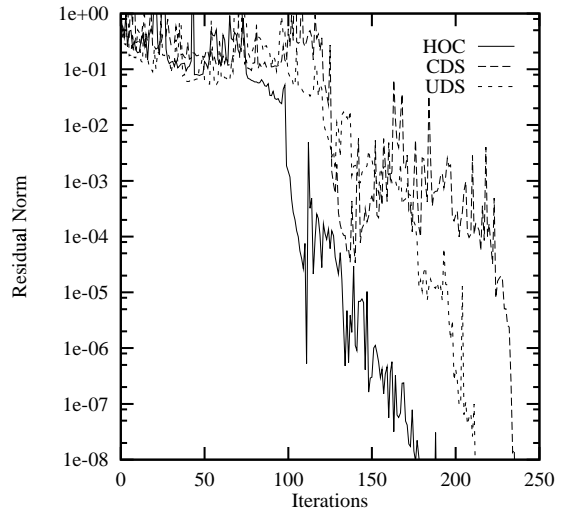


(b) $Re = 128, h = \frac{1}{64}$

Figure 4.11: Convergence plots for HOC, CDS and UDS using bi-conjugate gradient and diagonal scaling, $Re_h = 2$.

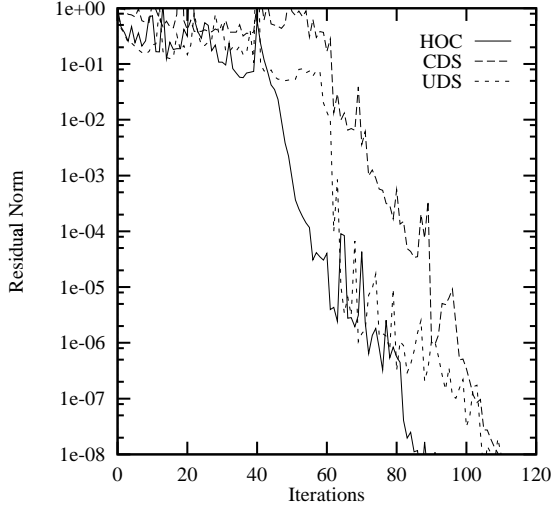


(a) $Re = 128, h = \frac{1}{32}$

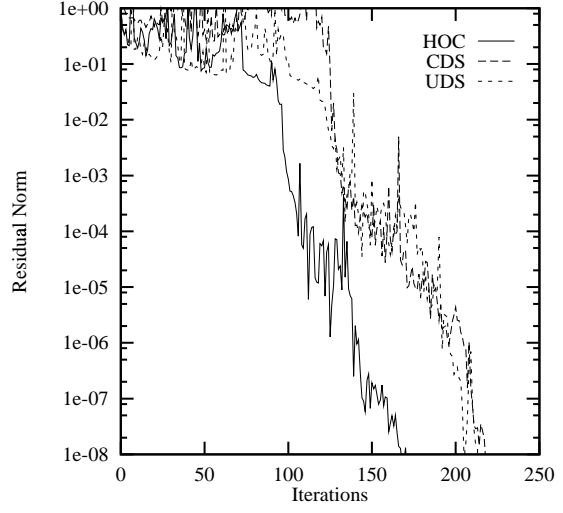


(b) $Re = 256, h = \frac{1}{64}$

Figure 4.12: Convergence plots for HOC, CDS and UDS using bi-conjugate gradient and diagonal scaling, $Re_h = 4$.



(a) $Re = 256, h = \frac{1}{32}$



(b) $Re = 512, h = \frac{1}{64}$

Figure 4.13: Convergence plots for HOC, CDS and UDS using bi-conjugate gradient and diagonal scaling, $Re_h = 8$.

chronously with other computations to maximize efficiency. In addition, 9-point stencils such as HOC run more efficiently (achieve higher MFLOP rates) than 5-point schemes such as CDS. This outcome is the result of the specific implementation of matrix-vector products in PCG and involves the transfer of data into cache. Basically, more operations can be performed between these transfers for a 9-point stencil than for a 5-point stencil, which results in higher efficiency. The details can be found in [94]. A comparison of matrix-vector product MFLOP rates is shown in Figure 4.14.

Within the context of implementing a software library such as PCG, the only user-level parallelization concern for the HOC method involves calculation of the difference operators $\delta_x c_{ij}$, $\delta_x f_{ij}$, etc., of the problem data c , d , and f that the HOC scheme requires. In a domain decomposition setting, calculation of these terms along processor boundaries requires off-processor information. This requirement was accommodated by allocating border points for c , d , and f , thus duplicating the storage of the problem data on processor boundaries. For the simple model

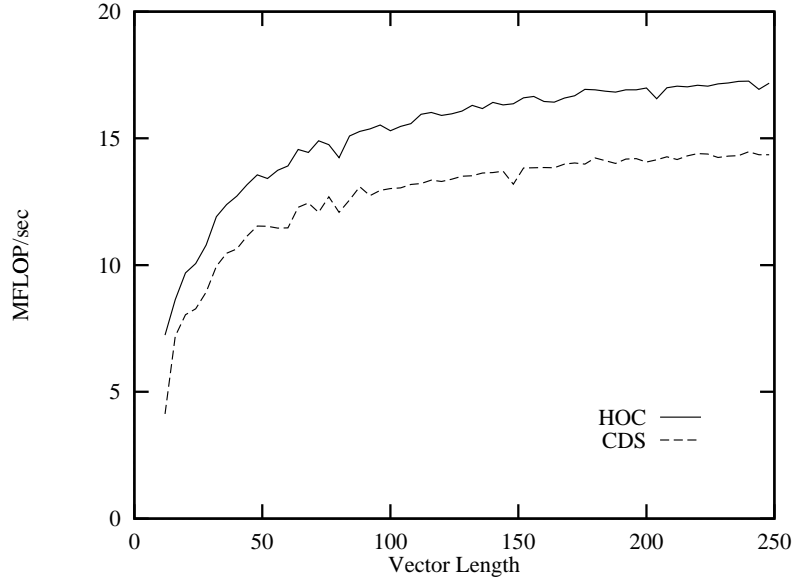


Figure 4.14: MFLOP rates for CDS and HOC matrix-vector products as a function of vector length. Data courtesy of McLay[94].

problems considered here, these border values could be computed directly. For a more complicated problem, such as (ψ, ζ) , the velocities u and v would have to be communicated among processors between successive approximations.

Figure 4.15 shows a surface and contour plot of the parallel HOC solution to the 2D model problem 1 for $Re = 20$. The problem was solved on a global 32×32 grid and a 4×4 processor partition on an Intel iPSC860 using conjugate gradient. Figure 4.16 is a speedup curve comparing parallel solution of HOC and CDS formulations. The grid sizes for these cases were chosen to be round numbers close to the limit that could be solved on a single processor. The HOC problem size is smaller because of its larger stencil and additional data storage requirements.

4.5 Summary

In this chapter we have studied the eigenvalues and condition numbers of HOC matrices to try and analyze their convergence properties for iterative algorithms.

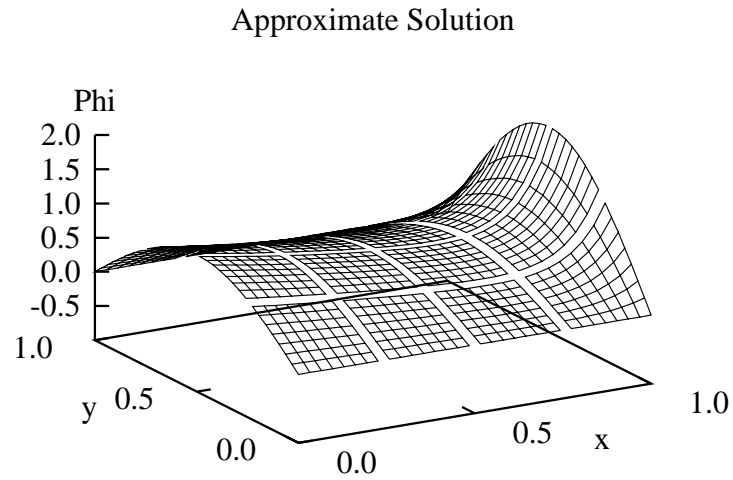


Figure 4.15: Surface and contour plot of a parallel HOC solution to the 2D model problem 1, $Re = 20$, solved on a 4×4 processor partition.

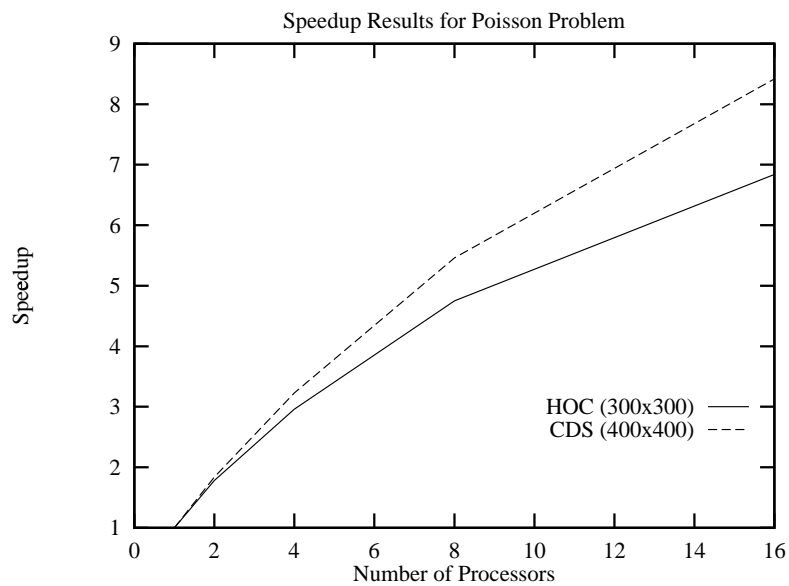


Figure 4.16: Speedup curve for parallel HOC and CDS Poisson solutions.

We determined a condition number limit for the 1D constant coefficient case and showed that these matrices are positive definite and have real eigenvalues. The limit itself was found to be higher than both CDS and UDS at all cell Reynolds numbers, although it is low enough over a reasonable range of Re_h that most iterative solvers should be able to handle HOC systems. In 2D, positive definiteness was proved for the cases when $ch \leq 2$ and $dh \leq 2$ by using Gershgorin theory. Experimental evidence suggests that 2D HOC matrices stay positive definite, but that complex conjugate pairs are possible at higher cell Reynolds numbers, although the imaginary components are always small compared to the real components. Iterative convergence comparisons (using conjugate gradient for pure diffusion and diagonally scaled bi-conjugate gradient for convection diffusion) of HOC with CDS and UDS surprisingly favored HOC, even though HOC condition numbers are higher. Finally, the 2D code for solving parallel HOC formulations was parallelized as a case study of adapting HOC schemes to parallel computer architectures. Although CDS can be solved slightly more quickly than HOC in parallel, the HOC scheme is more efficient in terms of MFLOP rates.

Chapter 5

HOC Schemes on Nonuniform Grids

5.1 Introduction

The HOC theory as developed to this point is restricted to uniform grids. This restriction precludes the solution of problems on non-rectangular domains or even problems in which non-square grid cells would be appropriate. Furthermore, many problems may be solved to much greater accuracy simply by refining the grid in areas of steep solution gradients, yet this option has not been previously available in HOC theory. In this chapter we address this issue and extend, for the first time, HOC formulations to nonuniform orthogonal grids.

5.2 1D Convection Diffusion

It is common practice in finite difference solutions to elliptic boundary-value problems to map the given problem from the physical domain Ω to a reference domain $\hat{\Omega}$ and to solve the transformed problem approximately on $\hat{\Omega}$ using a uniform difference grid. In fact, numerous constructions for mappings with desirable grid properties

have been devised (for example, see [138]). Since the HOC method in Section 2.3.1 has been constructed for uniform grids, this mapping formulation is a natural approach. To introduce the main ideas for extending the theory, let us consider the following form of the steady, 1D, convection diffusion equation,

$$-\frac{d^2\phi}{dx^2} + u(x)\frac{d\phi}{dx} = S(x), \quad (5.1)$$

with the familiar boundary conditions $\phi(0) = 0$, $\phi(1) = 1$.

5.2.1 HOC Formulation

Accordingly, let us construct an invertible map $x = x(\xi)$ with inverse map $\xi(x)$. Under the inverse map, a graded mesh on $0 \leq x \leq 1$ would be transformed to a uniform mesh on $0 \leq \xi \leq 1$. Transforming equation (5.1) gives

$$-\left(\frac{d\xi}{dx}\right)^2 \frac{d^2\hat{\phi}}{d\xi^2} + \left(\hat{u}\frac{d\xi}{dx} - \frac{d^2\xi}{dx^2}\right) \frac{d\hat{\phi}}{d\xi} = \hat{S}, \quad (5.2)$$

where $\hat{\phi}(\xi) = \phi(x(\xi))$, $\hat{u}(\xi) = u(x(\xi))$, $\hat{S}(\xi) = S(x(\xi))$, and the metric coefficients $\frac{d\xi}{dx}$ and $\frac{d^2\xi}{dx^2}$ must now be considered.

Provided the map is regular and non-degenerate (so that $\frac{d\xi}{dx} \neq 0$) we can write (5.2) conveniently in the form

$$-\frac{d^2\hat{\phi}}{d\xi^2} + c(\xi)\frac{d\hat{\phi}}{d\xi} = f(\xi), \quad (5.3)$$

where

$$c(\xi) = \frac{\hat{u}\frac{d\xi}{dx} - \frac{d^2\xi}{dx^2}}{\left(\frac{d\xi}{dx}\right)^2}, \quad f(\xi) = \frac{\hat{S}}{\left(\frac{d\xi}{dx}\right)^2}. \quad (5.4)$$

Now we have a governing equation that is of exactly the same form as (2.8), so the HOC scheme is exactly the same as (2.14), expressed here in the transformed variables:

$$-A_i\delta_\xi^2\hat{\phi}_i + C_i\delta_\xi\hat{\phi}_i = F_i + O(h^4), \quad (5.5)$$

where

$$A_i = 1 + \frac{h^2}{12} [c_i^2 - 2\delta_\xi c_i], \quad (5.6)$$

$$C_i = c_i + \frac{h^2}{12} [\delta_\xi^2 c_i - c_i \delta_\xi c_i], \quad (5.7)$$

$$F_i = f_i + \frac{h^2}{12} [\delta_\xi^2 f_i - c_i \delta_\xi f_i], \quad (5.8)$$

and c_i and f_i are defined by (5.4).

5.2.2 Numerical Studies

Consider the model test problem for (5.1) with $u = \text{constant}$, $S = 0$. The analytic solution is $\phi(x) = (e^{ux} - 1)/(e^u - 1)$ and for $u \gg 1$ has a steep layer near $x = 1$. To illustrate the mapping idea let us introduce the mapping function

$$x(\xi) = \xi + \frac{\gamma}{\pi} \sin \pi \xi, \quad 0 \leq \xi \leq 1, \quad (5.9)$$

where γ is the grading parameter. The map is invertible for $|\gamma| < 1$; $\gamma > 0$ corresponds to compression (clustering) to the right and similarly to the left for $\gamma < 0$. In the following convergence calculations we choose $\gamma = \frac{1}{2}$, which corresponds to a moderate grading to the right.

The test problem was computed on a sequence of uniformly refined grids $h = \frac{1}{4}, \frac{1}{8}, \dots, \frac{1}{64}$ for $u = 5$ and $u = 20$. The error $E = |\phi(x_i) - \phi_i|$ at a representative grid point $x_i = x(\xi_i = 0.75)$ is graphed in Figure 5.1 against mesh size h on a log-log scale for the UDS, CDS and HOC schemes. The rate exponent m is given by the asymptotic slope of the curves. The calculations for the high-order scheme utilize full knowledge of the analytic map (5.9) to compute the metric derivatives, $\frac{d\xi}{dx}$ and $\frac{d^2\xi}{dx^2}$, exactly, and the optimal $O(h^4)$ rate is obtained. These results also verify the HOC formulation for 1D convection diffusion with variable coefficient on a *uniform* grid, which was previously untested.

In practice the map may not be specified analytically and the metric coefficients may be obtained by $O(h^2)$ central differencing. For example, we know

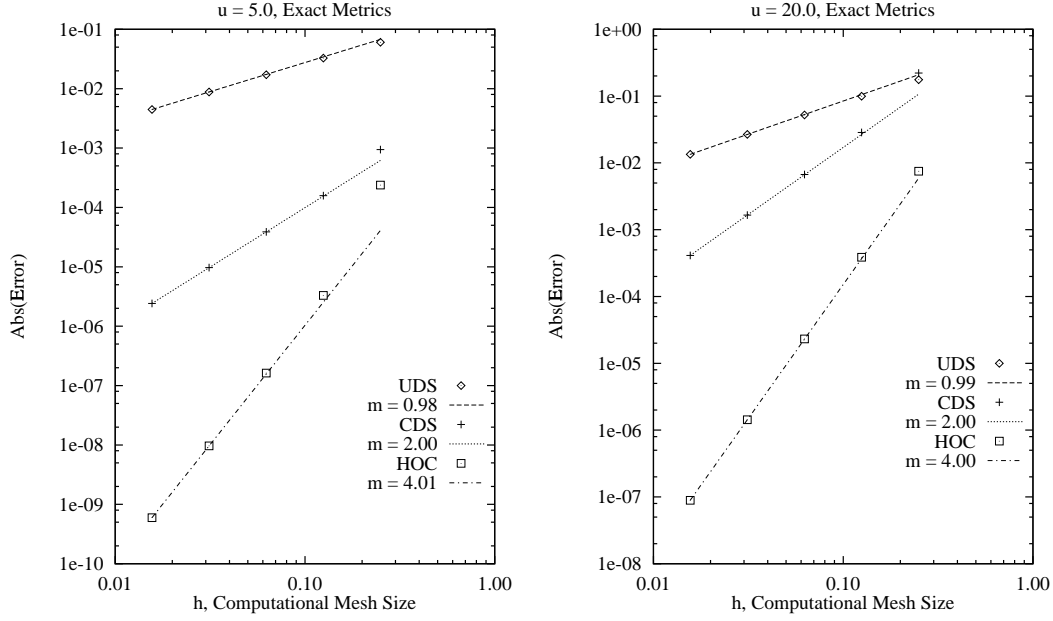


Figure 5.1: Convergence results for 1D convection diffusion on a nonuniform grid with exact metrics, $u = 5$ and 20 .

$\frac{d\xi}{dx} = \frac{1}{dx/d\xi}$, so

$$\begin{aligned}
 \left. \frac{d\xi}{dx} \right|_i &= \frac{1}{\delta_\xi x_i - \frac{h^2}{6} \left. \frac{d^3 x}{d\xi^3} \right|_i + O(h^4)}, \\
 &= \frac{1}{\delta_\xi x_i} \left[\frac{1}{1 - \frac{h^2}{6\delta_\xi x_i} \left. \frac{d^3 x}{d\xi^3} \right|_i + O(h^4)} \right], \\
 &= \frac{1}{\delta_\xi x_i} + \frac{h^2}{6(\delta_\xi x_i)^2} \left. \frac{d^3 x}{d\xi^3} \right|_i + O(h^4), \tag{5.10}
 \end{aligned}$$

where we have used the identity $\frac{1}{1+\epsilon} = 1 - \epsilon + \epsilon^2 - \dots$ to determine the truncation error. In a like manner, since $\frac{d^2 \xi}{dx^2} = -\frac{d^2 x}{d\xi^2} \left(\frac{d\xi}{dx} \right)^3$,

$$\begin{aligned}
 \left. \frac{d^2 \xi}{dx^2} \right|_i &= - \left[\delta_\xi^2 x_i - \frac{h^2}{12} \left. \frac{d^4 x}{d\xi^4} \right|_i + O(h^4) \right] \left[\frac{1}{\delta_\xi x_i} + \frac{h^2}{6(\delta_\xi x_i)^2} \left. \frac{d^3 x}{d\xi^3} \right|_i + O(h^4) \right]^3, \\
 &= - \left[\delta_\xi^2 x_i - \frac{h^2}{12} \left. \frac{d^4 x}{d\xi^4} \right|_i + O(h^4) \right] \left[\frac{1}{(\delta_\xi x_i)^3} + \frac{h^2}{2(\delta_\xi x_i)^4} \left. \frac{d^3 x}{d\xi^3} \right|_i + O(h^4) \right], \\
 &= -\frac{\delta_\xi^2 x_i}{(\delta_\xi x_i)^3} - \frac{h^2}{6} \left[\frac{3\delta_\xi^2 x_i}{(\delta_\xi x_i)^4} - \frac{1}{(\delta_\xi x_i)^3} \left. \frac{d^4 x}{d\xi^4} \right|_i \right] + O(h^4). \tag{5.11}
 \end{aligned}$$

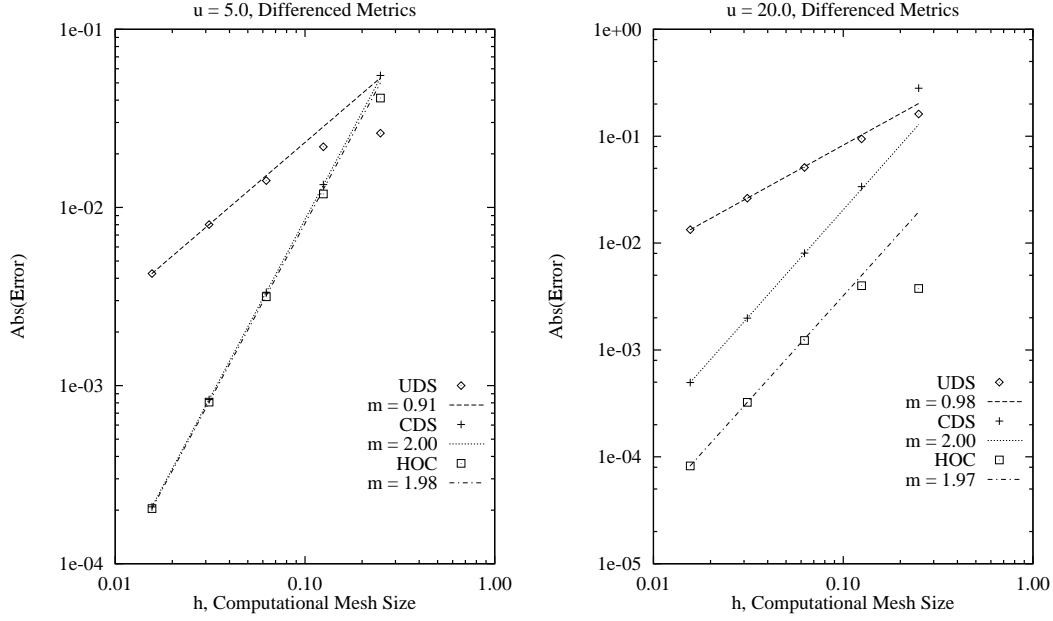


Figure 5.2: Convergence results for 1D convection diffusion on a nonuniform grid with differenced metrics, $u = 5$ and 20 .

Equations (5.10) and (5.11) are used in (5.4) to approximate c_i and f_i . The resulting approximation for c_i is

$$c_i = \hat{u} \delta_\xi x_i + \delta_\xi x_i \delta_\xi^2 x_i - \frac{h^2}{12} \left[\left(\frac{4\hat{u}}{\delta_\xi x_i} - \frac{2\delta_\xi^2 x_i}{(\delta_\xi x_i)^2} - 2 \right) \frac{d^3 x}{d\xi^3} \Big|_i + \frac{1}{\delta_\xi x_i} \frac{d^4 x}{d\xi^4} \Big|_i \right] + O(h^4).$$

Since we do not have approximations for $\frac{d^3 x}{d\xi^3}$ and $\frac{d^4 x}{d\xi^4}$, we expect $O(h^2)$ differencing of the grid metrics to pollute the overall approximation by $O(h^2)$.

We examine the effect of this approximation using the grid from the preceding test. The results are summarized in Figure 5.2. The effect of approximating the metric derivatives by the CDS is to degrade the asymptotic rate of the HOC scheme, reducing it to $O(h^2)$. The approximate solutions for the central and higher-order schemes are essentially identical for $u = 5$ but for $u = 20$ the higher order scheme is more accurate. Furthermore, comparisons of the two solutions for greater convection ($u = 50$) on a coarse grid ($h = \frac{1}{8}$) reveals that the HOC scheme is non-oscillatory

whereas the CDS still produces an oscillatory result (Figure 5.3). Note, however, how the grading improves both the HOC and CDS solutions compared to the same problem on a uniform grid in Figure 2.3.

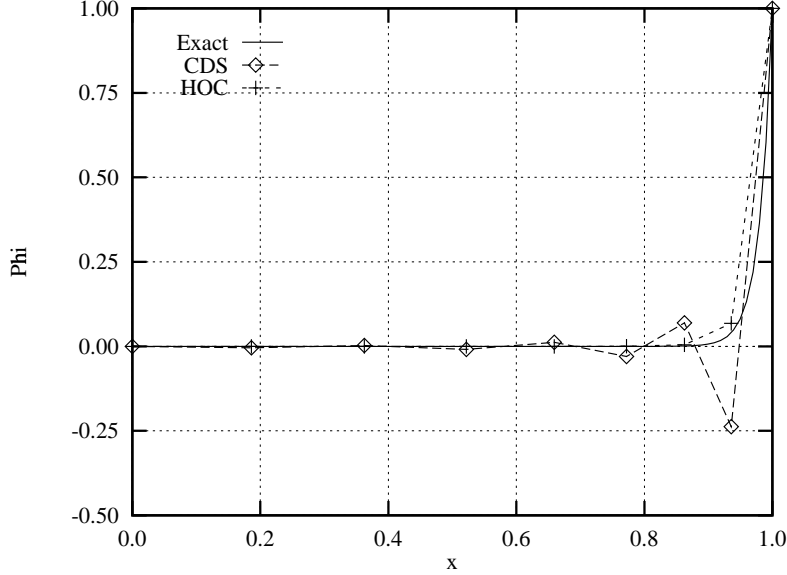


Figure 5.3: 1D convection diffusion results for the exact, oscillating CDS, and HOC scheme with differenced metrics, $u = 50$, $h = \frac{1}{8}$, on a nonuniform grid.

Gresho [47] argues that oscillations are an indication that the grid is not sufficiently fine to resolve the local solution characteristics, and advocates local refinement in the region of oscillations. He further asserts that a smooth solution may inspire undue confidence in an inaccurate approximation, thus implying oscillatory schemes are useful. If we use a non-oscillatory scheme then, we should at least make an effort to use any prior knowledge of the solution to insure that the grid is sufficiently fine to resolve the features of the flow.

The HOC results in Figure 5.3 are encouraging but the mesh gradation is mild and the Peclet number of 50 is quite moderate so the boundary layer near $x = 1$ is relatively modest. The ability of the method to function with more strongly graded meshes and at higher convection levels is therefore relevant. In fact, if faithful representation of the layer structure is desired then the mesh should be graded so that

there are a few grid points guaranteed to lie within the layer. Consequently, we considered the test problem for successively increasing convection levels corresponding to $u = 50, 100, 250$, and 500 . The same grading function (5.9) was applied with $\gamma = 0.6, 0.7, 0.8$, and 0.9 respectively. It can be shown for this problem that the boundary layer thickness, defined at the point where $\phi = 0.01$, is approximately $\frac{4.6}{u}$ when $u \gg 5$. This result was used to choose a unique h in each of the four cases such that three cells lie within the boundary layer. The HOC results in the layer regions are graphed in Figure 5.4 and compared with the analytical solution. The nodal superconvergence property is evident in each case and the approximation of the layer is indeed excellent.

5.2.3 HOC Metrics

If the map $x(\xi)$ is not known explicitly but satisfies a differential equation or similar auxiliary relation then it is possible to recover the $O(h^4)$ estimate in a manner analogous to the way in which the HOC scheme was developed for the governing transport equation. Consider the boundary value problem

$$\frac{d^2 x}{d\xi^2} + \pi^2 x = \pi^2 \xi, \quad (5.12)$$

with boundary conditions $x(0) = 0, x(1) = 1$, which corresponds to a Helmholtz PDE grid generator in 1D with a positive source term proportional to ξ . The exact solution is precisely the grading function $x(\xi)$ in (5.9). Let us assume now that the grid (and indirectly the map) is generated by solving (5.12) accurately using a uniform grid. Now (5.12) can be used as an auxiliary relation for the difference approximation of the metrics $\frac{d\xi}{dx}$ and $\frac{d^2 \xi}{dx^2}$ at grid point i . More specifically, $\frac{d\xi}{dx} = \frac{1}{dx/d\xi}$, so

$$\left. \frac{d\xi}{dx} \right|_i = \frac{1}{\delta_\xi x_i - \frac{h^2}{6} \left. \frac{d^3 x}{d\xi^3} \right|_i + O(h^4)}.$$

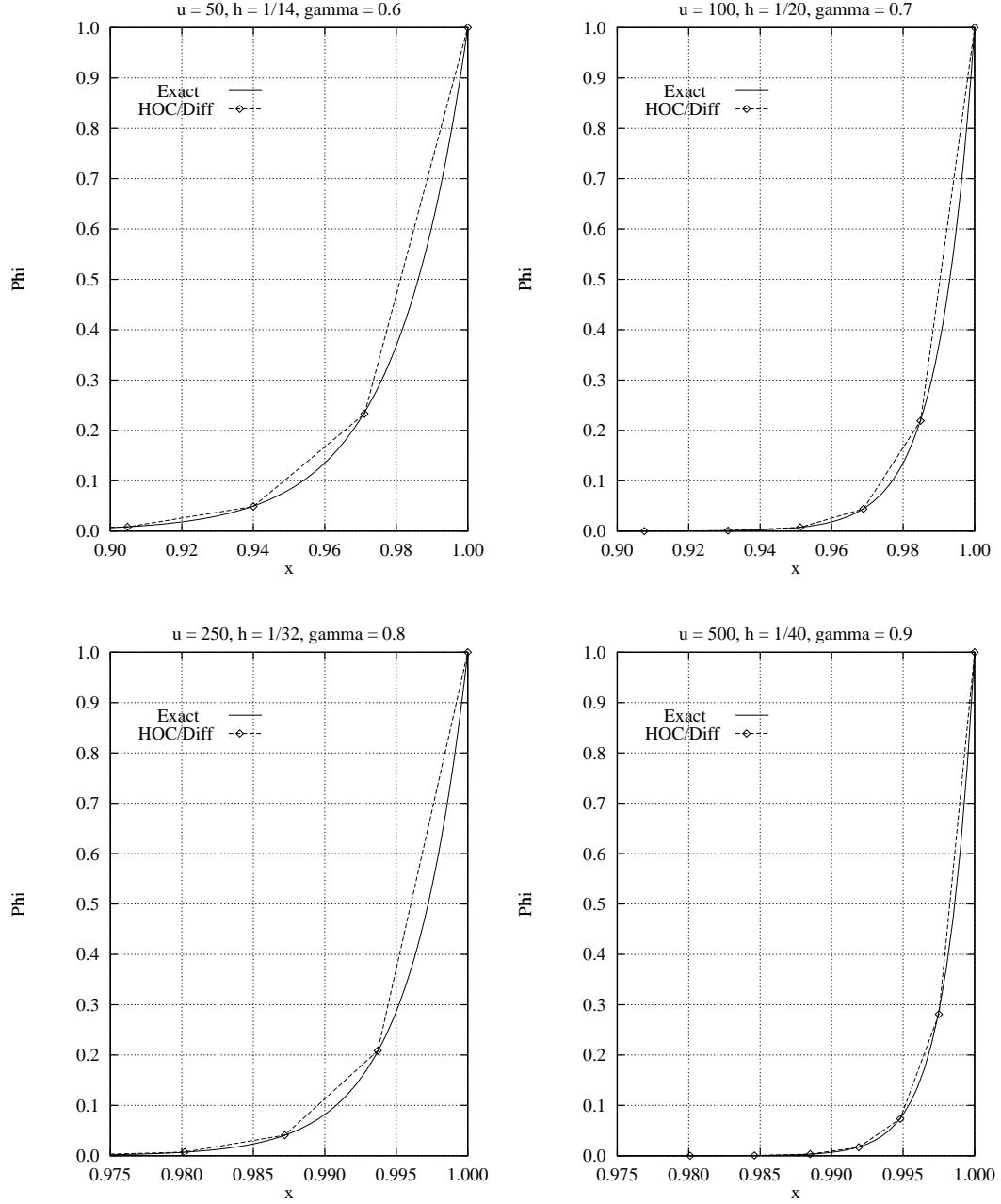


Figure 5.4: Boundary layer results for HOC scheme with differenced metrics.

Using (5.12),

$$\begin{aligned}\left.\frac{d\xi}{dx}\right|_i &= \frac{1}{\delta_\xi x_i - \frac{h^2\pi^2}{6}\left(1 - \frac{dx}{d\xi}\right)_i + O(h^4)}, \\ &= \frac{1}{\left(1 + \frac{h^2\pi^2}{6}\right)\delta_\xi x_i - \frac{h^2\pi^2}{6}} + O(h^4),\end{aligned}\tag{5.13}$$

where we have again used the identity $\frac{1}{1+\epsilon} = 1 - \epsilon + \epsilon^2 - \dots$ to determine the order of magnitude of the truncation error. Similarly, since $\frac{d^2\xi}{dx^2} = \frac{-d^2x/d\xi^2}{(dx/d\xi)^3}$, we can use (5.13) to obtain an $O(h^4)$ approximation to $\frac{d^2\xi}{dx^2}$,

$$\left.\frac{d^2\xi}{dx^2}\right|_i = \frac{-\pi^2(\xi_i - x_i)}{\left[\left(1 + \frac{h^2\pi^2}{6}\right)\delta_\xi x_i - \frac{h^2\pi^2}{6}\right]^3} + O(h^4).\tag{5.14}$$

Before equations (5.13) and (5.14) can be used in (5.4) to recover the optimal $O(h^4)$ result, we must consider the endpoints. Equations (5.5)–(5.8) require that the function c must be differenced in order to apply the HOC scheme on an interior point. The definition of c in (5.4) thus necessitates an approximation of the grid metrics at the endpoints. Fortunately, the form of (5.6)–(5.8) requires only $O(h^2)$ accuracy for the end point metrics in order to maintain an overall $O(h^4)$ method.

Letting δ_ξ^+ represent the forward difference operator,

$$\left.\frac{d\xi}{dx}\right|_i = \frac{1}{\delta_\xi^+ x_i - \frac{h}{2}\left.\frac{d^2x}{d\xi^2}\right|_i} + O(h^2).$$

Using (5.12) again,

$$\left.\frac{d\xi}{dx}\right|_i = \frac{1}{\delta_\xi^+ x_i - \frac{h}{2}\pi^2(\xi_i - x_i)} + O(h^2).$$

At the left endpoint, $i = 1$, and $x_1 = \xi_1 = 0$, so

$$\left.\frac{d\xi}{dx}\right|_1 = \frac{1}{\delta_\xi^+ x_1} + O(h^2),$$

and $\left.\frac{d^2\xi}{dx^2}\right|_1$ can be computed from (5.14). The right endpoint is treated similarly:

$$\left.\frac{d\xi}{dx}\right|_N = \frac{1}{\delta_\xi^- x_N} + O(h^2),$$

where N is the rightmost grid-point and δ_{ξ}^- represents the backward difference operator for the first derivative with respect to ξ .

Figure 5.5 shows the convergence results for the case where the metrics are computed using an auxiliary equation. The HOC method does in fact obtain the optimal $O(h^4)$ result¹.

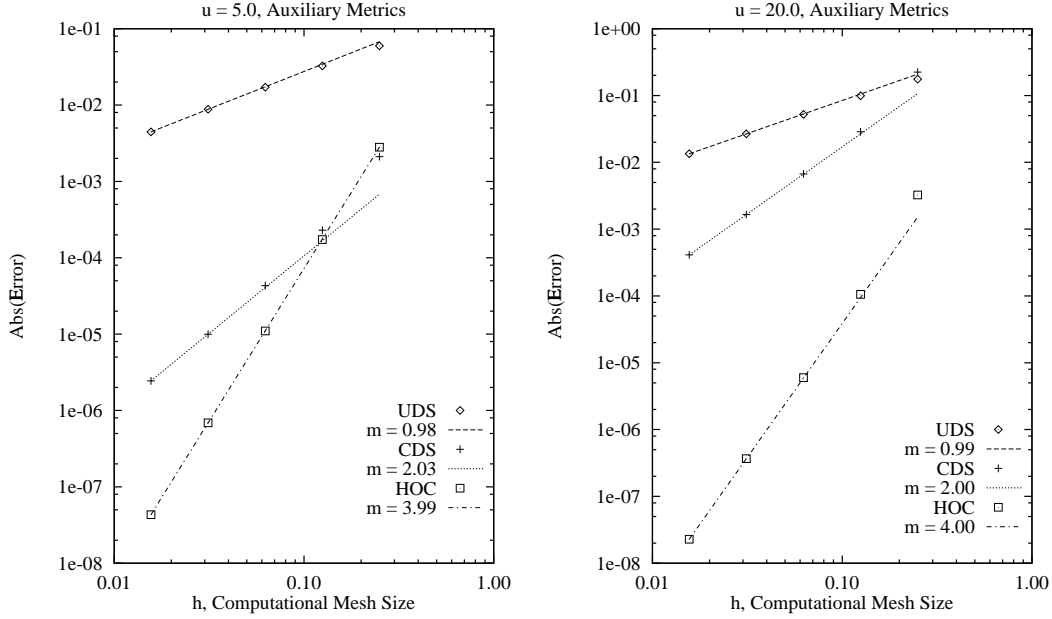


Figure 5.5: Convergence results for 1D convection diffusion on a nonuniform grid with approximated metrics using an auxiliary equation, $u = 5$ and 20 .

5.3 2D Convection Diffusion

This section extends the approach of section 5.2 from 1D to non-uniform grids in 2D. Accordingly, we begin with 2D convection diffusion on the physical domain Ω ,

$$-\left(\frac{\partial^2 \phi}{\partial x^2} + \frac{\partial^2 \phi}{\partial y^2}\right) + u(x, y) \frac{\partial \phi}{\partial x} + v(x, y) \frac{\partial \phi}{\partial y} = f(x, y), \quad (5.15)$$

¹As an alternative to utilizing a relation such as (5.12) in this way, one could simply use more adjacent grid points to approximate the metric derivatives more accurately. While this is counter to the goals of a compact representation, it is acceptable since the grid metric coefficients can be computed explicitly prior to solving the HOC systems.

where u and v are variable convection coefficients and f is the forcing function. We now transform the equation to a computational domain $\hat{\Omega}$ via mapping functions $x = x(\xi, \eta)$ and $y = y(\xi, \eta)$. If we let $\hat{\phi}(\xi, \eta) = \phi(x(\xi, \eta), y(\xi, \eta))$, etc., the transformation of equation (5.15) is

$$a(\xi, \eta) \frac{\partial^2 \hat{\phi}}{\partial \xi^2} + g(\xi, \eta) \frac{\partial^2 \hat{\phi}}{\partial \xi \partial \eta} + b(\xi, \eta) \frac{\partial^2 \hat{\phi}}{\partial \eta^2} + c(\xi, \eta) \frac{\partial \hat{\phi}}{\partial \xi} + d(\xi, \eta) \frac{\partial \hat{\phi}}{\partial \eta} = \hat{f}(\xi, \eta), \quad (5.16)$$

where

$$\begin{aligned} a(\xi, \eta) &= - \left(\frac{\partial \xi}{\partial x} \right)^2 - \left(\frac{\partial \xi}{\partial y} \right)^2, & b(\xi, \eta) &= - \left(\frac{\partial \eta}{\partial x} \right)^2 - \left(\frac{\partial \eta}{\partial y} \right)^2, \\ c(\xi, \eta) &= \hat{u} \frac{\partial \xi}{\partial x} + \hat{v} \frac{\partial \xi}{\partial y} - \frac{\partial^2 \xi}{\partial x^2} - \frac{\partial^2 \xi}{\partial y^2}, & d(\xi, \eta) &= \hat{u} \frac{\partial \eta}{\partial x} + \hat{v} \frac{\partial \eta}{\partial y} - \frac{\partial^2 \eta}{\partial x^2} - \frac{\partial^2 \eta}{\partial y^2}, \\ g(\xi, \eta) &= -2 \left(\frac{\partial \xi}{\partial x} \frac{\partial \eta}{\partial x} + \frac{\partial \xi}{\partial y} \frac{\partial \eta}{\partial y} \right). \end{aligned}$$

There are two significant complications to (5.16) that do not occur in the 1D case (5.3). First, there is now a second-order cross derivative present in the governing equation, that heretofore has not been approximated in an HOC formulation. Second, there are three second-order derivatives to model, each with an independent and variable coefficient, preventing us from scaling the problem to yield a diffusion coefficient of unity. Thus we require a new HOC formulation that is algebraically more complicated than those previously derived.

5.3.1 HOC Formulation

We begin, as always, by applying central differencing to (5.16) at node ij , which gives

$$a_{ij} \delta_\xi^2 \hat{\phi}_{ij} + g_{ij} \delta_\xi \delta_\eta \hat{\phi}_{ij} + b_{ij} \delta_\eta^2 \hat{\phi}_{ij} + c_{ij} \delta_\xi \hat{\phi}_{ij} + d_{ij} \delta_\eta \hat{\phi}_{ij} - \tau_{ij} = \hat{f}_{ij},$$

where the truncation error is

$$\begin{aligned} \tau_{ij} &= \frac{h^2}{12} \left[a \frac{\partial^4 \hat{\phi}}{\partial \xi^4} + 2g \left(\frac{\partial^4 \hat{\phi}}{\partial \xi^3 \partial \eta} + \frac{\partial^4 \hat{\phi}}{\partial \xi \partial \eta^3} \right) + b \frac{\partial^4 \hat{\phi}}{\partial \eta^4} + \right. \\ &\quad \left. 2c \frac{\partial^3 \hat{\phi}}{\partial \xi^3} + 2d \frac{\partial^3 \hat{\phi}}{\partial \eta^3} \right]_{ij} + O(h^4). \end{aligned} \quad (5.17)$$

Note that there are six (6) derivatives in the h^2 -term of the truncation error. HOC theory seeks to find alternative representations for these derivatives by differentiating the governing equation (5.16). Let us begin by differentiating (5.16) with respect to ξ and rearrange to get

$$\begin{aligned} \frac{\partial^3 \hat{\phi}}{\partial \xi^3} = & \frac{1}{a} \left[\frac{\partial \hat{f}}{\partial \xi} - \left(\frac{\partial a}{\partial \xi} + c \right) \frac{\partial^2 \hat{\phi}}{\partial \xi^2} - \left(\frac{\partial g}{\partial \xi} + d \right) \frac{\partial^2 \hat{\phi}}{\partial \xi \partial \eta} - g \frac{\partial^3 \hat{\phi}}{\partial \xi^2 \partial \eta} - \right. \\ & \left. \frac{\partial b}{\partial \xi} \frac{\partial^2 \hat{\phi}}{\partial \eta^2} - b \frac{\partial^3 \hat{\phi}}{\partial \xi \partial \eta^2} - \frac{\partial c}{\partial \xi} \frac{\partial \hat{\phi}}{\partial \xi} - \frac{\partial d}{\partial \xi} \frac{\partial \hat{\phi}}{\partial \eta} \right]. \end{aligned} \quad (5.18)$$

Similarly, with respect to η ,

$$\begin{aligned} \frac{\partial^3 \hat{\phi}}{\partial \eta^3} = & \frac{1}{b} \left[\frac{\partial \hat{f}}{\partial \eta} - \left(\frac{\partial b}{\partial \eta} + d \right) \frac{\partial^2 \hat{\phi}}{\partial \eta^2} - \left(\frac{\partial g}{\partial \eta} + c \right) \frac{\partial^2 \hat{\phi}}{\partial \xi \partial \eta} - g \frac{\partial^3 \hat{\phi}}{\partial \xi \partial \eta^2} - \right. \\ & \left. \frac{\partial a}{\partial \eta} \frac{\partial^2 \hat{\phi}}{\partial \xi^2} - a \frac{\partial^3 \hat{\phi}}{\partial \xi^2 \partial \eta} - \frac{\partial c}{\partial \eta} \frac{\partial \hat{\phi}}{\partial \xi} - \frac{\partial d}{\partial \eta} \frac{\partial \hat{\phi}}{\partial \eta} \right]. \end{aligned} \quad (5.19)$$

Expressions for $a \frac{\partial^4 \hat{\phi}}{\partial \xi^4}$ and $b \frac{\partial^4 \hat{\phi}}{\partial \eta^4}$ are found by differentiating twice and rearranging:

$$\begin{aligned} a \frac{\partial^4 \hat{\phi}}{\partial \xi^4} = & \frac{\partial^2 \hat{f}}{\partial \xi^2} - \left(\frac{\partial^2 a}{\partial \xi^2} + 2 \frac{\partial c}{\partial \xi} \right) \frac{\partial^2 \hat{\phi}}{\partial \xi^2} - \left(2 \frac{\partial a}{\partial \xi} + c \right) \frac{\partial^3 \hat{\phi}}{\partial \xi^3} - \\ & \left(\frac{\partial^2 g}{\partial \xi^2} + 2 \frac{\partial d}{\partial \xi} \right) \frac{\partial^2 \hat{\phi}}{\partial \xi \partial \eta} - \left(2 \frac{\partial g}{\partial \xi} + d \right) \frac{\partial^3 \hat{\phi}}{\partial \xi^2 \partial \eta} - g \frac{\partial^4 \hat{\phi}}{\partial \xi^3 \partial \eta} - \\ & \frac{\partial^2 b}{\partial \xi^2} \frac{\partial^2 \hat{\phi}}{\partial \eta^2} - 2 \frac{\partial b}{\partial \xi} \frac{\partial^3 \hat{\phi}}{\partial \xi \partial \eta^2} - b \frac{\partial^4 \hat{\phi}}{\partial \xi^2 \partial \eta^2} - \frac{\partial^2 c}{\partial \xi^2} \frac{\partial \hat{\phi}}{\partial \xi} - \frac{\partial^2 d}{\partial \xi^2} \frac{\partial \hat{\phi}}{\partial \eta}, \end{aligned} \quad (5.20)$$

$$\begin{aligned} b \frac{\partial^4 \hat{\phi}}{\partial \eta^4} = & \frac{\partial^2 \hat{f}}{\partial \eta^2} - \left(\frac{\partial^2 b}{\partial \eta^2} + 2 \frac{\partial d}{\partial \eta} \right) \frac{\partial^2 \hat{\phi}}{\partial \eta^2} - \left(2 \frac{\partial b}{\partial \eta} + d \right) \frac{\partial^3 \hat{\phi}}{\partial \eta^3} - \\ & \left(\frac{\partial^2 g}{\partial \eta^2} + 2 \frac{\partial c}{\partial \eta} \right) \frac{\partial^2 \hat{\phi}}{\partial \xi \partial \eta} - \left(2 \frac{\partial g}{\partial \eta} + c \right) \frac{\partial^3 \hat{\phi}}{\partial \xi \partial \eta^2} - g \frac{\partial^4 \hat{\phi}}{\partial \xi \partial \eta^3} - \\ & \frac{\partial^2 a}{\partial \eta^2} \frac{\partial^2 \hat{\phi}}{\partial \xi^2} - 2 \frac{\partial a}{\partial \eta} \frac{\partial^3 \hat{\phi}}{\partial \xi^2 \partial \eta} - a \frac{\partial^4 \hat{\phi}}{\partial \xi^2 \partial \eta^2} - \frac{\partial^2 c}{\partial \eta^2} \frac{\partial \hat{\phi}}{\partial \xi} - \frac{\partial^2 d}{\partial \eta^2} \frac{\partial \hat{\phi}}{\partial \eta}. \end{aligned} \quad (5.21)$$

Equations (5.18)–(5.21) provide us with independent substitutions for four of the six derivatives in (5.17), leaving $\frac{\partial^4 \hat{\phi}}{\partial \xi^3 \partial \eta}$ and $\frac{\partial^4 \hat{\phi}}{\partial \xi \partial \eta^3}$ unaccounted for. Unfortunately, there is the potential for only one more auxiliary equation (obtained by differentiating (5.16) by both ξ and η), which is not sufficient to provide compact representations for both of these derivatives, unless some further restriction is placed on

the governing equation. Notice that these terms are scaled by g in (5.20) and (5.21) and that $g = 0$ for orthogonal nonuniform grids. Restricting the formulation to this case we can again construct an HOC representation,

$$A_{ij}\delta_\xi^2\hat{\phi}_{ij} + G_{ij}\delta_\xi\delta_\eta\hat{\phi}_{ij} + B_{ij}\delta_\eta^2\hat{\phi}_{ij} + C_{ij}\delta_\xi\hat{\phi}_{ij} + D_{ij}\delta_\eta\hat{\phi}_{ij} + \frac{h^2}{12} \left[(a_{ij} + b_{ij})\delta_\xi^2\delta_\eta^2\hat{\phi}_{ij} + (2\delta_\eta a_{ij} + d_{ij} + d_{ij}^* a_{ij})\delta_\xi^2\delta_\eta\hat{\phi}_{ij} + \right. \quad (5.22)$$

$$\left. (2\delta_\xi b_{ij} + c_{ij} + c_{ij}^* b_{ij})\delta_\xi\delta_\eta^2\hat{\phi}_{ij} \right] = F_{ij} + O(h^4), \quad (5.23)$$

where the coefficients are given by

$$A_{ij} = a_{ij} + \frac{h^2}{12} \left[\delta_\xi^2 a_{ij} + \delta_\eta^2 a_{ij} + 2\delta_\xi c_{ij} + c_{ij}^* (\delta_\xi a_{ij} + c_{ij}) + d_{ij}^* \delta_\eta a_{ij} \right], \quad (5.24)$$

$$B_{ij} = b_{ij} + \frac{h^2}{12} \left[\delta_\xi^2 b_{ij} + \delta_\eta^2 b_{ij} + 2\delta_\eta d_{ij} + d_{ij}^* (\delta_\eta b_{ij} + d_{ij}) + c_{ij}^* \delta_\xi b_{ij} \right], \quad (5.25)$$

$$C_{ij} = c_{ij} + \frac{h^2}{12} \left[\delta_\xi^2 c_{ij} + \delta_\eta^2 c_{ij} + c_{ij}^* \delta_\xi c_{ij} + d_{ij}^* \delta_\eta c_{ij} \right], \quad (5.26)$$

$$D_{ij} = d_{ij} + \frac{h^2}{12} \left[\delta_\xi^2 d_{ij} + \delta_\eta^2 d_{ij} + c_{ij}^* \delta_\xi d_{ij} + d_{ij}^* \delta_\eta d_{ij} \right], \quad (5.27)$$

$$F_{ij} = \hat{f}_{ij} + \frac{h^2}{12} \left[\delta_\xi^2 \hat{f}_{ij} + \delta_\eta^2 \hat{f}_{ij} + c_{ij}^* \delta_\xi \hat{f}_{ij} + d_{ij}^* \delta_\eta \hat{f}_{ij} \right], \quad (5.28)$$

$$G_{ij} = \frac{h^2}{12} \left[2\delta_\eta c_{ij} + 2\delta_\xi d_{ij} + c_{ij}^* d_{ij} + d_{ij}^* c_{ij} \right], \quad (5.29)$$

with c_{ij}^* and d_{ij}^* given by

$$c_{ij}^* = \frac{c_{ij} - 2\delta_\xi a_{ij}}{a_{ij}},$$

$$d_{ij}^* = \frac{d_{ij} - 2\delta_\xi b_{ij}}{b_{ij}}.$$

Thus we have an HOC approximation to the 2D convection diffusion equation on a nonuniform, orthogonal grid.

Cartesian Grids. If we further restrict the grid to be strictly Cartesian, that is, $x = x(\xi)$ and $y = y(\eta)$ only, we will see some simplification. The mapped

coefficients are now given by

$$\begin{aligned} a &= -\left(\frac{d\xi}{dx}\right)^2, & b &= -\left(\frac{d\eta}{dy}\right)^2, \\ c &= \hat{u}\frac{d\xi}{dx} - \frac{d^2\xi}{dx^2}, & d &= \hat{v}\frac{d\eta}{dy} - \frac{d^2\eta}{dy^2}, \\ g &= 0. \end{aligned}$$

The approximation coefficients, A_{ij} and B_{ij} , also simplify to

$$\begin{aligned} A_{ij} &= a_i + \frac{h^2}{12} \left[\delta_\xi^2 a_i + 2\delta_\xi c_{ij} + c_{ij}^* (\delta_\xi a_i + c_{ij}) \right], \\ B_{ij} &= b_j + \frac{h^2}{12} \left[\delta_\eta^2 b_j + 2\delta_\eta d_{ij} + d_{ij}^* (\delta_\eta b_j + d_{ij}) \right], \end{aligned}$$

while the other coefficients, C_{ij} , D_{ij} , G_{ij} , and F_{ij} remain the same as in (5.26)–(5.29).

Constant Rectangular Grids. If we look at an even simpler class of 2D nonuniform grids, where $\Delta x \neq \Delta y$ are both constants, we see even further simplification to the approximation coefficients (5.24)–(5.29). If we define the cell aspect ratio, $\beta = \frac{\Delta x}{\Delta y}$, then we can let

$$\begin{aligned} x &= x_0 + \xi, \\ y &= y_0 + \frac{1}{\beta}\eta, \end{aligned}$$

where $\Delta x = h$ and $\Delta y = \frac{1}{\beta}h$. The mapping coefficients simplify to

$$\begin{aligned} a &= -1, & b &= -\beta^2, \\ c &= \hat{u}, & d &= \beta\hat{v}, \\ g &= 0. \end{aligned}$$

This leads to approximation coefficients of the form

$$\begin{aligned} A_{ij} &= -1 + \frac{1}{h^2} \left[2\delta_\xi \hat{u}_{ij} + \hat{u}_{ij}^2 \right], \\ B_{ij} &= -\beta^2 + \frac{1}{h^2} \left[2\beta\delta_\eta \hat{v}_{ij} + \left(\frac{\hat{v}_{ij}}{\beta} \right)^2 \right], \end{aligned}$$

$$\begin{aligned}
C_{ij} &= \hat{u}_{ij} + \frac{h^2}{12} \left[\delta_\xi^2 \hat{u}_{ij} + \delta_\eta^2 \hat{u}_{ij} + \hat{u}_{ij} \delta_\xi \hat{u}_{ij} + \frac{\hat{v}_{ij}}{\beta} \delta_\eta \hat{u}_{ij} \right], \\
D_{ij} &= \beta \hat{v}_{ij} + \frac{h^2}{12} \beta \left[\delta_\xi^2 \hat{v}_{ij} + \delta_\eta^2 \hat{v}_{ij} + \hat{u}_{ij} \delta_\xi \hat{v}_{ij} + \frac{\hat{v}_{ij}}{\beta} \delta_\eta \hat{v}_{ij} \right], \\
F_{ij} &= f_{ij} + \frac{h^2}{12} \left[\delta_\xi^2 f_{ij} + \delta_\eta^2 f_{ij} + \hat{u}_{ij} \delta_\xi f_{ij} + \frac{\hat{v}_{ij}}{\beta} \delta_\eta f_{ij} \right], \\
G_{ij} &= \frac{h^2}{12} \left[2\delta_\eta \hat{u}_{ij} + 2\beta \delta_\xi \hat{v}_{ij} + \left(\beta + \frac{1}{\beta} \right) \hat{u}_{ij} \hat{v}_{ij} \right].
\end{aligned}$$

5.3.2 Numerical Studies

To illustrate the 2D nonuniform HOC treatment, consider a 2D convection diffusion test case with solution

$$\phi(x, y) = \frac{(e^u - e^{ux})}{(e^u - 1)} \frac{(e^v - e^{vy})}{(e^v - 1)},$$

which is the tensor product of the compliment of the 1D layer solution given by equation (2.20). Dirichlet data corresponding to this solution is specified on each edge of the unit square and the components of the convection velocity comprise a vector with magnitude 50 at an angle of 45° above the x -axis. By inspection, the solution is close to unity over most of the domain with boundary layers adjacent to sides $x = 1$ and $y = 1$ where the solution decays rapidly to satisfy the boundary condition $\phi = 0$.

Since the test problem has layer behavior on two sides, a nonuniform graded mesh into each layer zone is very appropriate. Accordingly, we take the previous grading function (5.9) in each direction. This generates a tensor-product orthogonal grid that is progressively graded into the two wall layers. As a representative numerical test we set $\gamma = 0.6$ in (5.9) in each direction and solved the problem with the stated velocity vector using 15 grid points in each direction. The solution surface and contours obtained with this HOC scheme are shown in Figure 5.6 and are visually indistinguishable from the exact solution.

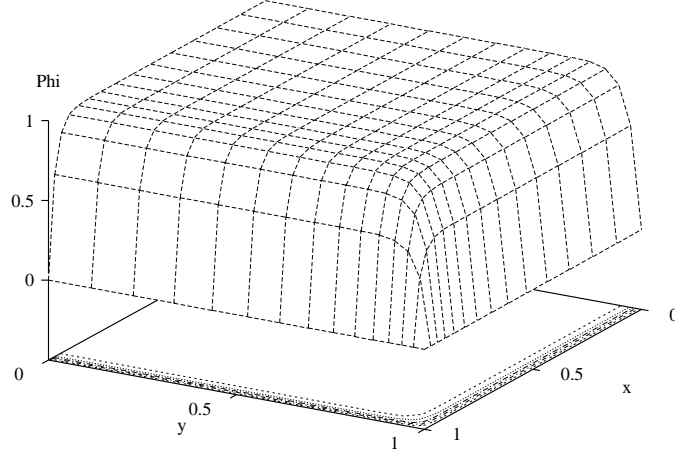


Figure 5.6: Surface and contour plot of the HOC solution to the 2D test problem on a nonuniform grid.

5.4 Summary

HOC methodology has been extended here to nonuniform orthogonal grids. In 1D, we see that the overall accuracy is limited by the accuracy of the mapping derivatives, $\frac{d\xi}{dx}$ and $\frac{d^2\xi}{dx^2}$. A method for deriving HOC mapping derivatives for the case where a differential-equation based grid generator is used was proposed and verified. Non-compact high-order differencing of the grid metrics is also a viable alternative for maintaining overall accuracy. In 2D, a completely new formulation was required to compactly approximate the mapped equation to high-order. It was determined that the grid must be orthogonal, that is, $\frac{d\xi}{dx} \frac{d\eta}{dy} + \frac{d\xi}{dy} \frac{d\eta}{dx} = 0$, in order for the $O(h^4)$ accuracy to be retained.

Chapter 6

Other Extensions to HOC Theory

6.1 Introduction

This chapter covers the extension of HOC schemes to several problem types that have previously not been approximated via HOC methodology. More specifically, Section 6.2 covers transient convection diffusion in 1D. Transient diffusion in 1D and 2D is treated in Sections 6.3 and 6.4. The nonlinear Poisson equation is then considered in Section 6.5 and Section 6.6 covers HOC formulations for the 3D Poisson equation.

6.2 Transient 1D Convection Diffusion

We seek now to explore a means by which existing steady-state HOC theory on uniform grids can be used to develop an HOC approximation to a 1D time-dependent convection diffusion problem. Accordingly, introduce the model equation

$$\frac{\partial \phi}{\partial t} + u \frac{\partial \phi}{\partial x} = a \frac{\partial^2 \phi}{\partial x^2} + S, \quad (6.1)$$

where t is time, a is constant, and $S = S(x)$ or $S = S(x, t)$ is a smooth source term. This can be rewritten conveniently as

$$-\frac{\partial^2 \phi}{\partial x^2} + c \frac{\partial \phi}{\partial x} = f, \quad (6.2)$$

where $c = \frac{u}{a}$ and $f = \frac{1}{a} \left(S - \frac{\partial \phi}{\partial t} \right)$. Since this now has the same form as equation (2.8), we can utilize the previous work to construct a semi-discrete HOC approximation to (6.1).

6.2.1 Semi-Discrete HOC Formulation

The semi-discrete approximation to (6.1) is obtained by taking equation (2.14), the HOC approximation to (6.2), and substituting our new definitions for c and f , which yields

$$\begin{aligned} - \left(1 + \frac{u^2 h^2}{12a^2} \right) \delta_x^2 \phi_i + \frac{u}{a} \delta_x \phi_i &= \frac{1}{a} \left[S_i - \frac{h^2}{12} \left(\frac{u}{a} \delta_x S_i - \delta_x^2 S_i \right) - \right. \\ &\quad \left. \frac{\partial \phi}{\partial t} \Big|_i + \frac{h^2}{12} \frac{\partial}{\partial t} \left(\frac{u}{a} \delta_x \phi_i - \delta_x^2 \phi_i \right) \right] + O(h^4). \end{aligned}$$

This can now be rewritten in the form

$$\begin{aligned} \frac{\partial \phi}{\partial t} \Big|_i - \frac{h^2}{12a} \frac{\partial}{\partial t} \left(u \delta_x \phi_i - a \delta_x^2 \phi_i \right) + u \delta_x \phi_i - \left(a + \frac{u^2 h^2}{12a} \right) \delta_x^2 \phi_i &= \\ S_i - \frac{h^2}{12a} \left(u \delta_x S_i - a \delta_x^2 S_i \right) + O(h^4). \end{aligned} \quad (6.3)$$

6.2.2 Temporal Differencing

Equation (6.3) gives us an expression that is fourth-order in space, but still needs a numerical approximation to the time derivatives. As an example, let us consider a class of time-differencing schemes at time-level n of the form

$$\begin{aligned} \delta_t^+ \phi_i^n - \frac{h^2}{12a} \left(u \delta_t^+ \delta_x \phi_i^n - a \delta_t^+ \delta_x^2 \phi_i^n \right) + (1 - \mu) \left[u \delta_x \phi_i^n - \left(a + \frac{u^2 h^2}{12a} \right) \delta_x^2 \phi_i^n \right] + \\ \mu \left[u \delta_x \phi_i^{n+1} - \left(a + \frac{u^2 h^2}{12a} \right) \delta_x^2 \phi_i^{n+1} \right] = (1 - \mu) \left[S_i^n - \frac{h^2}{12a} \left(u \delta_x S_i^n - a \delta_x^2 S_i^n \right) \right] + \\ \mu \left[S_i^{n+1} - \frac{h^2}{12a} \left(u \delta_x S_i^{n+1} - a \delta_x^2 S_i^{n+1} \right) \right] + O(h^4, \Delta t^p), \end{aligned} \quad (6.4)$$

where

$$\delta_t^+ \phi_i^n = \frac{\phi_i^{n+1} - \phi_i^n}{\Delta t},$$

and $0 \leq \mu \leq 1$. Here $\mu = 0$ corresponds to backward Euler, $\mu = 1$ corresponds to forward Euler, and $\mu = \frac{1}{2}$ corresponds to the trapezoidal rule, or Crank-Nicolson scheme. Crank-Nicolson is second-order accurate with respect to time and the other two schemes are first-order in time.

Note that the operators $\delta_t^+ \delta_x$ and $\delta_t^+ \delta_x^2$ in (6.4) insure that the coefficients for nodes $i \pm 1$ at time level $n + 1$ are non-zero, even if $\mu = 0$. In other words, HOC methods of this class are *implicit*, including forward Euler, similar to the mass matrix effect seen in the finite element method. This implies that certain nonlinear schemes that take advantage of explicit formulations will not be efficient within the HOC framework. This also implies that Runge-Kutta schemes, which require multiple solves (or “stages”) at each time-step, would be expensive.

The lack of an explicit forward-differencing HOC scheme eliminates the only real advantage forward Euler usually has over other time-differencing methods. For this reason it is not recommended, because forward Euler imposes strict stability restrictions on the time step that backward Euler and Crank-Nicolson do not. We now analyse the stability restrictions for the HOC schemes.

6.2.3 Stability Analysis

Appendix B gives a derivation of stability requirements of a general compact finite differencing scheme for a 1D transient problem. The conclusions are summarized here. If a stencil has coefficients as defined in Figure 6.1, we can define

$$d_0 = b_0^2 + (b_1 - b_{-1})^2 - a_0^2 - (a_1 - a_{-1})^2, \quad (6.5)$$

$$d_1 = 2[b_0(b_1 + b_{-1}) - a_0(a_1 + a_{-1})], \quad (6.6)$$

$$d_2 = 4(b_1 b_{-1} - a_1 a_{-1}). \quad (6.7)$$

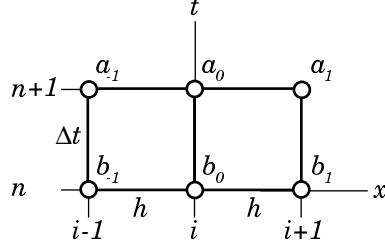


Figure 6.1: General stencil for a compact, 1D time-dependent problem.

We then have for a stable system,

$$d_0 + d_1 + d_2 \equiv 0, \quad (6.8)$$

$$d_1 + 2d_2 \geq 0, \quad (6.9)$$

$$d_1 \geq 0, \quad (6.10)$$

where equation (6.8) is an identity that always holds and we can use as an algebraic check. Relations (6.9)–(6.10) are requirements that we impose to insure stability.

Let us now determine the stability of the HOC scheme (6.4) by computing the corresponding a 's, b 's and d 's for this scheme.

If we introduce the Courant number $C = \frac{u\Delta t}{h}$ and the cell Reynolds number $Re_h = \frac{uh}{a}$, the stencil coefficients for the time-dependent HOC scheme can be expressed as

$$a_{-1} = \frac{1}{12} + \frac{Re_h}{24} - \mu \left(\frac{C}{2} + \frac{C}{Re_h} + \frac{CRe_h}{12} \right), \quad (6.11)$$

$$a_0 = \frac{5}{6} + \mu \left(\frac{2C}{Re_h} + \frac{CRe_h}{6} \right), \quad (6.12)$$

$$a_1 = \frac{1}{12} - \frac{Re_h}{24} + \mu \left(\frac{C}{2} - \frac{C}{Re_h} - \frac{CRe_h}{12} \right), \quad (6.13)$$

$$b_{-1} = \frac{1}{12} + \frac{Re_h}{24} + (1 - \mu) \left(\frac{C}{2} + \frac{C}{Re_h} + \frac{CRe_h}{12} \right), \quad (6.14)$$

$$b_0 = \frac{5}{6} - (1 - \mu) \left(\frac{2C}{Re_h} + \frac{CRe_h}{6} \right), \quad (6.15)$$

$$b_1 = \frac{1}{12} - \frac{Re_h}{24} - (1 - \mu) \left(\frac{C}{2} - \frac{C}{Re_h} - \frac{CRe_h}{12} \right). \quad (6.16)$$

Equations (6.11)–(6.16) are now used to determine the values for d_0 , d_1 and d_2 from (6.5)–(6.7),

$$\begin{aligned} d_0 &= -\frac{10C}{3Re_h} - \frac{CRe_h}{9} + (1 - 2\mu) \left(\frac{4C^2}{Re_h^2} + \frac{5C^2}{3} + \frac{C^2 Re_h^2}{36} \right), \\ d_1 &= \frac{8C}{3Re_h} + \frac{2CRe_h}{9} - (1 - 2\mu) \left(\frac{8C^2}{Re_h^2} + \frac{4C^2}{3} + \frac{C^2 Re_h^2}{18} \right), \\ d_2 &= \frac{2C}{3Re_h} - \frac{Re_h}{9} + (1 - 2\mu) \left(\frac{4C^2}{Re_h^2} - \frac{C^2}{3} + \frac{C^2 Re_h^2}{36} \right). \end{aligned}$$

As an algebraic check, we see that $d_0 + d_1 + d_2$ does in fact equal 0. The first stability criterion (6.9) gives

$$C(1 - 2\mu) \leq \frac{2}{Re_h}. \quad (6.17)$$

The second stability criterion (6.10) gives

$$C(1 - 2\mu) \leq \frac{48Re_h + 4Re_h^2}{144 + 24Re_h^2 + Re_h^4}. \quad (6.18)$$

Note that both (6.17) and (6.18) have the factor $1 - 2\mu$ on the left-hand side and that the right-hand sides are always non-negative, because $Re_h > 0$. As a result, the HOC method is stable for any combination of C and Re_h if $\mu \geq \frac{1}{2}$. Thus Crank-Nicolson and backward Euler are always stable. If $\mu < \frac{1}{2}$, then we have a more complicated stability curve, depicted in Figure 6.2. The crossover point where the two curves meet is at $Re_h = \sqrt{12} \approx 3.46$. Included in the graph for comparison are the well-known stability regions for CDS,

$$\begin{aligned} C(1 - 2\mu) &\leq \frac{2}{Re_h}, \\ C(1 - 2\mu) &\leq \frac{Re_h}{2}, \end{aligned}$$

and for UDS,

$$C(1 - 2\mu) \leq \frac{Re_h}{Re_h + 2}.$$

Unfortunately, the stability region for the HOC scheme is more restricted than both CDS and UDS. Of course, CDS is oscillatory for $Re_h > 2$ and UDS is overly diffusive

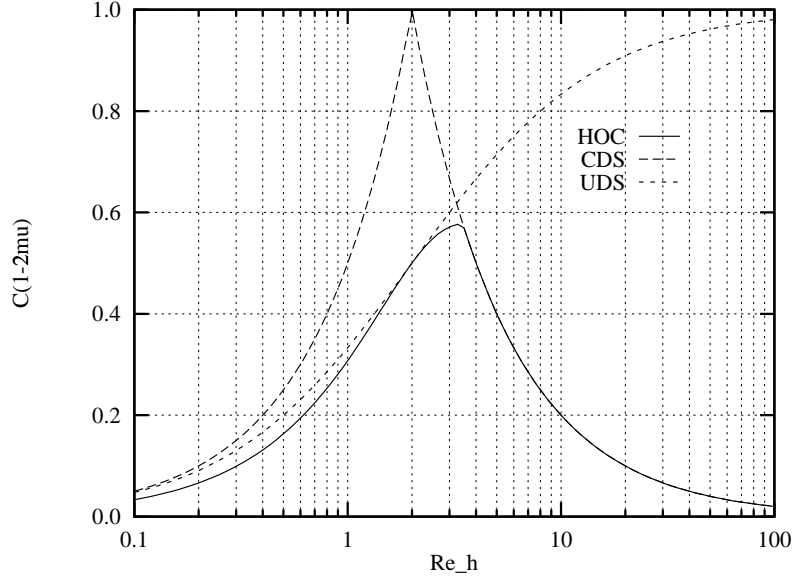


Figure 6.2: Stability restrictions for HOC, CDS and UDS. A scheme is stable in the region below its curve.

for large Re_h . Of course, backward Euler and Crank-Nicolson are unconditionally stable, and require no more work than forward Euler, since HOC schemes are implicit regardless of μ .

6.3 Transient 1D Diffusion

1D time-dependent diffusion is a special case of the previous formulation [simply set $u = 0$ in (6.4)]. It provides a convenient introduction to 2D time-dependent diffusion, and its stability analysis will necessarily be different, because the Courant number and cell Reynolds number are both zero when $u = 0$. Accordingly, let us now consider the transient Poisson equation,

$$\frac{\partial \phi}{\partial t} = a \frac{d^2 \phi}{dx^2} + S. \quad (6.19)$$

As before, we substitute $\frac{1}{a} \left(\frac{\partial \phi}{\partial t} - S \right)$ for f in the 1D HOC approximation to (6.19), and develop a scheme as in Section 6.2.1 to obtain a class of time-

differencing schemes at time-level n of the form

$$\begin{aligned} \delta_t^+ \phi_i^n + \frac{h^2}{12} \delta_t^+ \delta_x^2 \phi_i^n - a(1-\mu) \delta_x^2 \phi_i^n - a\mu \delta_x^2 \phi_i^{n+1} + O(h^4, \Delta t^p) = \\ (1-\mu) \left[S_i^n + \frac{h^2}{12} \delta_x^2 \phi_i^n \right] + \mu \left[S_i^{n+1} + \frac{h^2}{12} \delta_x^2 \phi_i^{n+1} \right], \end{aligned} \quad (6.20)$$

where $0 \leq \mu \leq 1$. Again, $\mu = 0$ corresponds to forward Euler, $\mu = 1$ corresponds to backward Euler, and $\mu = \frac{1}{2}$ corresponds to Crank-Nicolson. The Crank-Nicolson scheme is second-order accurate with respect to time while the other two schemes are first-order in time.

We now investigate the stability of (6.20). Applying the stability analysis of Section 6.2.3, the stencil coefficients are

$$\begin{aligned} a_{-1} = a_1 &= \frac{1}{12} - \mu \frac{a\Delta t}{h^2}, \\ a_0 &= \frac{5}{6} + \mu \frac{2a\Delta t}{h^2}, \\ b_{-1} = b_1 &= \frac{1}{12} + (1-\mu) \frac{a\Delta t}{h^2}, \\ b_0 &= \frac{5}{6} - (1-\mu) \frac{2a\Delta t}{h^2}. \end{aligned}$$

Note that since $u = 0$ for pure diffusion, $C = Re_h = 0$ and we cannot determine our stability region in terms of these quantities. The coefficients d_0 , d_1 and d_2 are given by

$$\begin{aligned} d_0 &= -\frac{10a\Delta t}{h^2} + (1-2\mu) \frac{4a^2\Delta t^2}{h^4}, \\ d_1 &= \frac{8a\Delta t}{3h^2} - (1-2\mu) \frac{8a^2\Delta t^2}{h^4}, \\ d_2 &= \frac{2a\Delta t}{3h^2} + (1-2\mu) \frac{4a^2\Delta t^2}{h^4}. \end{aligned}$$

As an algebraic check we see that $d_0 + d_1 + d_2 = 0$. The first stability requirement, $d_1 + 2d_2 \geq 0$, gives

$$\frac{4a\Delta t}{h^2} \geq 0,$$

which is always true. The second stability requirement, $d_1 \geq 0$, requires

$$\frac{a\Delta t}{h^2} (1-2\mu) \leq \frac{1}{3}. \quad (6.21)$$

Clearly, this puts a restriction on the relative size of Δt and h , depending on μ . Also, as with convection diffusion, if $\mu > \frac{1}{2}$, then the left-hand side of (6.21) is negative, leaving no restrictions on Δt and h . Thus, Crank-Nicolson and backward Euler are both unconditionally stable. If we compare (6.21) to the CDS stability requirement,

$$\frac{a\Delta t}{h^2}(1 - 2\mu) \leq \frac{1}{2},$$

we see that the restriction is slightly smaller for HOC. However, the higher accuracy will allow for larger mesh sizes, that in turn will allow for much larger time steps (since Δt can increase as h^2) that will more than compensate for the small difference in proportionality constants.

6.4 Transient 2D Diffusion

The HOC formulation for the 2D form of (6.19) can be derived in the same manner as (6.20). The result is

$$\begin{aligned} & \delta_t^+ \phi_{ij}^n + \frac{h^2}{12} [\delta_t^+ \delta_x^2 + \delta_t^+ \delta_y^2] \phi_{ij}^n - a(1 - \mu) \left[\delta_x^2 + \delta_y^2 + \frac{h^2}{6} \delta_x^2 \delta_y^2 \right] \phi_{ij}^n - \\ & a\mu \left[\delta_x^2 + \delta_y^2 + \frac{h^2}{6} \delta_x^2 \delta_y^2 \right] \phi_{ij}^{n+1} + O(h^4, \Delta t^p) = \\ & (1 - \mu) \left[S_{ij}^n + \frac{h^2}{12} (\delta_x^2 + \delta_y^2) S_{ij}^n \right] + \mu \left[S_{ij}^{n+1} + \frac{h^2}{12} (\delta_x^2 + \delta_y^2) S_{ij}^{n+1} \right], \end{aligned} \quad (6.22)$$

where p depends on μ as before.

Stability analysis also proceeds as in the 1D case, with the exception that we are looking for a Fourier expansion term of the form

$$\phi_{ij}^n = \alpha^n e^{I\theta_x i} e^{I\theta_y j},$$

where $I = \sqrt{-1}$. Equation (6.22) results in a magnification factor of amplitudes at consecutive time levels given by

$$G = \frac{\alpha^{n+1}}{\alpha^n} = \frac{4 + \cos \theta_x + \cos \theta_y + 4(1 - \mu)(\cos \theta_x \cos \theta_y + 2 \cos \theta_x + 2 \cos \theta_y - 5)}{4 + \cos \theta_x + \cos \theta_y - 4\mu(\cos \theta_x \cos \theta_y + 2 \cos \theta_x + 2 \cos \theta_y - 5)},$$

which has its strictest stability restriction when $\cos \theta_x = \cos \theta_y = -1$, where

$$G = \frac{1 - 16(1 - \mu)\frac{a\Delta t}{h^2}}{1 + 16\mu\frac{a\Delta t}{h^2}}.$$

This leads to an unstable solution whenever

$$\frac{a\Delta t}{h^2}(1 - 2\mu) > \frac{1}{8}. \quad (6.23)$$

We can compare this restriction to the CDS stability restriction for 2D diffusion [6],

$$\frac{a\Delta t}{h^2}(1 - 2\mu) > \frac{1}{4}.$$

Note that as in the 1D case, HOC has a tighter stability restriction, but that the ability to use coarser grids compensates for this and allows larger time-steps. Also, relationship (6.21) is unconditionally stable for $\mu \geq \frac{1}{2}$, just as relationship (6.23).

6.5 Nonlinear Poisson

We now move from the transient problem to the nonlinear steady problem where $f = f(\phi)$ in (2.32). This case is of interest in many reaction-diffusion transport problems. The previous HOC approach is still valid because the key assumption on f was that it was a smooth function of spatial coordinates, and this is still presumed true in the present nonlinear case. The linear case $f = k\phi + g$, where $g = g(x)$ and k is constant can be handled trivially in the previous formulation by simply including $k\phi_{ij}$ in the discrete operator and replacing f by g on the right, prior to approximating the truncation error by differentiating the governing equation. Hence, we will focus on the nonlinear case.

The nonlinear case will require us to use an iterative method such as successive approximation to solve the resulting nonlinear algebraic system. We should also be aware of the possibility of non-unique solutions, but as an introduction of HOC schemes applied to nonlinear problems, such obstacles will not be our primary concern.

To introduce the main ideas in a simple setting let us return to an intermediate step in the development of the HOC scheme for the 1D Poisson equation, in which the truncation error substitution has been made but not approximated,

$$-\delta_x^2 \phi_i = f_i + \frac{h^2}{12} \left. \frac{d^2 f}{dx^2} \right|_i. \quad (6.24)$$

Recall that the $O(h^6)$ approximation would require evaluating the fourth derivative of f in the truncation error. If f is a given analytic function of position then this can be evaluated explicitly. However, in the nonlinear problem, this is not the case and hence a compact $O(h^6)$ scheme cannot generally be constructed.

The simplest approach for formulating an HOC approximation to (6.24) is to substitute $\delta_x^2 f_i$ for $\left. \frac{d^2 f}{dx^2} \right|_i$ in (6.24) to obtain our familiar HOC formulation,

$$-\delta_x^2 \phi_i + O(h^4) = f_i + \frac{h^2}{12} \delta_x^2 f_i,$$

and successively approximate the solution by lagging the right-hand side. Alternatively, we could apply Newton's method to the HOC scheme. This approach generally has much better convergence properties than successive approximation and will be described in the following section.

Instead of the above approach, we could recognize that

$$\frac{d^2 f}{dx^2} = f'' \left(\frac{d\phi}{dx} \right)^2 + f' \frac{d^2 \phi}{dx^2},$$

where the prime ($'$) indicates differentiation with respect to ϕ . We could substitute this term into (6.24) and again apply successive approximation or Newton's method. However, it is not clear that we gain anything by making this substitution. If $f(\phi)$ has a simple analytical form (for example, ϕ^2), then this approach may allow even higher-order formulations, but for a general f this is not the case. Hence, we opt for the simpler formulation.

We choose to apply Newton's method to our HOC schemes in order to converge to an approximate solution. In general, a set of nonlinear algebraic equations

$$g_i(\phi) = 0,$$

where $i = 1, 2, \dots, N$ and $\phi = \{\phi_1, \phi_2, \dots, \phi_N\}$ can be updated from an initial guess or previous iterate by solving the Jacobian system

$$\sum_{j=1}^N \left(\frac{\partial g_i}{\partial \phi_j} \right)^{(n)} \Delta \phi_j = -g_i(\phi^{(n)}), \quad i = 1, 2, \dots, N,$$

at each Newton iterate $n = 0, 1, 2, \dots$ for

$$\Delta \phi_j = \phi_j^{(n+1)} - \phi_j^{(n)}.$$

This procedure can be continued until $\Delta \phi_j$ or g_i (or both) is smaller than some prescribed convergence tolerance.

For the HOC scheme for the 1D Poisson equation, we can define g_i to be

$$g_i(\phi) = \delta_x^2 \phi_i + f_i + \frac{h^2}{12} \delta_x^2 f_i = 0,$$

which results in a tridiagonal Jacobian of the form

$$\begin{aligned} \frac{\partial g_i}{\partial \phi_{i-1}} &= \frac{1}{h^2} + \frac{f'_{i-1}}{12}, \\ \frac{\partial g_i}{\partial \phi_i} &= -\frac{2}{h^2} + \frac{5}{6} f'_i, \\ \frac{\partial g_i}{\partial \phi_{i+1}} &= \frac{1}{h^2} + \frac{f'_{i+1}}{12}, \end{aligned}$$

where f' is defined to be $\frac{df}{d\phi}$.

The 2D Poisson equation has a fourth-order compact approximation given by (2.38). If we define g_{ij} in the same manner as we just defined g_i , the nine non-zero Jacobian matrix coefficients are given by

$$\begin{aligned} \frac{\partial g_{i,j}}{\partial \phi_{i,j}} &= -\frac{10}{3h^2} + \frac{2}{3} f'_{i,j}, \\ \frac{\partial g_{i,j}}{\partial \phi_{i\pm 1,j}} &= \frac{2}{3h^2} + \frac{1}{12} f'_{i\pm 1,j}, \\ \frac{\partial g_{i,j}}{\partial \phi_{i,j\pm 1}} &= \frac{2}{3h^2} + \frac{1}{12} f'_{i,j\pm 1}, \\ \frac{\partial g_{i,j}}{\partial \phi_{i\pm 1,j\pm 1}} &= \frac{1}{6h^2}. \end{aligned}$$

6.6 3D Linear Poisson

The relative simplicity of the Poisson equation makes it a good candidate for our first attempt at an HOC scheme in 3D. The central difference scheme for (2.32) in 3D is

$$-\delta_x^2 \phi_{ijk} - \delta_y^2 \phi_{ijk} - \delta_z^2 \phi_{ijk} - \tau_{ijk} = f_{ijk}, \quad (6.25)$$

where the truncation error has the form

$$\begin{aligned} \tau_{ijk} = & -\frac{h^2}{12} \left[\frac{\partial^4 \phi}{\partial x^4} + \frac{\partial^4 \phi}{\partial y^4} + \frac{\partial^4 \phi}{\partial z^4} \right]_{ijk} - \\ & \frac{h^4}{360} \left[\frac{\partial^6 \phi}{\partial x^6} + \frac{\partial^6 \phi}{\partial y^6} + \frac{\partial^6 \phi}{\partial z^6} \right]_{ijk} + O(h^6). \end{aligned} \quad (6.26)$$

As in section 2.5, we have included both $O(h^2)$ and $O(h^4)$ terms in (6.26) because we wish to approximate all of them in order to yield an $O(h^6)$ scheme. Also note that (6.25) is a 7-point stencil, as illustrated in Figure 6.3, in which the resulting matrix coefficients for the neighboring grid points are also displayed.

6.6.1 HOC Formulation

To obtain compact approximations to the $O(h^2)$ terms in (6.26), we take the appropriate derivatives of (2.32) to write

$$\frac{\partial^4 \phi}{\partial x^4} = -\frac{\partial^2 f}{\partial x^2} - \frac{\partial^4 \phi}{\partial x^2 \partial y^2} - \frac{\partial^4 \phi}{\partial x^2 \partial z^2}, \quad (6.27)$$

$$\frac{\partial^4 \phi}{\partial y^4} = -\frac{\partial^2 f}{\partial y^2} - \frac{\partial^4 \phi}{\partial x^2 \partial y^2} - \frac{\partial^4 \phi}{\partial y^2 \partial z^2}, \quad (6.28)$$

$$\frac{\partial^4 \phi}{\partial z^4} = -\frac{\partial^2 f}{\partial z^2} - \frac{\partial^4 \phi}{\partial x^2 \partial z^2} - \frac{\partial^4 \phi}{\partial y^2 \partial z^2}. \quad (6.29)$$

Substituting (6.27)–(6.29) into (6.26), we obtain

$$\begin{aligned} \tau_{ijk} = & \frac{h^2}{12} \nabla^2 f_{ijk} + \frac{h^2}{6} \left[\frac{\partial^4 \phi}{\partial x^2 \partial y^2} + \frac{\partial^4 \phi}{\partial y^2 \partial z^2} + \frac{\partial^4 \phi}{\partial x^2 \partial z^2} \right]_{ijk} - \\ & \frac{h^4}{360} \left[\frac{\partial^6 \phi}{\partial x^6} + \frac{\partial^6 \phi}{\partial y^6} + \frac{\partial^6 \phi}{\partial z^6} \right]_{ijk} + O(h^6). \end{aligned} \quad (6.30)$$

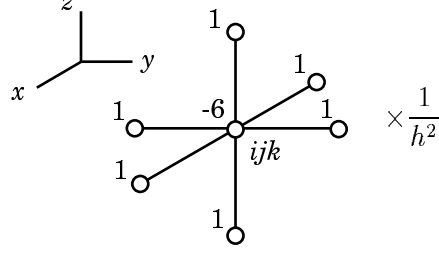


Figure 6.3: 7-Point CDS stencil for the 3D Laplace operator, shown with corresponding matrix coefficients.

The $O(h^4)$ approximation is therefore

$$\begin{aligned}
 -\delta_x^2 \phi_{ijk} - \delta_y^2 \phi_{ijk} - \delta_z^2 \phi_{ijk} - \frac{h^2}{6} \left[\delta_x^2 \delta_y^2 \phi_{ijk} + \delta_y^2 \delta_z^2 \phi_{ijk} + \delta_x^2 \delta_z^2 \phi_{ijk} \right] = \\
 f_{ijk} + \frac{h^2}{12} \left[\delta_x^2 f_{ijk} + \delta_y^2 f_{ijk} + \delta_z^2 f_{ijk} \right] + O(h^4) \quad (6.31)
 \end{aligned}$$

Note that (6.31) corresponds to a 19-point stencil, encompassing all the adjacent nodes of the mesh located on the three grid planes that intersect the node ijk , but not the corner points of the surrounding cube. This stencil and its matrix coefficients are illustrated in Figure 6.4. This is also the stencil shape a 3D, HOC *convection* diffusion approximation would take.

Again, as with the 2D case, we want to obtain a compact $O(h^6)$ approximation if one is possible. Substituting the finite difference expressions for the cross derivatives of ϕ and their truncation error terms into (6.30) gives us

$$\begin{aligned}
 \tau_{ijk} = & \frac{h^2}{12} \nabla^2 f_{ijk} + \frac{h^2}{6} \left[\delta_x^2 \delta_y^2 \phi_{ijk} + \delta_y^2 \delta_z^2 \phi_{ijk} + \delta_x^2 \delta_z^2 \phi_{ijk} \right] - \\
 & \frac{h^4}{72} \left[\frac{\partial^6 \phi}{\partial x^4 \partial y^2} + \frac{\partial^6 \phi}{\partial x^2 \partial y^4} + \frac{\partial^6 \phi}{\partial y^4 \partial z^2} + \frac{\partial^6 \phi}{\partial y^2 \partial z^4} + \frac{\partial^6 \phi}{\partial x^4 \partial z^2} + \frac{\partial^6 \phi}{\partial x^2 \partial z^4} \right]_{ijk} - \\
 & \frac{h^4}{360} \left[\frac{\partial^6 \phi}{\partial x^6} + \frac{\partial^6 \phi}{\partial y^6} + \frac{\partial^6 \phi}{\partial z^6} \right]_{ijk} + O(h^6), \quad (6.32)
 \end{aligned}$$

Clearly, to get a *compact* $O(h^6)$ approximation, we require compact expressions for the partial derivatives of order six in (6.32). Although more complicated than the

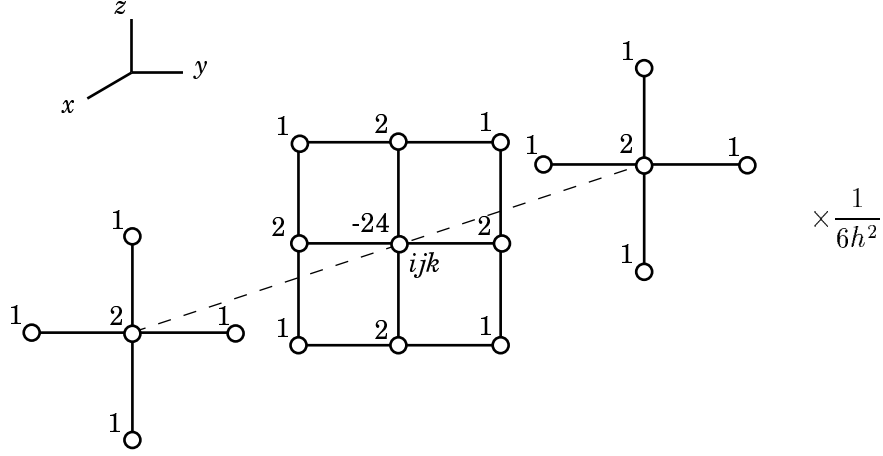


Figure 6.4: 19-Point $O(h^4)$ HOC stencil for the 3D Laplace operator, shown with corresponding matrix coefficients.

2D case, this can actually be done by further differentiating (2.32). The required expressions are

$$\frac{\partial^6 \phi}{\partial x^6} = -\frac{\partial^4 f}{\partial x^4} - \frac{\partial^6 \phi}{\partial x^4 \partial y^2} - \frac{\partial^6 \phi}{\partial x^4 \partial z^2}, \quad (6.33)$$

$$\frac{\partial^6 \phi}{\partial y^6} = -\frac{\partial^4 f}{\partial y^4} - \frac{\partial^6 \phi}{\partial x^2 \partial y^4} - \frac{\partial^6 \phi}{\partial y^4 \partial z^2}, \quad (6.34)$$

$$\frac{\partial^6 \phi}{\partial z^6} = -\frac{\partial^4 f}{\partial z^4} - \frac{\partial^6 \phi}{\partial x^2 \partial z^4} - \frac{\partial^6 \phi}{\partial y^2 \partial z^4}, \quad (6.35)$$

and

$$\frac{\partial^6 \phi}{\partial x^2 \partial y^2 \partial z^2} = -\frac{\partial^4 f}{\partial y^2 \partial z^2} - \frac{\partial^6 \phi}{\partial y^4 \partial z^2} - \frac{\partial^6 \phi}{\partial y^2 \partial z^4}, \quad (6.36)$$

$$\frac{\partial^6 \phi}{\partial x^2 \partial y^2 \partial z^2} = -\frac{\partial^4 f}{\partial x^2 \partial z^2} - \frac{\partial^6 \phi}{\partial x^4 \partial z^2} - \frac{\partial^6 \phi}{\partial x^2 \partial z^4}, \quad (6.37)$$

$$\frac{\partial^6 \phi}{\partial x^2 \partial y^2 \partial z^2} = -\frac{\partial^4 f}{\partial x^2 \partial y^2} - \frac{\partial^6 \phi}{\partial x^4 \partial y^2} - \frac{\partial^6 \phi}{\partial x^2 \partial y^4}. \quad (6.38)$$

The key here is that using (6.33)–(6.38), we can algebraically eliminate all the derivatives of ϕ in (6.32) except for $\frac{\partial^6 \phi}{\partial x^2 \partial y^2 \partial z^2}$, which has a compact approximation! (See Table 6.1 for its definition.) This operator brings the eight corner points into

Table 6.1: Definition of 3D Cross Derivative δ -Operator on a Uniform Mesh

Operator	Formula
$\delta_x^2 \delta_y^2 \delta_z^2 \phi_{ijk}$	$ \begin{aligned} & \frac{-8\phi_{ijk}}{h^6} + \\ & \frac{4(\phi_{i-1,j,k} + \phi_{i+1,j,k} + \phi_{i,j-1,k} + \phi_{i,j+1,k} + \phi_{i,j,k-1} + \phi_{i,j,k+1})}{h^6} + \\ & \frac{-2(\phi_{i,j-1,k-1} + \phi_{i,j+1,k-1} + \phi_{i-1,j,k-1} + \phi_{i+1,j,k-1} + \phi_{i-1,j-1,k} + \phi_{i+1,j-1,k} + \phi_{i+1,j+1,k})}{h^6} + \\ & -2 \frac{(\phi_{i-1,j+1,k} + \phi_{i,j-1,k+1} + \phi_{i,j+1,k+1} + \phi_{i-1,j,k+1} + \phi_{i+1,j,k+1})}{h^6} + \\ & \frac{\phi_{i-1,j-1,k-1} + \phi_{i+1,j-1,k-1} + \phi_{i-1,j+1,k-1} + \phi_{i+1,j+1,k-1}}{h^6} + \\ & \frac{\phi_{i-1,j-1,k+1} + \phi_{i+1,j-1,k+1} + \phi_{i-1,j+1,k+1} + \phi_{i+1,j+1,k+1}}{h^6} \end{aligned} $

our $O(h^6)$ approximation, which follows from

$$\begin{aligned}
 -\delta_x^2 \phi_{ijk} + \delta_y^2 \phi_{ijk} + \delta_z^2 \phi_{ijk} + \frac{h^2}{6} \left[\delta_x^2 \delta_y^2 \phi_{ijk} + \delta_y^2 \delta_z^2 \phi_{ijk} + \delta_x^2 \delta_z^2 \phi_{ijk} \right] + \\
 \frac{h^4}{30} \delta_x^2 \delta_y^2 \delta_z^2 \phi_{ijk} = f_{ijk} + \frac{h^2}{12} \nabla^2 f_{ijk} + \frac{h^4}{360} \nabla^4 f_{ijk} + \quad (6.39) \\
 \frac{h^4}{180} \left(\frac{\partial^4 f}{\partial x^2 \partial y^2} + \frac{\partial^4 f}{\partial y^2 \partial z^2} + \frac{\partial^4 f}{\partial x^2 \partial z^2} \right)_{ijk} + O(h^6).
 \end{aligned}$$

Note that the derivatives of f of fourth order in (6.39) cannot be differenced compactly. Thus, these terms must be known analytically or at least to $O(h^2)$ accuracy to achieve $O(h^6)$ convergence. If these terms are not known, we are forced to resort to (6.31). The $O(h^6)$ stencil in (6.39) involves all 27 grid points, depicted in Figure 6.5.

6.6.2 Global Error Norm

Previously in this dissertation, convergence with respect to mesh size has been determined by measuring the error at a grid-point common to a series of increasingly fine meshes. We wish now to examine a different measure of the error, for two reasons. First, successively halving the mesh size in 3D quickly produces extremely large problems which we wish to avoid. Second, we wish to demonstrate that a global measure of the error also exhibits high-order convergence for HOC methods.

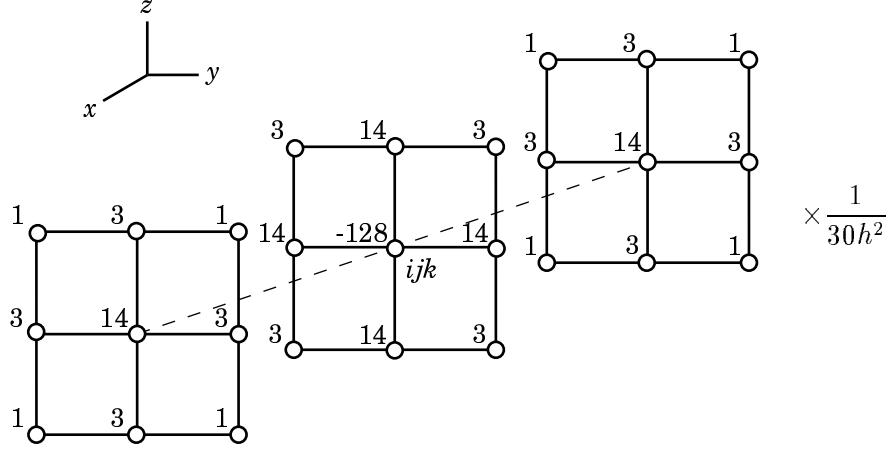


Figure 6.5: 27-Point $O(h^6)$ HOC stencil for the 3D Laplace operator, shown with corresponding matrix coefficients.

Accordingly, first note that the numerical schemes in this work generate a class of linear systems that can be expressed in exact form as

$$\mathbf{M}_m \boldsymbol{\phi} = \mathbf{f}_m - \sum_{p=m}^{\infty} \mathbf{c}_p h^p, \quad (6.40)$$

where m is the order of accuracy of the approximation scheme, \mathbf{M}_m is the coefficient matrix, $\boldsymbol{\phi}$ is the vector of nodal unknowns, $\{\mathbf{c}_p\}$ are truncation error coefficient vectors, and \mathbf{f}_m is the right-hand-side vector. Of course, we do not solve (6.40), but rather the approximate equation,

$$\mathbf{M}_m \boldsymbol{\phi}_h = \mathbf{f}_m.$$

For computations in exact arithmetic, the error then satisfies

$$\mathbf{e} = \boldsymbol{\phi}_h - \boldsymbol{\phi} = \sum_{p=m}^{\infty} \mathbf{M}_m^{-1} \mathbf{c}_p h^p.$$

Dropping the higher-order terms, we see that

$$\mathbf{e} \approx \mathbf{M}_m^{-1} \mathbf{c}_m h^m, \quad (6.41)$$

and we expect the asymptotic behavior of the error at interior node ijk to be $e_{ijk} \sim O(h^m)$ in the limit as $h \rightarrow 0$, as has been demonstrated here in 1D and 2D.

If, however, we desire an estimate of a global measure of the error, we can take some appropriate norm of (6.41),

$$E = \|\mathbf{e}\| \approx \|\mathbf{M}_m^{-1} \mathbf{c}_m\| h^m,$$

and provided $\|\mathbf{M}_m^{-1} \mathbf{c}_m\|$ is *independent* of h , the convergence rate of the global error in this norm is then also $O(h^m)$. Finding such a norm is not trivial, however, since we are comparing measures of error among different-sized vector spaces. Consider the simple distance norm ($\|\cdot\|_d$) for the error on a uniform 3D mesh of N total grid points,

$$\begin{aligned} \|\mathbf{e}\|_d &= \left(\sum_{ijk} e_{ijk}^2 \right)^{1/2}, \\ &= \left[N \times O(h^{2m}) \right]^{1/2}. \end{aligned}$$

But we know that $N = O(h^{-3})$ for a uniform 3D mesh, so it follows that

$$\|\mathbf{e}\|_d = O(h^{m-3/2}).$$

We therefore choose the discrete L^2 norm (for example, see [156]),

$$\|\mathbf{e}\| \equiv \left(\frac{\sum_{ijk} e_{ijk}^2}{N} \right)^{1/2}, \tag{6.42}$$

as the definition of our norm for the purposes of convergence analysis.

6.6.3 Numerical Experiments

We now carry out numerical experiments for some representative test problems to verify the $O(h^4)$ and $O(h^6)$ theoretical estimates for the above schemes in (6.31) and (6.39).

Problem 1. As a first test case consider (2.32) in $(0,1)^3$ with $f = 0$ and boundary conditions

$$\begin{aligned}\phi &= \sin \pi y \sin \pi z, & x &= 0, \\ \phi &= 2 \sin \pi y \sin \pi z, & x &= 1, \\ \phi &= 0, & y, z &= \{0, 1\}.\end{aligned}$$

The exact solution is

$$\phi = \frac{\sin \pi y \sin \pi z}{\sinh \pi \sqrt{2}} \left[2 \sinh(\pi \sqrt{2} x) + \sinh(\pi \sqrt{2}(1 - x)) \right].$$

We solved this problem on a series of meshes, $h = \frac{1}{2}, \frac{1}{4}, \frac{1}{6}, \frac{1}{8}$, and $\frac{1}{10}$ and computed the norm defined in (6.42) of the exact error. The results for the CDS, fourth-order compact (HOC4), and sixth-order compact (HOC6) schemes are presented in Figure 6.6(a). The rates of convergence were as predicted.

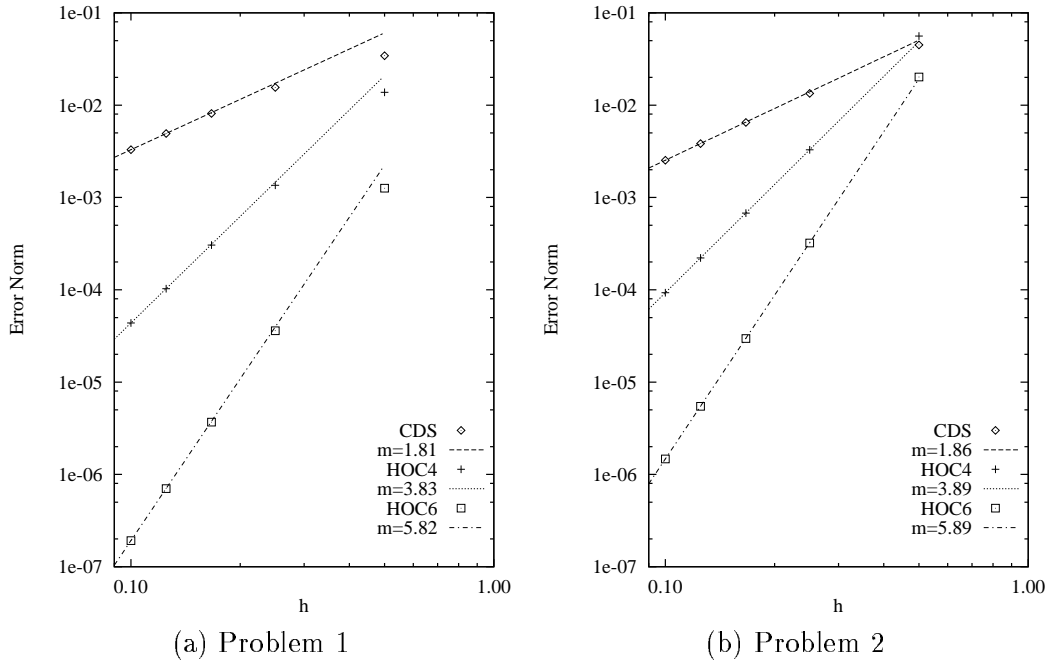


Figure 6.6: Convergence rates for 3D model problems, (a) Problem 1, (b) Problem 2.

Problem 2. As a second test case we constructed a problem with a non-zero forcing function. For the same domain Ω as before with $\phi = 0$ on the entire boundary $\partial\Omega$ and forcing function

$$f = -3\pi^2 \sin \pi x \sin \pi y \sin \pi z,$$

the exact solution to (2.32) is

$$\phi = \sin \pi x \sin \pi y \sin \pi z.$$

The results for the same sequence of meshes as for Problem 1 are presented in Figure 6.6(b). Again, the predicted convergence rates were achieved.

6.7 Summary

This chapter has covered the extension of HOC theory to a number of new problem types, including transient convection diffusion, nonlinear Poisson, and 3D linear Poisson problems. The transient problems were expressed in HOC semi-discrete form, from which any number of different time-marching techniques could be employed. As an example, we integrated the approximations in time by simple differencing, although other more complicated techniques might be more appropriate. For example, the Lax-Wendroff method would be consistent with the HOC methodology, and Runge-Kutta would yield temporal truncation errors of the same order as the spatial truncation errors. Nevertheless, the differencing formulas illustrate general aspects of transient HOC schemes. For example, most time-marching HOC schemes are implicit, even forward Euler. The stability criteria developed for 1D and 2D problems are technically more restrictive than criteria for other schemes, but the higher spatial accuracy allows for coarser grids that in turn allow larger time steps than other schemes.

A simple class of nonlinear reaction-diffusion problems, where the forcing function is a nonlinear function of ϕ was considered. The HOC formulation was

developed, and the Newton method was applied as an example of a representative iterative scheme.

The last extension considered was the 3D linear Poisson problem. Because of the computational cost restrictions imposed by 3D problems, these may be the avenue of greatest promise for HOC schemes, but the algebraic complexity of developing such schemes is formidable. This formulation should be seen as a first step towards developing a broader class of HOC schemes in 3D. The results obtained were similar to 2D Poisson, in which an $O(h^4)$ scheme was achievable for any forcing function, and an $O(h^6)$ scheme was obtained for the case when the fourth derivatives of the forcing function were known.

Chapter 7

Conclusions

This dissertation involves the development and extension of HOC finite difference theory for boundary value problems in computational mechanics. To illustrate the benefits of the approach, the HOC scheme has been applied successfully to convection diffusion problems and the (ψ, ζ) form of the 2D, incompressible Navier-Stokes equations. An analysis of convergence properties, as well as the application of HOC methods to nonuniform grids, transient problems, nonlinear problems, and 3D problems were also considered.

The (ψ, ζ) formulation also required development of new HOC expressions for the velocity components and wall boundary conditions. Numerical results demonstrated that the fourth-order BCs can be oscillatory for a moving wall (such as in the driven cavity problem), but are non-oscillatory for stationary walls. The $O(h^3)$ BC formulation is non-oscillatory and can be used when appropriate. Comparison of coarse grid HOC results for the vorticity and velocity components compare favorably with fine grid results in the literature.

Analysis of the matrix properties of HOC schemes revealed that the condition number (in 1D) is predicted to be higher than for CDS and UDS for all values of the cell Reynolds number, suggesting that HOC systems are harder to solve. However, computational experiments indicated that HOC matrices remain positive

definite, thus making them viable candidates for gradient-type iterative solvers. Furthermore, experiments with conjugate gradient and diagonally scaled bi-conjugate gradient resulted in *faster* convergence for HOC matrices than CDS and UDS, possibly indicating that HOC eigenvalues are more tightly clustered or that diagonal scaling is a particularly good preconditioner for HOC matrices.

HOC schemes were formulated for the convection diffusion equation on nonuniform grids via mapping functions for the first time. The 1D case was instructive for demonstrating that the overall accuracy of the method is restricted to the accuracy to which the mapping derivatives are known. A method for computing HOC metrics was presented for the case where the mapping functions satisfy a differential equation (as is the case for grids created by a Helmholtz grid generator). Without this type of extra knowledge, users will be forced to use non-compact differencing to obtain high-order accurate grid metrics. The HOC formula for the 2D convection diffusion equation on nonuniform grids is one of the most complicated ever developed to date, and it was found that fourth-order accuracy is restricted to problems solved on orthogonal grids. Grids that meet this restriction still face the metric pollution problem if the mapping derivatives are not known to sufficient accuracy.

HOC schemes were also extended to transient problems by using existing HOC theory to develop a semi-discrete formulation. Any type of time-marching scheme could then be used, although the semi-discrete form indicates that explicit HOC schemes will be difficult to obtain. As an example of a time-marching method, simple weighted temporal differencing (allowing for the study of forward and backward Euler, as well as Crank-Nicolson) was applied. It was found that forward Euler and Crank-Nicolson are always stable, but if the weighting factor $\mu < \frac{1}{2}$, then a slightly more restrictive stability requirement is imposed on HOC schemes as compared to CDS and UDS. Of course, the allowance for coarser grids when using the HOC scheme alleviates this restriction.

Possible approaches to solving the nonlinear Poisson problem, where the

forcing function f is a nonlinear function of the solution ϕ (such as occur in many reaction-diffusion transport problems), were proposed. Simple formulas for the Newton method applied the the HOC approximation to 1D and 2D problems were developed.

Finally, the HOC methodology was applied to a 3D linear Poisson problem. As with 2D Poisson, $O(h^6)$ accuracy is obtainable if the fourth derivatives of the forcing function are known by using a full 27-point compact stencil. If not, a 19-point $O(h^4)$ scheme is available for any forcing function.

This dissertation has shown that problems with smooth problem data that can be discretized with (orthogonal) structured meshes can be solved to great accuracy with HOC schemes. More importantly, these problems can be solved to much lower (but still acceptable) accuracy on extremely coarse grids compared to more standard schemes. This savings in computer memory, computational effort and time make HOC schemes an attractive choice for appropriate problems.

Still, HOC schemes have not gained widespread popularity, possibly due to two overriding concerns. One, the class of problems to which HOC schemes could be applied was somewhat narrow, largely because of grid restrictions and regularity requirements for the solution and problem data, and two, the algebraic complexity of deriving HOC schemes for a given problem can be daunting. Hopefully, this dissertation has addressed the first concern and provided an expanded set of HOC approximations that will be of use to researchers. As to the second concern, it would appear that automation of the algebraic process of deriving HOC schemes would be the avenue of greatest promise. This might be possible with the use of existing symbolic manipulation software products such as MACSYMA [116], MATHEMATICA [150], or MAPLE [23], although successful automation has not yet been achieved.

This dissertation has attempted to expand the set of problems that can be solved using HOC finite difference schemes, but many more areas could be studied to expand this set even further. Accordingly, I suggest the following recommendations

for further study:

Mixed methods. Breaking a problem into a lower-order system with simpler relationships will provide additional auxiliary equations and should make algebraic substitutions less complicated.

Boundary conditions. HOC theory should provide for a wider range of boundary conditions, which could be approached in the same manner as the HOC (ψ, ζ) wall BCs.

Fourth-order wall boundary conditions. It may be possible to obtain non-oscillatory, compact, $O(h^4)$ wall boundary conditions on a moving wall. For example, the convective term in the fourth-order wall boundary condition could be upwinded to suppress oscillations while maintaining $O(h^4)$ accuracy.

Nonuniform stream-function vorticity. The HOC (ψ, ζ) theory and nonuniform grid theory should be combined. The formulas for the transport equations are already constructed, but the velocity relationships and wall boundary conditions still need to be modified for nonuniform grids.

Material discontinuities. Although this problem was partially addressed in [86], whether or not $O(h^4)$ accuracy can be achieved (or under what conditions) is still an open question.

Time-marching. More advanced (and higher accurate) time-marching schemes should be analyzed.

Symbolic manipulators. More work should be done to automate or at least aid the process of constructing HOC schemes.

Nonorthogonal grids. Mixed methods *might* provide a means to construct an HOC scheme for nonorthogonal grids. Alternatively, the scheme presented in this dissertation might be extended and tested on nonorthogonal grids to determine if the resulting numerical pollution is significant.

Flux limiters. How HOC approximations could be used in the context of flux-limiting and other schemes (such as TVD) should be studied.

Appendix A

Truncation Errors for Compact Difference Operators

The basic truncation errors that are of interest in this dissertation for first- and second-order derivatives are listed here for reference.

A.1 1D Difference Operators

Central difference operators:

$$\left. \frac{d\phi}{dx} \right|_i = \delta_x \phi_i - \frac{h^2}{6} \left. \frac{d^3\phi}{dx^3} \right|_i - \frac{h^4}{120} \left. \frac{d^5\phi}{dx^5} \right|_i + O(h^6), \quad (\text{A.1})$$

$$\left. \frac{d^2\phi}{dx^2} \right|_i = \delta_x^2 \phi_i - \frac{h^2}{12} \left. \frac{d^4\phi}{dx^4} \right|_i - \frac{h^4}{360} \left. \frac{d^6\phi}{dx^6} \right|_i + O(h^6). \quad (\text{A.2})$$

Forward difference operator:

$$\left. \frac{d\phi}{dx} \right|_i = \delta_x^+ \phi_i - \frac{h}{2} \left. \frac{d^2\phi}{dx^2} \right|_i - \frac{h^2}{6} \left. \frac{d^3\phi}{dx^3} \right|_i - \frac{h^3}{24} \left. \frac{d^4\phi}{dx^4} \right|_i + O(h^4). \quad (\text{A.3})$$

Backward difference operator:

$$\left. \frac{d\phi}{dx} \right|_i = \delta_x^- \phi_i + \frac{h}{2} \left. \frac{d^2\phi}{dx^2} \right|_i - \frac{h^2}{6} \left. \frac{d^3\phi}{dx^3} \right|_i + \frac{h^3}{24} \left. \frac{d^4\phi}{dx^4} \right|_i + O(h^4). \quad (\text{A.4})$$

A.2 2D Cross Derivative Operators

Central difference operators:

$$\left. \frac{\partial^2 \phi}{\partial x \partial y} \right|_{ij} = \delta_x \delta_y \phi_{ij} - \frac{h^2}{6} \left[\frac{\partial^4 \phi}{\partial x^3 \partial y} + \frac{\partial^4 \phi}{\partial x \partial y^3} \right]_{ij} + O(h^4), \quad (\text{A.5})$$

$$\left. \frac{\partial^3 \phi}{\partial x \partial y^2} \right|_{ij} = \delta_x \delta_y^2 \phi_{ij} - \frac{h^2}{12} \left[\frac{\partial^5 \phi}{\partial x^4 \partial y} + 2 \frac{\partial^5 \phi}{\partial x^2 \partial y^3} \right]_{ij} + O(h^4), \quad (\text{A.6})$$

$$\left. \frac{\partial^3 \phi}{\partial x^2 \partial y} \right|_{ij} = \delta_x^2 \delta_y \phi_{ij} - \frac{h^2}{12} \left[\frac{\partial^5 \phi}{\partial x^4 \partial y} + 2 \frac{\partial^5 \phi}{\partial x^2 \partial y^3} \right]_{ij} + O(h^4), \quad (\text{A.7})$$

$$\left. \frac{\partial^4 \phi}{\partial x^2 \partial y^2} \right|_{ij} = \delta_x^2 \delta_y^2 \phi_{ij} - \frac{h^2}{12} \left[\frac{\partial^6 \phi}{\partial x^4 \partial y^2} + \frac{\partial^6 \phi}{\partial x^2 \partial y^4} \right]_{ij} + O(h^4). \quad (\text{A.8})$$

Appendix B

General Stability for Compact Schemes

To investigate the numerical stability of compact finite difference operators, we apply von Neumann analysis. In general, we can label the stencil coefficients of any compact, single time-step formula in the manner illustrated by Figure B.1, where the numerical scheme is represented by

$$\sum_{j=-1}^1 a_j \phi_{i+j}^{n+1} = \sum_{k=-1}^1 b_k \phi_{i+k}^n.$$

If we let

$$\phi_i^n = \alpha^n e^{I\theta i},$$

where α^n is the amplitude of ϕ at time level n , $I = \sqrt{-1}$, the phase angle $\theta = \frac{2\pi h}{\lambda_x}$, and λ_x is the wavelength. It is easy to show [104] that the amplitude magnification factor, $G = \frac{\alpha^{n+1}}{\alpha^n}$, satisfies

$$|G|^2 - 1 = \frac{B(\theta) - A(\theta)}{A(\theta)}, \quad (\text{B.1})$$

where

$$\begin{aligned} A(\theta) &= a_0^2 + (a_1 - a_{-1})^2 + 2a_0(a_1 + a_{-1}) \cos \theta + 4a_1 a_{-1} \cos^2 \theta, \\ B(\theta) &= b_0^2 + (b_1 - b_{-1})^2 + 2b_0(b_1 + b_{-1}) \cos \theta + 4b_1 b_{-1} \cos^2 \theta. \end{aligned}$$

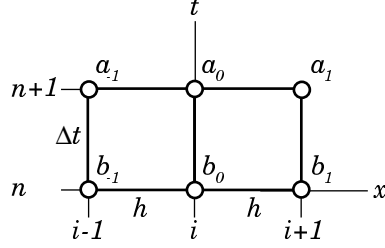


Figure B.1: General stencil for a compact, 1D, time-dependent problem.

For a stable system, $|G|^2 - 1 \leq 0$. This, coupled with the fact that it is also easy to show that $A(\theta) > 0$ always holds true, means that the numerator of (B.1) must be less than zero for a general compact stencil to be stable. We therefore express our stability criterion as

$$F(\chi) = d_0 + d_1\chi + d_2\chi^2 \leq 0,$$

where $\chi = \cos(\theta)$ and

$$d_0 = b_0^2 + (b_1 - b_{-1})^2 - a_0^2 - (a_1 - a_{-1})^2, \quad (\text{B.2})$$

$$d_1 = 2[b_0(b_1 + b_{-1}) - a_0(a_1 + a_{-1})], \quad (\text{B.3})$$

$$d_2 = 4(b_1b_{-1} - a_1a_{-1}). \quad (\text{B.4})$$

We can further simplify this stability restriction by noting that

$$\begin{aligned} F(1) &= d_0 + d_1 + d_2, \\ &= (b_{-1} + b_0 + b_1)^2 - (a_{-1} + a_0 + a_1)^2, \\ &= 0, \end{aligned} \quad (\text{B.5})$$

where we have used the fact that $\sum_{j=-1}^1 a_j = \sum_{k=-1}^1 b_k$ for a conservative system. Since $F(\chi)$ is a parabola, this result means that $F'(1) = d_1 + 2d_2 \geq 0$ is our first requirement for stability. To insure that the parabola is nonpositive over $-1 \leq \chi \leq 1$, we must also require $F(-1) = d_0 - d_1 + d_2 = -2d_1 \leq 0$. Our stability criteria are

therefore

$$d_1 + 2d_2 \geq 0, \tag{B.6}$$

$$d_1 \geq 0. \tag{B.7}$$

Relations (6.9) and (6.10) provide two simple restrictions that we can apply to any compact, single-time-step scheme to determine stability requirements.

Bibliography

- [1] S. Abarbanel and A. Kumar. Compact higher-order schemes for the Euler equations. *Journal of Scientific Computing*, 3:275–288, 1988.
- [2] A. R. Abdullah and D. J. Evans. New explicit methods for the numerical solution of the diffusion-convection equation. In *Proceedings of the Third International Conference on Numerical Methods in Laminar and Turbulent Flows*, pages 951–962, Seattle, 1983.
- [3] L. M. Adams, R. J. Leveque, and D. M. Young. Analysis of the SOR iteration for the 9-point Laplacian. *SIAM Journal on Numerical Analysis*, 25(5):1156–1180, October 1988.
- [4] A. P. Alamdary. Vectorization and microtasking of UTCHEM on the CRAY X-MP. Technical report, University of Texas Petroleum Engineering Department, 1988.
- [5] U. Ananthakrishnaiah, R. Manohar, and J. W. Stephenson. High-order methods for elliptic equations with variable coefficients. *Numerical Methods for Partial Differential Equations*, 3:219–227, 1987.
- [6] D. A. Anderson, J. C. Tannehill, and R. H. Pletcher. *Computational Fluid Mechanics and Heat Transfer*. Hemisphere Publishing Corporation, New York, 1984.

- [7] E. Anderson, Z. Bai, C. Bischof, J. Demmel, J. Dongarra, J. Du Croz, A. Greenbaum, S. Hammarling, A. McKenney, S. Ostrouchov, and D. Sorensen. *LAPACK Users' Guide, Release 2.0*. SIAM. http://www.netlib.org/lapack/lug/lapack_lug.html.
- [8] B. Armaly. Experimental and theoretical investigation of backward-facing step flow. *Journal of Fluid Mechanics*, 127:473–496, 1983.
- [9] E. Barragy. *Parallel Finite Element Methods and Iterative Solution Techniques for Viscous Incompressible Flows*. PhD thesis, The University of Texas at Austin, 1993.
- [10] E. Barragy and G. F. Carey. Stream function vorticity solution using high- p element-by-element techniques. *Communications in Numerical Methods in Engineering*, 9:387–395, 1993.
- [11] D. Bradley, M. Missaghi, and S. B. Chin. A Taylor series approach to numerical accuracy and a third-order scheme for strong convective flows. *Computer Methods in Applied Mechanics and Engineering*, 69:133–151, 1988.
- [12] A. Brandt. Multi-level adaptive solutions to boundary value problems. *Mathematics and Computers*, 31:333–390, 1977.
- [13] A. Brandt. Guide to multigrid development. In W. Hackbush and V. Trottenberg, editors, *Multigrid Methods: Proceedings, Köln-Porz, 1981*, pages 220–312, New York, 1982. Springer-Verlag.
- [14] G. F. Carey and H. T. Dinh. Grading functions and mesh redistribution. *SIAM Journal on Numerical Analysis*, 22:1028–1040, 1985.
- [15] G. F. Carey and R. Krishnan. Penalty approximation of Stokes flow. *Computer Methods in Applied Mechanics and Engineering*, 35(2):169–206, November 1982.

- [16] G. F. Carey and R. McLay. Local pressure oscillation and boundary treatment for the 8-node quadrilateral. *International Journal for Numerical Methods in Fluids*, 6:165–172, 1986.
- [17] G. F. Carey and J. T. Oden. *Finite Elements: Fluid Mechanics, Volume VI*. Prentice Hall, Englewood Cliffs, New Jersey, 1986.
- [18] M. H. Carpenter, D. Gottlieb, and S. Abarbanel. The stability of numerical boundary treatments for compact high-order finite-difference schemes. *Journal of Computational Physics*, 108:272–295, 1993.
- [19] J. E. Castillo, J. M. Hyman, M. Yu. Shashkov, and S. Steinberg. High-order mimetic finite difference methods on nonuniform grids. In *International Conference on Spectral and High Order Methods—Preliminary Proceedings*, pages 11–1–11–15, Houston, Texas, 1995.
- [20] J. E. Castillo, J. M. Hyman, M. Yu. Shashkov, and S. Steinberg. The sensitivity and accuracy of fourth order finite difference schemes on nonuniform grids in one dimension. *Journal of Computers & Mathematics with Applications*, to appear.
- [21] J. E. Castillo and M. Yu. Shashkov. Grid generation methods consistent with finite-difference schemes. Technical Report LA-UR-93-2932, Los Alamos National Laboratory, Los Alamos, NM, 1993.
- [22] T. F. Chan. Stability analysis of finite difference schemes for the advection-diffusion equation. *SIAM Journal on Numerical Analysis*, 21:272–284, 1984.
- [23] B. Char. *Maple V Language Reference Manual*. New York, 1991.
- [24] G. Chen and Z. Yang. Compact second-order upwind finite difference schemes for the convection-diffusion equations. *Journal of Hydrodynamics*, 4(4):32–42, October 1992.

- [25] G. Chen and Z. Yang. Perturbational fourth-order upwind finite difference scheme for the convection-diffusion equation. *Journal of Hydraulics*, 5(1):82–97, January 1993.
- [26] S. I. Cheng. Accuracy of difference formulation of Navier-Stokes equations. Technical report, A. M. S. Department, Princeton University, Princeton, New Jersey, 1968.
- [27] W. C. Connett, W. L. Golik, and A. L. Schwartz. Superconvergent grids for two-point boundary value problems. *Mathematica Applicad e Computacional*, 10:43–58, 1991.
- [28] H. J. Crowder and C. Dalton. Errors in the use of non-uniform mesh systems. *Journal of Computation Physics*, 7:32–45, 1971.
- [29] A. Datta Gupta, L. W. Lake, G. A. Pope, and K. Sepehrnoori. High-resolution monotonic schemes for reservoir fluid flow simulation. *In Situ*, 15(3):289–317, 1991.
- [30] J. L. Davis. *Finite Difference Methods in Dynamics of Continuous Media*. New York, 1986.
- [31] C. de Boor and H. O. Kreiss. On the condition of the linear systems associated with discretized bvps of odes. *SIAM Journal on Numerical Analysis*, 23(5):936–939, October 1986.
- [32] E. K. de Rivas. On the use of nonuniform grids on finite-difference equations. *Journal of Computational Physics*, 9:202–210, 1972.
- [33] G. de Vahl Davis and G. D. Mallinson. An evaluation of upwind and central difference approximations by a study of recirculating flow. *Computers and Fluids*, 4:29–43, 1976.

- [34] S. C. R. Dennis and J. D. Hudson. Compact h^4 finite difference approximations to operators of Navier-Stokes type. *Journal of Computational Physics*, 85:390–416, 1989.
- [35] S. C. R. Dennis and Q. Wing. Generalized finite differences for operators of Navier-Stokes type. In F. G. Zhuang and Y. L. Zhu, editors, *Proceedings of the 10th International Conference on Numerical Methods in Fluid Dynamics*, volume 264 of *Lecture Notes in Physics*, pages 222–228. Springer-Verlag, 1986.
- [36] D. Ding and L. F. L. Philio. Operator-splitting algorithm for three-dimensional convection-diffusion problems. *Journal of Hydrodynamics*, 5(1):22–34, January 1993.
- [37] J. K. Dukowicz and J. D. Ramshaw. Tensor viscosity method for convection in numerical fluid dynamics. *Journal of Computational Physics*, 32:71–79, 1979.
- [38] H. Fasel. Investigation of the stability of boundary layers by a finite-difference model of the Navier-Stokes equations. *Journal of Fluid Mechanics*, 78:355–383, 1976.
- [39] C. K. Forester. Higher order monotonic convective differencing schemes. *Journal of Computational Physics*, 23:1–22, 1977.
- [40] G. E. Forsythe and W. R. Wasow. *Finite Difference Methods for Partial Differential Equations*. Wiley, New York, 1960.
- [41] E. C. Gartland, Jr. Discrete weighted mean approximation of a model convection-diffusion equation. *SIAM Journal on Scientific and Statistical Computing*, 3(4):460–472, December 1982.
- [42] D. K. Gartling. A test problem for outflow boundary conditions—flow over a backward-facing step. *International Journal for Numerical Methods in Fluids*, 11:953–967, 1990.

- [43] U. Ghia, K. N. Ghia, and C. T. Shin. High Re solutions for incompressible flow using Navier-Stokes equations and a multi-grid method. *Journal of Computational Physics*, pages 387–411, 1982.
- [44] J. C. Gilbert and J. Nocedal. Global convergence properties of conjugate gradient methods for optimization. *SIAM Journal on Optimization*, 2(1):21–42, 1992.
- [45] S. K. Godunov and V. S. Ryabenkii. *Difference Schemes*. North-Holland, Amsterdam, 1987.
- [46] R. Gordon, J. F. Lee, and R. Mittra. Technique for using the finite difference frequency domain method with a non-uniform mesh. *Archiv für Elektronik und Übertragungstechnik: Electronics and Communication*, 47(3):143–148, May 1993.
- [47] P. M. Gresho and R. L. Lee. Don’t suppress the wiggles—they’re telling you something! *Computers and Fluids*, 9:223–253, 1981.
- [48] P. Grisvard. *Elliptic Problems in Nonsmooth Domains*. Pitman Advanced Publications Program, Boston, 1985.
- [49] P. Grisvard, editor. *Singularities and Constructive Methods for Their Treatment: Proceedings of the Conference held in Oberwolfach, West Germany*. Springer-Verlag, New York, 1985.
- [50] G. Guj and F. Stella. Numerical solutions of high- Re recirculating flows in vorticity-velocity form. *International Journal for Numerical Methods in Fluids*, 8:405–416, 1988.
- [51] M. M. Gupta and et. al. Single-cell high order difference method for steady state advection-diffusion equation. In *Proceedings of the Symposium—International Association for Hydraulic Research*, pages 101–108, 1982.

- [52] M. M. Gupta, R. P. Manohar, and J. W. Stephenson. A single cell high order scheme for the convection-diffusion equation with variable coefficients. *International Journal for Numerical Methods in Fluids*, 4:641–651, 1984.
- [53] T. Han, J. A. C. Humphrey, and B. E. Launder. A comparison of hybrid and quadratic-upstream differencing in high Reynolds number elliptic flows. *Computer Methods in Applied Mechanics and Engineering*, 29:81–95, 1981.
- [54] A. Harten, B. Engquist, S. Osher, and S. R. Chakravarthy. Uniformly high order accurate essentially non-oscillatory schemes II. *Journal of Computational Physics*, 83:231–303, August 1987.
- [55] A. Harten, B. Engquist, S. Osher, and S. R. Chakravarthy. Uniformly high order accurate essentially non-oscillatory schemes III. *Journal of Computational Physics*, 71(2):231–303, 1987.
- [56] P. W. Hemker. Mixed defect correction iteration for the accurate solution of the convection diffusion equation. In W. Hackbusch and U. Trottenberg, editors, *Multigrid Methods: Proceedings, Köln-Porz, 1981*, Lecture Notes in Mathematics, pages 485–501, New York, 1982. Springer-Verlag.
- [57] P. W. Hemker. Defect correction and higher order schemes for the multi grid solution of the steady Euler equations. In W. Hackbusch and U. Trottenberg, editors, *Multigrid Methods II: Proceedings of 2nd European Conference on Multigrid Methods held at Cologne, October 1–4, 1985*, pages 149–165, New York, 1985. Springer-Verlag.
- [58] W. D. Henshaw, H. O. Kreiss, and L. G. Reyna. Smallest scale estimates for the Navier-Stokes equations for incompressible flow. *Archive for Rational Mechanics and Analysis*, 112(1):21–44, 1990.
- [59] F. B. Hildebrand. *Finite Difference Equations and Simulations*. Englewood Cliff, 1968.

- [60] R. S. Hirsh. Higher order accurate difference solution of fluid mechanics problems by a compact differencing technique. *Journal of Computational Physics*, 9(1):90–109, 1975.
- [61] J. D. Hoffman. Relationship between the truncation errors of centered finite-difference approximations on uniform and nonuniform meshes. *Journal of Computational Physics*, 46:469–474, 1982.
- [62] T. J. R. Hughes and A. N. Brooks. A multi-dimensional upwind scheme with no crosswind diffusion. In *Finite Element Methods in Convection Dominated Flow*, volume 34, pages 19–35, New York, 1979. ASME Winter Annual Meeting.
- [63] S. S. Iyengar. *Structuring Biological Systems : A Computer Modeling Approach*. CRC Press, Boca Raton, FL, 1992.
- [64] M. K. Jain, R. K. Jain, and R. K. Mohanty. Fourth-order finite difference method for three dimensional elliptic equations with nonlinear first-derivative terms. *Numerical Methods for Partial Differential Equations*, 8(6):575–591, November 1992.
- [65] L. Jameson. On the wavelet-optimized finite difference method. Technical Report CR-191601, NASA, 1994.
- [66] R. W. Johnson and R. J. MacKinnon. Equivalent versions of the QUICK scheme for finite-difference and finite volume numerical methods. *Communications in Applied Numerical Methods*, 8:841–847, 1992.
- [67] W. D. Joubert, G. F. Carey, R. T. McLay, N. A. Berner, H. Kohli, A. Lorber, and Y. Shen. *PCG Reference Manual, Version 1.0 α* . Center for Numerical Analysis, The University of Texas at Austin.
- [68] H. M. Jurgens and D. W. Zingg. Implementation of a high-accuracy finite-difference scheme for linear wave phenomena. In *International Conference on*

- Spectral and High Order Methods—Preliminary Proceedings*, pages 16–1–16–10, Houston, Texas, 1995.
- [69] J. Kacur, A. Handlovicova, and M. Kacurova. Solution of nonlinear diffusion problems by linear approximation schemes. *SIAM Journal on Numerical Analysis*, 30(6):1703–1722, December 1993.
 - [70] A. Karlsson and L. Fuchs. Fast and accurate solution of time-dependent incompressible flow. In *Proceedings of the Third International Conference on Numerical Methods in Laminar and Turbulent Flows*, pages 606–616, Seattle, 1983.
 - [71] G. Karniadakis, M. Israeli, and S. Orszag. High-order splitting methods for the incompressible Navier-Stokes equations. *Journal of Computational Physics*, 97:414–443, 1991.
 - [72] P. Knupp and S. Steinberg. *The Fundamentals of Grid Generation*. CRC Press, Boca Raton, 1993.
 - [73] R. I. Kreis, F. C. Thames, and H. A. Hassan. Applications of a variational method for generating adaptive grids. *AIAA Journal*, 24(3):404–410, March 1986.
 - [74] H. O. Kreiss. Central difference schemes and stiff boundary value problems. *BIT*, 24(4):560–567, 1984.
 - [75] H. O. Kreiss, T. Manteuffel, B. Swartz, B. Wendroff, and A. White. Supra-convergent schemes on irregular grids. *Mathematics and Computers*, 47:537–554, 1986.
 - [76] H. O. Kreiss, N. K. Nichols, and D. L. Brown. Numerical methods for stiff two-point boundary value problems. *SIAM Journal on Numerical Analysis*, 23(2):325–368, April 1986.

- [77] Y. K. Kwok and K. K. Tam. Stability analysis of three-level difference schemes for initial-boundary problems for multidimensional convective-diffusion equations. *Communications in Numerical Methods in Engineering*, 9(7):595–605, July 1993.
- [78] P. D. Lax and B. Wendroff. Difference schemes for hyperbolic equations with high order of accuracy. *Communications on Pure and Applied Mathematics*, 17:381–398, 1964.
- [79] S. K. Lele. Compact finite difference schemes with spectral-like resolution. *Journal of Computational Physics*, 103:16–42, 1992.
- [80] B. P. Leonard. A consistency check for estimating truncation error due to upstream differencing. *Applied Mathematical Modelling*, 2:239–244, December 1978.
- [81] B. P. Leonard. A stable and accurate convective modeling procedure based on quadratic upstream interpolation. *Computer Methods in Applied Mechanics and Engineering*, 19:59–98, 1979.
- [82] A. Lerat and R. Peyret. *The Problem of Spurious Oscillations in the Numerical Solution of the Equations of Gas Dynamics*, volume 35 of *Lecture Notes in Physics*, pages 251–256. Springer-Verlag, 1975.
- [83] M. A. Leschziner. Practical evaluation of three finite difference schemes for the computation of steady-state recirculating flows. *Computer Methods in Applied Mechanics and Engineering*, 23:293–312, 1980.
- [84] S. Y. Lin and T. M. Wu. An adaptive multigrid finite-volume scheme for incompressible Navier-Stokes equations. *International Journal for Numerical Methods in Fluids*, 17:687–710, 1993.

- [85] A. A. Lorber and G. F. Carey. A vector-parallel scheme for Navier-Stokes computations at multi-gigaflop performance rates. *International Journal for Numerical Methods in Fluids*, 21(6):445, September 1995.
- [86] R. J. MacKinnon and G. F. Carey. Analysis of material interface discontinuities and superconvergent fluxes in finite difference theory. *Journal of Computational Physics*, 75(1):151–167, 1988.
- [87] R. J. MacKinnon and G. F. Carey. Superconvergent derivatives: A Taylor series analysis. *International Journal for Numerical Methods in Engineering*, 28:489–509, 1989.
- [88] R. J. MacKinnon and G. F. Carey. Nodal superconvergence and solution enhancement for a class of finite element and finite difference methods. *SIAM Journal on Scientific and Statistical Computing*, 11(2):343–353, March 1990.
- [89] R. J. MacKinnon, G. F. Carey, and P. Murray. A procedure for calculating vorticity boundary conditions in the streamfunction-vorticity method. *Communications in Applied Numerical Methods*, 6:47–48, 1990.
- [90] R. J. MacKinnon and R. W. Johnson. Differential equation based representation of truncation errors for accurate numerical simulation. *International Journal for Numerical Methods in Fluids*, 13:739–757, 1991.
- [91] R. J. MacKinnon and M. A. Langerman. A compact high-order finite-element method for elliptic transport problems with variable coefficients. *Numerical Methods for Partial Differential Equations*, 10:1–19, 1994.
- [92] C. W. Mastin. Error analysis and difference equations on curvilinear coordinate systems. In S.V. Parter, editor, *Large Scale Scientific Computation, Proceedings of a Conference Conducted by the Mathematical Research Center, the University of Wisconsin-Madison, May 17–19, 1983*, pages 195–214. Academic Press, Inc., 1984.

- [93] C. W. Mastin and J. F. Thompson. Errors in finite difference computations on curvilinear coordinate systems. Technical Report MSSU-EIRS-ASE-80-4, Mississippi State University, Engineering & Industrial Research Station, 1980.
- [94] R. T. McLay, S. L. Swift, and G. F. Carey. Maximizing sparse matrix–vector product performance in MIMD computers. *Journal of Parallel Supercomputing*, to appear.
- [95] L. M. Milne-Thompson. *The Calculus of Finite Differences*. New York, 1981.
- [96] A. R. Mitchell and D. F. Griffiths. *The Finite Difference Method in Partial Differential Equations*. T. Wiley, 1980.
- [97] S. Mokhtari and B. P. Leonard. Analysis of oscillatory convection schemes. *Bulletin of the American Physical Society*, 32, 1987.
- [98] K. W. Morton. Stability of finite difference approximations to a diffusion-convection equation. *International Journal for Numerical Methods in Engineering*, 15:677–683, 1980.
- [99] K. Muralidhar, M. Varghese, and K. M. Pillai. Application of an operator-splitting algorithm for advection-diffusion problems. *Numerical Heat Transfer: An International Journal of Computation and Methodology: Part A: Applications*, 23(1):99–113, January–February 1993.
- [100] B. J. Noye. New third-order finite-difference method for transient one-dimensional advection-diffusion. *Communications in Applied Numerical Methods*, 6(4):279–288, May 1990.
- [101] B. J. Noye. Compact unconditionally stable finite difference method for transient one-dimensional advection-diffusion. *Communications in Applied Numerical Methods*, 7(7):501–512, October 1991.

- [102] B. J. Noye and K. J. Hayman. An accurate five-point explicit finite difference method for solving the one-dimensional diffusion equation. In B. J. Noye and R. L. May, editors, *Computational Techniques and Applications, CTAC-85*, pages 205–216. Elsevier, 1986.
- [103] B. J. Noye and K. J. Hayman. Explicit two-level finite-difference methods for the two-dimensional diffusion equation. *International Journal of Computer Mathematics*, 42(3–4):223–236, 1992.
- [104] B. J. Noye and H. H. Tan. A third-order semi-implicit finite difference method for solving the one-dimensional convection-diffusion equation. *International Journal for Numerical Methods in Engineering*, 26(7):1615–1629, July 1988.
- [105] B. J. Noye and H. H. Tan. Finite difference methods for solving the two-dimensional advection-diffusion equation. *International Journal for Numerical Methods in Fluids*, 9(1):75–98, January 1989.
- [106] P. Olsson. High-order entropy conserving difference methods for nonlinear conservation laws. In *International Conference on Spectral and High Order Methods—Preliminary Proceedings*, pages 35–1–35–5, Houston, Texas, 1995.
- [107] S. Osher and C. W. Shu. Efficient implementation of essentially non-oscillatory shock capturing schemes. *Journal of Computational Physics*, 77:439–471, 1988.
- [108] S. Osher and C. W. Shu. Efficient implementation of essentially non-oscillatory shock capturing schemes II. *Journal of Computational Physics*, 83(1):32–79, 1989.
- [109] R. L. Panton. *Incompressible Flow*. Wiley, New York, 1984.
- [110] J. C. Patterson. General derivative approximations for finite difference schemes. *International Journal for Numerical Methods in Engineering*, 19:1235–1241, 1983.

- [111] M. Z. Pindera. Method of local corrections for high speed viscous flows. In *Proceedings of the 33rd Heat Transfer and Fluid Mechanics Institute*, pages 115–130, 1993.
- [112] M. Z. Pindera, H. Q. Yang, A. J. Przekwas, and K. Tucker. Assessment of modern methods of numerical simulations of high speed flows. Technical Report 92-0052, AIAA, Reno, NV, January 1992.
- [113] H. S. Price. Monotone and oscillation matrices applied to finite difference approximations. *Mathematics and Computers*, 22:489–516, 1968.
- [114] H. S. Price, R. S. Varga, and J.E. Warren. Applications of oscillation matrices to diffusion-convection equations. *Journal of Mathematical Physics*, 45:301–311, 1966.
- [115] G. D. Raithby. A critical evaluation of upstream differencing applied to problems involving fluid flow. *Computer Methods in Applied Mechanics and Engineering*, 9:75–103, 1976.
- [116] R. H. Rand. *Computer Algebra in Applied Mathematics: An Introduction to MACSYMA*. Pitman Advanced Publishing Program, Boston, 1984.
- [117] J. N. Reddy. On the accuracy and existence of solutions to primitive variable models of viscous incompressible fluids. *International Journal of Engineering Science*, 16:921–929, 1978.
- [118] R. D. Richtmyer and K. W. Morton. *Difference Methods for Initial Value Problems*. Interscience, second edition, 1967.
- [119] A. Rigal. Numerical analysis of two-level finite difference schemes for unsteady diffusion-convection problems. *International Journal for Numerical Methods in Engineering*, 28:1001–1021, 1989.

- [120] P. Roache. *Computational Fluid Dynamics*. Hermosa Press, Albuquerque, NM, 1972.
- [121] P. Roache. Finite difference methods for the steady-state Navier-Stokes equations. In *Proceedings of the Third International Conference on Numerical Methods in Fluid Mechanics*, volume 1, pages 138–145. Springer-Verlag, 1973.
- [122] P. J. Roache. On artificial viscosity. *Journal of Computational Physics*, 10:169–184, 1972.
- [123] K. V. Roberts and N. O. Weiss. Convective difference schemes. *Mathematics of Computation*, 20:272–299, 1966.
- [124] E. M. Rönquist. A domain decomposition solver for the steady Navier-Stokes equations. In *International Conference on Spectral and High Order Methods—Preliminary Proceedings*, pages 39–1–39–17, Houston, Texas, 1995.
- [125] A. A. Samarskii, V. F. Tishkin, A. P. Favorskii, and M. Yu. Shashkov. Operational finite-difference schemes. *Differential Equations*, pages 863–885, 1982.
- [126] H. Schreiber and H. B. Keller. Driven cavity flows by efficient numerical techniques. *Journal of Computational Physics*, 49:310–333, 1983.
- [127] H. Schreiber and H. B. Keller. Spurious solutions in driven cavity calculations. *Journal of Computational Physics*, 49:165–173, 1983.
- [128] J. N. Scott and Y. P. Yao. Stability criteria for a general class of finite difference schemes for convective diffusion equation. Technical Report 92-0424, AIAA, Reno, NV, January 1992.
- [129] J. M. M. Sousa, C. F. N. B. Silva, and J. C. F. Pereira. Accuracy comparison of high-order finite difference schemes for the evolution of two-dimensional finite-amplitude disturbances. In *International Conference on Spectral and*

- High Order Methods—Preliminary Proceedings*, pages 64–1–64–8, Houston, Texas, 1995.
- [130] D. B. Spalding. A novel finite difference formulation for differential expressions involving both first and second derivatives. *International Journal for Numerical Methods in Engineering*, 4:551–559, 1972.
 - [131] W. F. Spotz. Superconvergent finite difference methods with applications to viscous flow. Master’s thesis, University of Texas at Austin, 1991.
 - [132] W. F. Spotz and G. F. Carey. High-order compact finite difference methods with applications to viscous flow. Technical Report TICAM 94-03, Texas Institute for Computational and Applied Mathematics, 1993.
 - [133] W. F. Spotz and G. F. Carey. High-order compact scheme for the stream-function vorticity equations. *International Journal for Numerical Methods in Engineering*, 38(20):3497–3512, October 30 1995.
 - [134] W. F. Spotz and G. F. Carey. A high-order compact formulation for the 3D Poisson equation. *Numerical Methods for Partial Differential Equations*, 12:235–243, 1996.
 - [135] G. Strang. *Linear Algebra and Its Applications*. Harcourt Brace Jovanovich, Inc., San Diego, third edition, 1988.
 - [136] G. D. Stubbley, G. D. Raithby, and A. B. Strong. Proposal for a new discrete method based on an assessment of discretization errors. *Numerical Heat Transfer*, 3:411–428, 1980.
 - [137] A. Suresh and H. T. Huynh. Numerical experiments on a new class of non-oscillatory schemes. Technical Report 92-0421, AIAA, Reno, NV, January 1992.

- [138] J. F. Thompson, Z. U. A. Warsi, and C. W. Mastin. *Numerical Grid Generation: Foundations and Applications*. Elsevier Science Publishing Co., New York, 1985.
- [139] W. W. Tworzydło. The FDM in arbitrary curvilinear co-ordinates — formulation, numerical approach, and applications. *International Journal for Numerical Methods in Engineering*, 28:261–277, 1989.
- [140] A. I. van de Vooren and A. C. Vliegenthart. On the 9-point difference formula for Laplace’s equation. *Journal of Engineering Mathematics*, 1:187–202, 1967.
- [141] P. J. van der Houven. *Finite Difference Methods for Solving Partial Differential Equations*. Amsterdam, 1968.
- [142] H. D. Victory. On finite difference methods for solving discrete-ordinate transport equations. *SIAM Journal on Numerical Analysis*, 23(1):78–108, February 1986.
- [143] W. G. Vincenti and C. H. Kruger. *Introduction to Physical Gas Dynamics*. John Wiley and Sons, Inc., New York, 1965.
- [144] R. A. Walters and G. F. Carey. Analysis of spurious oscillation modes for the shallow water and Navier-Stokes equations. *Computers and Fluids*, 11(1):51, 1983.
- [145] Y. L. Wang and P. A. Longwell. Laminar flow in inlet section of parallel flow. *American Institute of Chemical Engineers Journal*, 10(3):323–329, May 1964.
- [146] R. F. Warming and R. M. Beam. Upwind second-order difference schemes and applications in aerodynamic flows. *AIAA Journal*, 14:1241, 1976.
- [147] J. J. Westerink and D. Shea. Consistent higher degree Petrov-Galerkin methods for the solution of the transient convection-diffusion equation. *International Journal for Numerical Methods in Engineering*, 28:1077–1101, 1989.

- [148] N. S. Wilkes and C. P. Thompson. An evaluation of higher-order upwind differencing for elliptic flow problems. In *Proceedings of the Third International Conference on Numerical Methods in Laminar and Turbulent Flows*, pages 248–257, Seattle, 1983.
- [149] J. Wilkinson. *The Algebraic Eigenvalue Problem*. Clarendon Press, Oxford, 1965.
- [150] Stephen Wolfram. *Mathematica: A System for Doing Mathematics by Computer*. Addison Wesley, Redwood City, California, second edition, 1991.
- [151] H. H. Wong and G. D. Raithby. Improved finite difference methods based on a critical evaluation of the approximation errors. *Numerical Heat Transfer*, 2:139–163, 1979.
- [152] W. S. Yousif and D. J. Evans. High order difference group explicit (Hodge) methods. *Communications in Applied Numerical Methods*, 2(5):449–462, September–October 1986.
- [153] D. W. Zingg, E. M. Epstein, and H. M. Jurgens. A comparison of finite-difference schemes for computational aeroacoustics. Technical Report 95-0162, AIAA, 1995.
- [154] D. W. Zingg, H. Lomax, and H. M. Jurgens. An optimized finite-difference scheme for wave propagation problems. Technical Report 93-0459, AIAA, 1993.
- [155] D. W. Zingg, H. Lomax, and H. M. Jurgens. High-accuracy finite-difference schemes for linear wave propagation. *SIAM Journal on Scientific Computing*, 17(2):328, March 1996.
- [156] M. Zlámal. Superconvergence and reduced integration in the finite element method. *Mathematics and Computers*, 32:663–685, 1978.

Vita

William Frederick Spotz was born at the U.S. Air Force Hospital in Wiesbaden, West Germany, August 31, 1967 to William Henry and Beverly Jean Spotz. During high school in Houston, he worked two summers for Barrios Technologies. After enrolling at the University of Texas in the fall of '85, William spent three summers working for IBM. During the school year, he worked part-time in the UT Computational Fluid Dynamics Laboratory. In May '89, he graduated with a Bachelor of Science in Aerospace Engineering with High Honors and entered the Graduate School the following fall semester, where he worked as a research and teaching assistant as well as a computer lab consultant and received his Masters of Science in December '91. In January '93 he married Katherine Simons and moved back to Houston, where he continued working on his dissertation at U.T. Austin via the Internet.

Permanent Address: 2125 Pine
Boulder, CO 80302

This dissertation was typeset with L^AT_EX 2_ε¹ by the author.

¹L^AT_EX 2_ε is an extension of L^AT_EX. L^AT_EX is a collection of macros for T_EX. T_EX is a trademark of the American Mathematical Society. The macros used in formatting this dissertation were written by Dinesh Das, Department of Computer Sciences, The University of Texas at Austin.